Engineering Applications of Artificial Intelligence 117 (2023) 105532

Contents lists available at ScienceDirect

Engineering Applications of Artificial Intelligence

journal homepage: www.elsevier.com/locate/engappai

Survey paper

Automated liver tissues delineation techniques: A systematic survey on machine learning current trends and future orientations

Ayman Al-Kababji [a,*], Faycal Bensaali [a], Sarada Prasad Dakua [b], Yassine Himeur [a,c]

[a] Department of Electrical Engineering, Qatar University, Doha, Qatar
[b] Department of Surgery, Hamad Medical Corporation, Doha, Qatar
[c] College of Engineering and Information Technology, University of Dubai, Dubai, UAE

ARTICLE INFO

MSC:
00-01
99-00

Keywords:
Liver
Hepatic-tumors
Hepatic-vessels
Machine learning
Survey
Semantic segmentation

ABSTRACT

Machine learning and computer vision techniques have grown rapidly in recent years due to their automation, suitability, and ability to generate astounding results. Hence, in this paper, we survey the key studies that are published between 2014 and 2022, showcasing the different machine learning algorithms researchers have used to segment the liver, hepatic tumors, and hepatic-vasculature structures. We divide the surveyed studies based on the tissue of interest (hepatic-parenchyma, hepatic-tumors, or hepatic-vessels), highlighting the studies that tackle more than one task simultaneously. Additionally, the machine learning algorithms are classified as either supervised or unsupervised, and they are further partitioned if the amount of work that falls under a certain scheme is significant. Moreover, different datasets and challenges found in literature and websites containing masks of the aforementioned tissues are thoroughly discussed, highlighting the organizers' original contributions and those of other researchers. Also, the metrics used excessively in the literature are mentioned in our review, stressing their relevance to the task at hand. Finally, critical challenges and future directions are emphasized for innovative researchers to tackle, exposing gaps that need addressing, such as the scarcity of many studies on the vessels' segmentation challenge and why their absence needs to be dealt with sooner than later.

1. Introduction

Two million deaths annually around the world are credited to hepatic diseases (Asrani et al., 2019). Half of these deaths are related to complications caused by liver cirrhosis, and the other half are due to hepatitis and hepatocellular carcinoma (HCC) (Asrani et al., 2019). Unfortunately, it is also a hub for metastasis originating from adjacent organs such as the colon, rectum, pancreas, stomach, esophagus, breasts, lungs, etc. (UCSF Department of Surgery, 2020). Regardless of the tumors' origin, the liver and its lesions are routinely analyzed in primary tumor staging (Christ et al., 2017). In particular, HCC comprises a genetically and molecularly heterogeneous group of cancers commonly arising in chronically damaged livers (Christ et al., 2017). However, screening for liver-related diseases can reduce mortality (Nasiri et al., 2020). Early detection and accurate delineation of hepatic tumors can help a physician decide on more appropriate treatment planning.

As important as the liver is, many developed imaging modalities such as computerized tomography (CT), magnetic resonance imaging (MRI), positron-emitting computerized tomography (PET-CT), and ultrasound (US) are used for the liver's morphological and volumetric analysis and diagnosis of associated diseases (Campadelli et al., 2009; Gotra et al., 2017). They are useful, especially for their capability of giving surgeons insights into the current state of organs non-invasively. With the existence of such modalities, computer-aided detection (CAD) systems have become significantly important. Furthermore, CT, MRI, and PET-CT can generate 2-dimensional (2D) slices of the human body that are combined to generate 3-dimensional (3D) holistic organ volumes for surgeons to analyze. Thus, they bear more advantages than the US modality in providing clearer and more informative image slices. Moreover, thanks to CT scans' higher signal-to-noise ratio and better spatial resolution, they produce more accurate anatomical information about the visualized structures, and this imaging technique is preferred by diagnosticians (Campadelli et al., 2009). Moreover, relative to MRI, CT scans have a shorter acquisition time (Gotra et al., 2017). In contrast, the patient is more exposed to radiation in modalities like CT. Additionally, the chances of developing fatal cancers from CT scans are 1 in 2,000, which is fairly small; however, with the increased number of scans, the chances become higher (Chang, 2018).

* Corresponding author.
E-mail addresses: aa1405810@qu.edu.qa (A. Al-Kababji), f.bensaali@qu.edu.qa (F. Bensaali), SDakua@hamad.qa (S.P. Dakua), yassine.himeur@qu.edu.qa (Y. Himeur).

https://doi.org/10.1016/j.engappai.2022.105532
Received 30 April 2022; Received in revised form 29 September 2022; Accepted 13 October 2022
Available online 21 November 2022

Abbreviations

1D	1-dimensional
2D	2-dimensional
2.5D	2.5-dimensional
3D	3-dimensional
3D-IRCADb	3D Image Reconstruction for Comparison of Algorithm Database
4D	4-dimensional
AdaBoost	Adaptive boosting
AH-Net	Anisotropic hybrid network
AHCNet	Attention hybrid connection blocks network
AI	Artificial intelligence
ANN	Artificial neural network
ANU-Net	Attention mechanism and nested U-Net
ASM	Active shape models
ASD	Average symmetric surface distance
ASPP	Atrous spatial pyramid pooling
AUC	Area under curve
BCE	Binary cross-entropy
BRISK	Scalable key points
BtCV	Multi-Atlas Labeling Beyond the Cranial Vault
Conv-LSTM	Convolutional LSTM
CAD	Computer-aided detection
CaRF	Cascaded random forest
CCGAN	Cascaded conditional GANs
CdAE	Convolutional denoising autoencoders
CE-CT	Contrast-enhanced CT
CE-MRI	Contrast-enhanced MRI
CE-US	Contrast-enhanced US
CFCN	Cascaded 2D FCN
CHAOS	Combined (CT-MR) Healthy Abdominal Organ Segmentation
CNN	Convolutional neural network
CoFCN	Conjugate FCN
CompNet	Complementary network
CRF	conditional random field
cSE	Squeeze and channel excitation
CT	Computerized tomography
CT-ORG	CT Volumes with Multiple Organ Segmentations
CU-ResNet	Cascaded U-ResNet
D-BCE	Dice and BCE
DA	Domain adaptation
DAP	Deep atlas prior
DBN	Deep belief network
DC-GAN	Densely-connected GAN
DDL	Deep data-driven loss
DenseU-Net	Densely-connected U-Net
DI2IN	Deep image-to-image network
DL	Deep learning
DPC	Dice/case
DMO	deformable model optimization
DNN	Deep neural network
DRR	Digitally reconstructed radiographs
DSC	Dice similarity coefficient
DSN	Deeply supervised network
DT	Decision tree
DV-Net	Dense V-Net
ELM	Extreme learning machine
FC	Fuzzy connectedness
FFCM	Fast FCM
FCM	Fuzzy c-means
FCN	Fully convolutional network
FKFCM	Fast kernelized FCM
FP	False positive
FPR	False positive rate
FN	False negative
FRN	fractal residual network
G-ResNet	Graph convolutions-based ResNet
GAN	Generative adversarial network
GAT	Graph attention layers
GC	Graph-cut
GCCM	Graphical connectivity constraint module
GDSC	Global DSC
GLC-UNet	Global and local context U-Net
GNN	Graph neural network
GO	Genetic optimizer
GPU	Graphics processing unit
GWO	Grey wolf optimization
H-DenseUNet	Hybrid DenseU-Net
HCC	Hepatocellular carcinoma
HD	Hausdorff Distance
HNN	Holistic nested network
HPM-Net	hierarchical progressive multi-scale network
IoU	Intersection-over-union
ISBI	IEEE International Symposium on Biomedical Imaging
JI	Jaccard index
KFCM	Kernelized FCM
KNN	K-nearest neighbors
LDOG	Local direction of gradient
LER-CN	Liver extraction residual convolutional network
LF	Laplacian forest
LiTS	Liver Tumor Segmentation Challenge
LR	Logistic regression
LSM	Level-set methods
LSTM	Long short-term memory
LTEM	Laws texture energy measure
LU-Net	Lightweight U-Net
LVSNet	Liver vessel segmentation network
MC-FCN	Multi-channel FCN
MC-FC-ResNet	Multi-channel 3D FCN ResNet
MCG	Multi-scale candidate generation
MICCAI	Medical Image Computing and Computer Assisted Intervention
MIDAS-LT	MIDAS Liver Tumor
MIMO-FAN	Multiple-input and multiple-output feature abstraction network
ML	Machine learning
mm	Millimeter
MPNet	Multi-planar network
MPU-Net	Multi-planar U-Net
MRF	Markov random field
MRI	Magnetic resonance imaging
MSD	Maximum symmetric surface distance

MSF	Mean shape fitting
MSDC	Medical Segmentation Decathlon Challenge
MSDC-T3	MSDC Task 3
MSDC-T8	MSDC Task 8
mU-Net	modified U-Net
NMF	Non-negative matrix factorization
NRC	Noise removal component
NS	Neutrosophic sets
OAN-RCs	Organ-attention networks with reverse connections
P-UNet	Perpendicular U-Net
PaNN	Prior-aware neural network
PCA	Principal component analysis
PE	Project and excite
PET-CT	Positron-emitting CT
PPV	Positive predictive value
PSO	Particle swarm optimization
RA-UNet	Residual attention-aware U-Net
RECIST	Response evaluation criteria in solid tumors
RF	Random forest
RIU-Net	U-Net equipped with residual and InceptionV3 modules
RMSD	Root-mean-square symmetric surface distance
ROC	Receiver operating characteristic
RUCB	Relaxed upper confident bound
RVD	Relative volumetric distance
RW	Random walks
SAEs	Stacked autoencoders
SAR-U-Net	ASPP-based residual U-Net
SIRT	Selective internal radiation therapy
SLIC	Simple linear iterative clustering
SLIVER07	Segmentation of the LIVER Competition 2007
SPC	Structural preservation component
SSM	Statistical shape models
SU-UNet	Self-updating U-Net
SURF	Robust features
SVC	Soft voting classifier
SVM	Support vector machine
TCIA	The Cancer Imaging Archive
TD-GAN	Task-driven GAN
TL	Transfer learning
TN	True negative
TNR	True Negative Rate
TOI	Tissue of interest
TP	True positive
TPCNN	Two-path CNN
TPR	True Positive Rate
U^2-Net	universal U-Net
U-ResNet	U-Net ResNet
US	Ultrasound
VA	Volume attention
VAE	Variational autoencoder
VascuSynth	Vascular Synthesizer
VISCERAL	Visual Concept Extraction Challenge in Radiology
VOE	Volumetric overlap error

CT, MRI, and PET-CT allow clinicians, physicians, and surgeons to have a clearer insight into the body organs non-invasively. CT scans, for instance, provide three different anatomical views for the organs from transversal, sagittal, and coronal planes, allowing medical personnel to tackle the organ of interest from different angles. Such modalities are utilized extensively by medical personnel for countless clinical applications, including organic cancer diagnosis, organ transplantation, and surgical planning (Wang et al., 2018). All these procedures apply in the case of the liver, where different cancerous cells exist, such as HCC, cysts, metastases, etc. Additionally, such modalities are used for adaptive radiation therapy, which is a radiation treatment plan that imposes modifications based on the patient's functional changes during a course of radiation (Liang et al., 2018). In another clinical procedure, a pre-procedural CT or MRI scan can help in interventional endoscopy for pancreatic and biliary diseases as image guidance can be supportive in intra-procedural navigation (Gibson et al., 2018a) to specific gastrointestinal positions as the endoscope's field of view is small and lacks visual orientation cues (Gibson et al., 2017). Also, medical image registration can aid medical practitioners in observing the motion of intra-patient organs in the middle of procedures (Heinrich, 2019). Thus, it is evident how important these modalities are in increasing the quality of life and expectancy for numerous patients.

All the aforementioned reasons justify the idea of segmenting human organs, especially the liver, its tumors, and vessels, to aid medical personnel in disease diagnosis. Not only is it important to segment liver and tumors pre-procedural, but numerous advantages also prevail when performing post-procedural segmentation on a follow-up CT scan. For instance, through medical image registration, a realization can be achieved about whether the conducted procedure successfully stopped the disease. Furthermore, tumor burden quantification, which measures the volume of all tumors within the liver (Vivanti et al., 2017), is important when discussing tumors' progression within the liver. Early diagnosis and accurate segmentation of hepatic tumors can help doctors plan an appropriate treatment procedure (Nasiri et al., 2020). Additionally, a follow-up CT scan, which segments the liver and the tumors, is also of interest since diseases' progression can be documented for further analysis and treatment procedure planning. However, the norm currently in clinical routines is to manually or semi-automatically segment the liver from CT and MRI modalities. Even though, in some scenarios, these techniques can be more accurate than automatic ones (Zheng et al., 2017a), the underlying issues of manual and semi-automatic techniques are represented by their subjectivity (i.e., dependency on the radiologists' experience), intra- and inter-radiologist variance, and time-consumption (Hu et al., 2016), especially for experts whose time is extremely valuable. Thus, comes the importance of using automatic methods with high segmentation performance.

Many devised automatic segmentation techniques have been applied in the last two decades. They can be categorized into statistical-based and learning-based approaches, where the former can be represented by scans intensities' statistical distribution, including atlases, statistical shape models (SSM), active shape models (ASM), level-set methods (LSM), and graph-cut (GC) methods (Yang et al., 2017). Usually, these methods are challenged by boundary leakage and under- or over-segmentation (Zheng et al., 2017a). On the other hand, the latter depends on either hand-crafted features as in conventional machine learning (ML) algorithms or empirically-found features as in the case of convolutional neural network (CNN), which is a special structure of the artificial neural network (ANN). The medical image segmentation field made the most significant leap riding on the wave of deep CNNs (Wang et al., 2018), where they reached a state of capability that enabled them to generate expert-like segmentations in extremely minimal time. Hence, ML techniques are essential and effective tools in analyzing highly complex data from the medical fields (Garg and Mago, 2021).

However, creating an accurate segmentation of the liver, hepatic tumors, and hepatic vessels is still a challenge. During data acquisition, the variance within the dataset constructs obstacles in front of the model's performance, such as the different scanning protocols with different voxel densities/scanners resolution and different contrast agents

with varying levels of contrast enhancements (Christ et al., 2017). On the other hand, from an organs point of view, the low-contrast boundaries exhibited between the liver and surrounding organs create areas of fuzziness that are hard for models to classify, which are translated into over- or under-segmentation (Hu et al., 2016). Moreover, the highly varying liver shapes and/or sizes among people, especially abnormalities introduced by surgical resection (Christ et al., 2017), render it harder for liver segmentation techniques, particularly for SSM and similar predictors (Hu et al., 2016). Challenges of segmenting what is within the liver are introduced by the heterogeneity of tumors' sizes and shapes, and intra-hepatic veins (vessels) irregularities, which further complicates the segmentation task (Hu et al., 2016; Christ et al., 2017). Thus, creating a detailed 3D liver segmentation is one of the most challenging tasks that need addressing.

Similar to what Garg and Mago (2021) did, but with a more in-depth review of the ML techniques focusing on the liver, this paper highlights their use in the liver's segmentation from medical images (including the tumors and vessels) by:

- Reviewing the state-of-the-art automated algorithms incorporating/based on novel ML
- Specifying all the publicly-available datasets' for liver, tumors, and/or vessels segmentation challenge
- Highlighting the metrics currently in use for evaluating the model's segmentation performance
- Presenting the literature based on ML to segment liver, tumors, and/or vessels during 2014–2022
- Providing a list of open research issues and future directions for improving the available existing datasets and the automatic segmentation techniques

The remainder of this paper is organized as follows. Section 2 highlights the existing datasets, which can be utilized for the aforementioned cause. Section 3 describes the objective metrics that evaluate created models for performance comparison. Section 4 delves into the related works, where a comparison of compartments is shown and discussed. Section 5 shows our critical discussion of the survey and promotes open challenges. Future directions that we observe during the conducted survey are presented in Section 6, and finally, we conclude the paper in Section 7.

2. Publicly available challenges and datasets

This section provides a brief historical background and a summary of the literature's datasets/challenges' specifications. Each dataset's origins and specifications are discussed and then summarized in Table 1. Some of the mentioned datasets/challenges were hosted by well-known medical conferences such as the Medical Image Computing and Computer Assisted Intervention (MICCAI) conference and the IEEE International Symposium on Biomedical Imaging (ISBI). The organizers would present the datasets in a competition format pushing researchers to participate by creating healthy peer-pressure environments. Other datasets were shared publicly by different research institutions encouraging researchers to create better algorithms.[1]

2.1. Inclusion/exclusion criteria

This paper comprehensively highlights and presents datasets that include liver, tumors, and/or vessel delineations, solely or with other organs' ground-truth masks.

However, if the ground-truth labels for either liver, tumors, or vessels were not created, we refrain from including that particular dataset. Lastly, we define ground-truth labels as tissues' delineation (i.e., segmentation), not the localization of said tissues.

[1] Some of the datasets were investigated with the aid of ITK-SNAP (Yushkevich et al., 2006). Available at: www.itksnap.org

2.2. Historical background, comparison, and summary of challenges/datasets

Throughout the last decade and a half, many datasets of different imaging modalities such as CT, contrast-enhanced CT (CE-CT), MRI, and contrast-enhanced MRI (CE-MRI) have been published. Moreover, with the recent development of ML and artificial intellignece (AI) technologies, medical faculty understood how important it is to incorporate such tools to enhance healthcare quality. Thus, datasets' sizes have considerably increased, which is also noticeable in the case of our review paper, as highlighted later in this section.

The Segmentation of the LIVER Competition 2007 (SLIVER07) occurred in a workshop named "3D Segmentation in the Clinic: A Grand Challenge" in conjunction with MICCAI 2007. It is considered the first-ever workshop in the liver segmentation field, where it paved the way for the rest of the open-source datasets/challenges, and the results of it are summarized in Heimann et al. (2009). Three years later, 3D Image Reconstruction for Comparison of Algorithm Database (3D-IRCADb) is gathered by the IRCAD institute in France, which includes patients' anonymized medical images. In total, the dataset has 22 venous phase CE-CT scans divided into: (1) 3D-IRCADb01, which contains 10 males and 10 females with 75% having hepatic tumors; (2) 3D-IRCADb02, which contains 2 CT scans with other abdominal organs segmented. It is worth noting that the majority of literature focuses on the 3D-IRCADb01 group and is normally divided into training and testing records accordingly. In the same year, a very small dataset is also published, called the MIDAS Liver Tumor (MIDAS-LT) Segmentation Dataset. It is a part of a bigger initiative to provide a collection of archived, analyzed, and publicly accessed datasets called MIDAS (Kitware Inc., 2010a).

Later on, Vascular Synthesizer (VascuSynth) software is created for synthesizing tubular-shaped structures such as human organ vessels or other tree-like structures. Due to the absence of datasets with manually segmented vessels for training, the creators (Hamarneh and Jassi, 2010; Jassi and Hamarneh, 2011) aimed to create synthesized data to support the cause of automated segmentation of tubular structures in 3D medical images. The software can simulate volumetric vascular images by iteratively growing vascular trees based on either user-defined or spatially varying oxygen demand maps. Moreover, the software generates the corresponding ground-truth segmentations, the tree hierarchy, the bifurcation locations, and the branch properties. In 2015, Multi-Atlas Labeling Beyond the Cranial Vault (BtCV) - Workshop and Challenge extends multi-atlas segmentation beyond the skull vault to include the cervix and abdomen segmentation. Thus, the liver, among other organs (kidneys, gallbladder, esophagus, stomach, etc.), is segmented. The dataset contains many segmentations and registrations, but the number of liver segmentation records is 50 venous phase CE-CT scans. On the same year, Pancreas-CT dataset is launched containing pancreas manual delineations available on The Cancer Imaging Archive (TCIA) website (Roth et al., 2016). It originally had 82 records when first published in 2015. However, in 2020, 2 records were removed (#25 & #70) as they were duplicates of Record #2 with slight variations. This dataset is included because the liver delineations are created along with other organs for 43 records (42 after removing the duplicate Record #25) from this dataset (Gibson et al., 2018a). It is worth noting that the specifications mentioned in Table 1 are for those records with liver delineation provided in Gibson et al. (2018a). The following year, Visual Concept Extraction Challenge in Radiology (VISCERAL) Anatomy3 is published. The challenge is concerned with multi-organ segmentation providing ground-truth labeling of up to 20 organs (liver, pancreas, spleen, kidneys, lungs, aorta, urinary bladder, gallbladder, etc.). The full list can be found in Hanbury (2016), and the results of all the workshops are summarized in Jimenez-del-Toro et al. (2016).

A breakthrough in the liver and tumors segmentation happened with the Liver Tumor Segmentation Challenge (LiTS) in 2017, This challenge was conducted in both ISBI and MICCAI to provide researchers with ground-truth labels for the liver and tumors within.

The challenge is to automatically segment liver tumors/lesions in CT volumes and estimate the tumors' burden, along with the typical liver segmentation challenge. The dataset can be found in (Christ, 2017), and the summary of the challenge results is summarized in (Bilic et al., 2019) (Noting that 3D-IRCADb01 is part of the training set of LiTS. records 28 – 47 (Jiang et al., 2019)). A year later, the Medical Segmentation Decathlon Challenge (MSDC) was held in MICCAI, where it uniquely focuses on the segmentation generalizability of a model on 10 different biomedical tasks. In this review, we only report the liver-related tasks, which are Task 3 and Task 8; however, details regarding all the tasks are summarized in (Simpson et al., 2019). We refer to Task 3 and Task 8 datasets as MSDC-T3 and MSDC-T8, respectively. As a matter of fact, MSDC-T3 is the same as the LiTS dataset, where the training sets are identical, but the testing set in MSDC-T3 is re-shuffled. It is worth noting that the authors in (Tian et al., 2019) publicly created and shared both the liver annotations for the MSDC-T8 443 CT records and the Couinaud's annotations for 193. The following year, CT Volumes with Multiple Organ Segmentations (CT-ORG) Dataset is published as an extension of the LiTS dataset and is publicly accessible via the TCIA website (Clark et al., 2013). It contains 140 CT scans where the creators Rister et al. (2019) added extra 9 PET-CT scans over the LiTS training set and extended the segmentation to multiple organs (lungs, bones, liver, kidneys, bladder, and brain). Lastly, the Combined (CT-MR) Healthy Abdominal Organ Segmentation (CHAOS) Challenge was held in ISBI 2019, aiming to segment abdominal multi-organ tumor-free CT and MRI data. The dataset has both CT and MRI (T1 and T2 weighted) parts, where there is no inter-modality connection (i.e., the CT and MRI data are from random patients, not counterparts for the same patient). The summary of this challenge is reported in Kavur et al. (2021).

In Table 1, each dataset's positives and negatives are highlighted explicitly. It can be noticed that the most comprehensive dataset (from a liver point of view) is the MSDC-T8 due to the presence of many records in that dataset, along with the vessels' segmentation availability. Moreover, a summary of the reviewed challenges and datasets is depicted in this table. It highlights the website from where researchers can retrieve the datasets, the type of modality used, and the inclusion of contrast enhancement agents. Also, it highlights the training/testing ratio along with the physical and computerized dimensions for each dataset.

3. Standard segmentation evaluation metrics

This section discusses the most considered metrics within the liver segmentation literature, highlighting the used notations, the inclusion/exclusion criteria, and the significance each metric presents. Before discussing the metrics, we highlight the used notations.

- A refers to the ground-truth label voxels set
- B is the predicted voxels set by the created models
- $|\cdot|$ is the set cardinality
- $\|\cdot\|$ represents the Euclidean distance
- $S(\cdot)$ indicates the set of surface voxels
- True positive (TP) is the set of correctly classified tissue of interest (TOI) pixels/voxels
- True negative (TN) is the set of truly classified background pixels/voxels, noting that background voxels describe any voxel which does not belong to the TOI of the study.
- False positive (FP) is the set of incorrectly classified background pixels/voxels
- False negative (FN) is the set of incorrectly classified TOI pixels/voxels

Moreover, all the frequently used metrics in the literature are included in this section highlighting the measurement each one conveys. Two main types of metrics have been identified in the literature: (1) percentile metrics; and (2) distance metrics. Percentile metrics are the ones that end up being between 0 and 1 (or 100%) to indicate a percentage. In contrast, distance metrics are measurements of the difference between ground-truth mask A and segmented mask B in real-life physical units.

3.1. Percentile metrics

3.1.1. Jaccard index (JI)

JI is a fundamental metric to understand how close is the generated prediction in overlapping with the ground-truth label. It is also known as the Tanimoto index, or intersection-over-union (IoU) metric (Heimann et al., 2009). Eq. (1) shows two equivalent definitions of the JI metric.

$$JI = \frac{|A \cap B|}{|A \cup B|} = \frac{TP}{TP + FP + FN} \tag{1}$$

Intuitively, perfect prediction is when JI equals 1, meaning that $|A \cap B|$ is the same as $|A \cup B|$. In other words, there are no wrong predictions (i.e., FP and $FN = 0$), and the volumes are perfectly similar. In contrast, JI equating to 0 means that no intersection exists between the ground-truth and prediction, or TP is 0, meaning that the TOI was completely misclassified.

3.1.2. Precision/positive predictive value (PPV)

Precision aims to investigate the over-segmentation aspect of the model by dividing the total number of correctly classified TOI voxels over the total positively classified voxels (i.e., true and false) as indicated by Eq. (2).

$$Precision/PPV = \frac{TP}{TP + FP} \tag{2}$$

A value of 1 indicates an ideal segmentation scenario for correctly classifying background voxels. In contrast, a value of 0 is the extreme case of incorrectly classifying all TOI voxels.

3.1.3. Recall/sensitivity/true positive rate (TPR)

Recall, on the other hand, investigates the under-segmentation aspect of the model, by dividing the correctly classified TOI voxels over the "actual" number of TOI voxels, as shown by Eq. (3).

$$Recall/Sensitivity/TPR = \frac{TP}{TP + FN} \tag{3}$$

Recall varies between 0 and 1, where 1 indicates perfect segmentation of all TOI voxels, and 0 indicates the exact opposite.

3.1.4. Dice similarity coefficient (DSC)

DSC (or Dice) is the F1 Score counterpart for images, which is a harmonic mean of both precision and recall. In a sense, it measures the similarity between ground-truth set A and generated prediction B. The original DSC for a single image is defined in Eq. (4).

$$DSC = 2\frac{|A \cap B|}{|A| + |B|} = \frac{2TP}{2TP + FP + FN} \tag{4}$$

Similar to the JI metric, the two extreme cases are 0 and 1, where the former emphasizes the absence of any similarity, and the latter indicates perfect similarity between A and B.

The organizers of the LiTS workshop further formulated two metrics from DSC, highlighting a key difference: how the DSC is summed in each case. By this distinction, Dice/case is aimed to account equally for both small tumors and large tumors and not be highly influenced by the large ones (Bilic et al., 2019).

Global DSC (GDSC) encapsulates the segmentations of all volumes and compares them to all respective labels in a single shot as if all the volumes were concatenated into one. Thus, having a similar effect to Eq. (4) for the whole test set.

Table 1
Summary of available datasets and their characteristics (Heimann et al., 2007; IRCAD, 2010; Kitware Inc., 2010b; Landman et al., 2015; Selver et al., 2019).

Dataset	Year	Available Masks	Modality	Size (Train/Test)	Voxels Dimensions (Height × Width × Depth mm^3)	Volumes Dimensions (Height × Width × Slice)	Positives	Negatives
SLIVER07 (Heimann et al., 2007)	2007	Liver	CE-CT	30 (20/10)	(0.54 ~ 0.86) × (0.54 ~ 0.86) × (0.5 ~ 5)	512 × 512 × (64 ~ 502)	– The earliest publicly available dataset to have liver masks	– Small size (↓) – Does not have liver tumors and vessels
3D-IRCADb (IRCAD, 2010)	≤ 2010	Liver (Tumors, Vessels)	CE-CT	22 (N/A)	(0.56 ~ 0.96) × (0.56 ~ 0.96) × (1 ~ 4)	512 × 512 × (74 ~ 260)	– First dataset to include liver tumors – Records metadata are mentioned	– Small size (↓↓) – The Majority does not have liver vessels
MIDAS-LT (Kitware Inc., 2010b)	2010	Tumors in Liver	CT	4 (N/A)	(1.73 ~ 1.85) × (1.73 ~ 1.85) × (1.73 ~ 1.85)	(177 ~ 189) × (177 ~ 189) × (98 ~ 259)	– N/A	– Very small size (↓↓↓) – Very few segmented tumors
BtCV (Landman et al., 2015)	2015	Liver & Others	CE-CT	50 (30/20)	(0.54 ~ 0.98) × (0.54 ~ 0.98) × (2.5 ~ 5)	512 × 512 × (85 ~ 198)	– Many segmented organs	– Medium size – Does not have liver tumors and vessels
Pancreas-CT (Roth et al., 2016)	2015	Pancreas, Liver & Others	CE-CT	42 (N/A)	(0.66 ~ 0.98) × (0.66 ~ 0.98) × (0.5 ~ 1)	512 × 512 × (186 ~ 466)	– Has both pancreas and liver masks – High resolution	– Medium size (↑) – Does not have liver tumors and vessels
VISCERAL Anatomy3 (Hanbury, 2016)	2016	Liver & Others	CT	30 (20/10)	(0.97 ~ 1.40) × (0.97 ~ 1.40) × 3	–	– Multiple modalities – Large size (↑↑) – Highest number of segmented organs (~20 ground-truth organs)	– Hard to access – Does not have liver tumors and vessels
			CE-CT	30 (20/10)	(0.60 ~ 0.79) × (0.60 ~ 0.79) × 3	–		
			MRI	30 (20/10)	1.25 × 1.25 × 5	–		
			CE-MRI	30 (20/10)	(0.84 ~ 1.30) × (0.84 ~ 1.30) × (3 ~ 8)	–		
LiTS (Christ, 2017)	2017	Liver (Tumors)	CE-CT	201 (131/70)	(0.55 ~ 1.00) × (0.55 ~ 1.00) × (0.45 ~ 6)	512 × 512 × (42 ~ 1026)	– Large size (↑↑) – Many tumors are segmented in 131 records	– Does not have liver vessels
MSDC-T8 (Cardoso et al., 2018)	2018	Liver (Tumors, Vessels)	CE-CT	443 (303/140)	(0.56 ~ 0.97) × (0.56 ~ 0.97) × (0.8 ~ 8)	512 × 512 × (24 ~ 251)	– Largest abdominal dataset (↑↑↑) – Contains all liver masks (liver, tumors, vessels)	– N/A
CT-ORG (Rister et al., 2019)	2019	Liver (Tumors) & Others	CT CE-CT PET-CT	140 (119/21)	(0.55 ~ 1.37) × (0.55 ~ 1.37) × (0.7 ~ 5)	512 × 512 × (74 ~ 987)	– Builds up over LiTS and adds 9 more records – Has other segmented organs	– Does not have liver vessels
CHAOS (Selver et al., 2019)	2019	Liver	CE-CT	40 (20/20)	(0.70 ~ 0.80) × (0.70 ~ 0.80) × (3 ~ 3.2)	512 × 512 × (77 ~ 105)	– Multiple modalities – Large size (↑↑)	– Does not have liver tumors and vessels
		Liver, Kidneys & Spleen	MRI	120 (60/60)	(1.36 ~ 1.89) × (1.36 ~ 1.89) × (5.5 ~ 9)	256 × 256 × (26 ~ 50)		

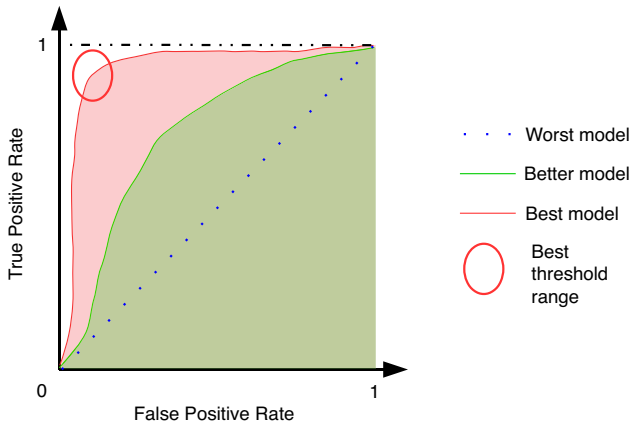

Fig. 1. ROC and AUC for multiple models.

Dice/Case (DPC) calculates DSC per volume and then averages the DSC of all the volumes in the test set. Adjustment to the DSC formula is shown in Eq. (5).

$$DPC = \frac{1}{N}\sum_{i=1}^{N} 2\frac{|A_i \cap B_i|}{|A_i| + |B_i|} = \frac{1}{N}\sum_{i=1}^{N} \frac{2TP_i}{2TP_i + FP_i + FN_i} \tag{5}$$

where N represents the number of volumes in the testing set and i represents the i^{th} volume from those N volumes.

3.1.5. Specificity/true negative rate (TNR)

As depicted in Eq. (6), specificity investigates the model's capability in classifying background voxels correctly.

$$Specificity/TNR = \frac{TN}{TN + FP} \tag{6}$$

Ranging between 0 and 1, the former denotes a misclassification of all background voxels, and the latter resembles a proper classification of all background voxels.

3.1.6. False positive rate (FPR)/fallout

As shown by Eq. (7), and complementary to the specificity definition, it highlights the amount of error the model is making when classifying background voxels.

$$FPR/Fallout = 1 - Specificity = \frac{FP}{FP + TN} \tag{7}$$

Contrary to specificity, a value of 0 is a good indicator of the model's ability in predicting background voxels. On the other hand, a value of 1 is an extreme scenario where the model wrongly classified all background voxels.

3.1.7. Receiver operating characteristic (ROC) and area under ROC curve (AUC)

ROC curve takes advantage of the TPR and FPR metrics to measure the contribution of using a certain threshold, for which, the voxel will be classified as either a TOI or background voxel. It encompasses the resulting TPR and FPR for every threshold between 0 and 1, showing the ideal threshold range to be at the top left corner for a specific model. The AUC metric can compare multiple models with varying thresholds, where the larger the area is, the better the model is for different threshold values. Fig. 1 illustrates the underlying benefits of using ROC curves in comparing trained models.

3.1.8. Volumetric overlap error (VOE)

VOE is the complementary metric of JI, which is known as Jaccard distance, knowing that VOE is a special case for volumetric sets. It measures the spatial error represented between the voxels of A and B (Heimann et al., 2009) and is described by Eq. (8).

$$VOE = 1 - \frac{|A \cap B|}{|A \cup B|} = \frac{FP + FN}{TP + FP + FN} \tag{8}$$

VOE ranges between 0 and 1, where the former means that the voxels of B are perfectly and correctly lying over A's voxels, and the latter indicates the absence of overlapping voxels between the voxels of A and B.

3.1.9. Relative volumetric distance (RVD)

RVD measures the difference between volume A and B, and is an indicator of whether the set of voxels encompassed by B is an under- or over-segmentation by comparing it with A's voxels (Heimann et al., 2009). Eq. (9) highlights this metric.

$$RVD(A, B) = \frac{|B| - |A|}{|A|} \tag{9}$$

This metric can be positive, negative or zero, whereas being positive indicates that B is over-segmenting the original volume, being negative indicates an under-segmentation case, and being zero as having identical volumes. RVD should not be used alone as it does not necessarily indicate an overlap between A and B (Heimann et al., 2009).

3.2. Distance metrics

The distance measurements extensively used in literature are mentioned here, each measurement captures a certain spatial aspect, and all of them are measured in millimeter (mm).

3.2.1. Average symmetric surface distance (ASD)

ASD measures the minimum distance that can be found between a surface voxel in A to another surface voxel in B. Since it is a symmetric metric, the same applies to B with respect to A. Then, the average is taken over all the calculated distances. Surface voxel is a name given to a voxel with at least one non-TOI voxel (i.e., background voxel) from its 18-neighboring voxels, as shown in Fig. 2. To define ASD, we first have to define the minimum distance between an arbitrary voxel v and $S(A)$:

$$d(v, S(A)) = \min_{s_A \in S(A)} \|v - s_A\| \tag{10}$$

where s_A is a single surface voxel distance from the surface voxels set $S(A)$.

Using Eq. (10), we can now define ASD as following:

$$ASD(A, B) = \frac{1}{|S(A)| + |S(B)|}\left(\sum_{s_A \in S(A)} d(s_A, S(B)) + \sum_{s_B \in S(B)} d(s_B, S(A))\right) \tag{11}$$

From Eq. (11) and the definition of Euclidean distance, it can be seen that this metric is always positive. The value converges to 0 when the highest spatial similarity is achieved. However, the larger the value, the worse the overlap between volumes A and B and dissimilarity starts to be observed.

3.2.2. Root-mean-square symmetric surface distance (RMSD)

RMSD is significantly related to the ASD definition described by Eq. (11). The root-mean-square of ASD is the summation of distances squared under the square root as defined by Eq. (12).

$$RMSD(A, B) = \sqrt{\frac{1}{|S(A)| + |S(B)|}\left(\sum_{s_A \in S(A)} d^2(s_A, S(B)) + \sum_{s_B \in S(B)} d^2(s_B, S(A))\right)} \tag{12}$$

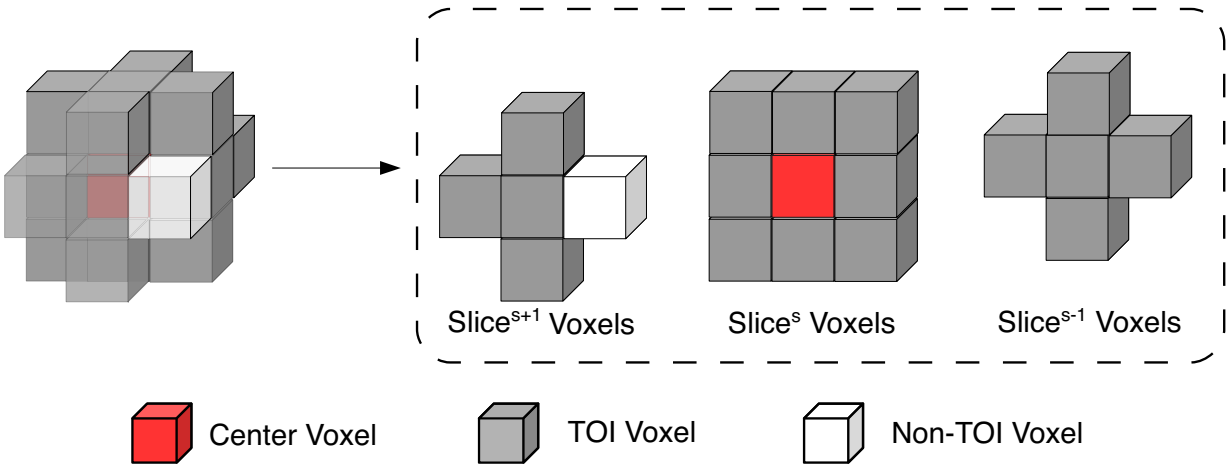

Fig. 2. A surface voxel (red) with 1 non-TOI adjacent voxel (white) and 17 TOI voxels (grey).

The benefit of defining such metric is the weight bestowed over large deviations, making the metric more sensitive to outliers (Heimann et al., 2009). Equivalently, the best value for this metric should be 0, and the bigger it is, the worse the volumes' overlap is.

3.2.3. Maximum symmetric surface distance (MSD)/Hausdorff distance (HD)

MSD, famously known as HD as well, searches for the maximum distance, defined by Eq. (10), that can be found between volumes A and B.

$$MSD(A,B) = \max\left\{\max_{s_A \in S(A)} d(s_A, S(B)), \max_{s_B \in S(B)} d(s_B, S(A))\right\} \tag{13}$$

This metric gives the maximum distance error between A and B, and thus, is extremely sensitive to outliers (Heimann et al., 2009).

3.3. Discussion

Selecting the appropriate metric for a specific medical image segmentation task is of utmost importance. The abovementioned evaluation metrics are essential for a transparent, objective, and fair performance comparison and assessment; however, little concern was given to discussing their limitations. Overall, one main advantage of the percentile metrics over the distance-based ones is their fixed value range [0, 1] (also reported as [0, 100]). This helps easily compare the results reported in different studies, unlike the distance-based metrics with their unfixed value range (-∞, ∞). However, the main problem with percentile-based metrics is that they account only for the number of correctly classified or misclassified pixels without reflecting volumes' spatial distribution. On the other hand, another issue with distance-based metrics is the variety of methods used to define region borders based on the selected neighborhood size (Taha and Hanbury, 2015). Additionally, as reported in Yeghiazaryan and Voiculescu (2015), using only one metric among the abovementioned ones to evaluate automatic liver segmentation techniques is unsuitable to serve as a reliable metric that can reflect all the aspects of segmentation accuracy and errors. However, adopting multiple metrics can avoid their limitations and make them complement each other.

One more thing to highlight, we would find that in earlier studies, researchers typically use the VOE, RVD, ASD, RMSD, and HD metrics to compare their segmentations with the ground truth. On the contrary, more recent studies utilize precision, recall, and DSC scores. This is a result of ML algorithms' influence on more recent studies. It is quite rare to find a study that would try to compete on all the aforementioned metrics such as our study in Al-Kababji et al. (2022). Moreover, most studies also refrain from using the Specificity metric, which is quite useless in the context of liver segmentation, especially when having a large volume where the liver's voxels constitute a very small part of it.

4. Categorization of ML techniques

In this section, surveyed works are categorized based on two main components within the context of liver segmentation: (1) how the volumes are input to the ML algorithms; and (2) the targeted tissue to be classified. Not only different types of inputs and tissues are compared, but also the different ML algorithms that have tackled each tissue classification within the liver, showing a summary between them and allowing the readers to compare each one's methodology and results.

4.1. Based on input shape

When reviewing the literature, slices are inserted into the networks in different shapes and dimensions. CNNs, by their many forms, can accept inputs with different dimensions. The importance of discussing the input dimensions prevails when we know that these dimensions also affect the CNN architecture, where filter sizes, convolutional layers, and pooling layers will be designed differently. This subsection highlights works utilizing different input dimensions: 2D, 3D, 2.5-dimensional (2.5D), 4-dimensional (4D), hybrid, patches, or multi-level scaled-down slices. Fig. 3 visually explains the difference between different input shapes while being fed into an agnostic ML algorithm.

4.1.1. 2D input

Originally, CNNs are developed to work with inputs in their 2D form, i.e., images. Many works opt for the utilization of 2D inputs, where slices from the imaging modalities are inserted into the CNN in a slice-by-slice fashion. Each slice is segmented in a single forward pass isolated from adjacent slices as in Christ et al. (2016) for example, where a 3D conditional random field (CRF) has to be used to impose 3D context. If the slices were fed sequentially (for the same volume) into the CNN model but randomizing the volumes, the model could implicitly understand that there is a 3D context within. However, the emphasis is not strong, and this 3D context quickly dissipates if the training was randomized within volumes as well.

4.1.2. 3D input

3D inputs are used to involve the volumetric context in the segmentation task. It is helpful to use slices in their 3D form, meaning multiple slices are inserted into a single CNN, and the segmentation is carried out in one shot over all of slices in the forward pass. Consequently, the network learns the importance of 3D context around the TOI; thus,

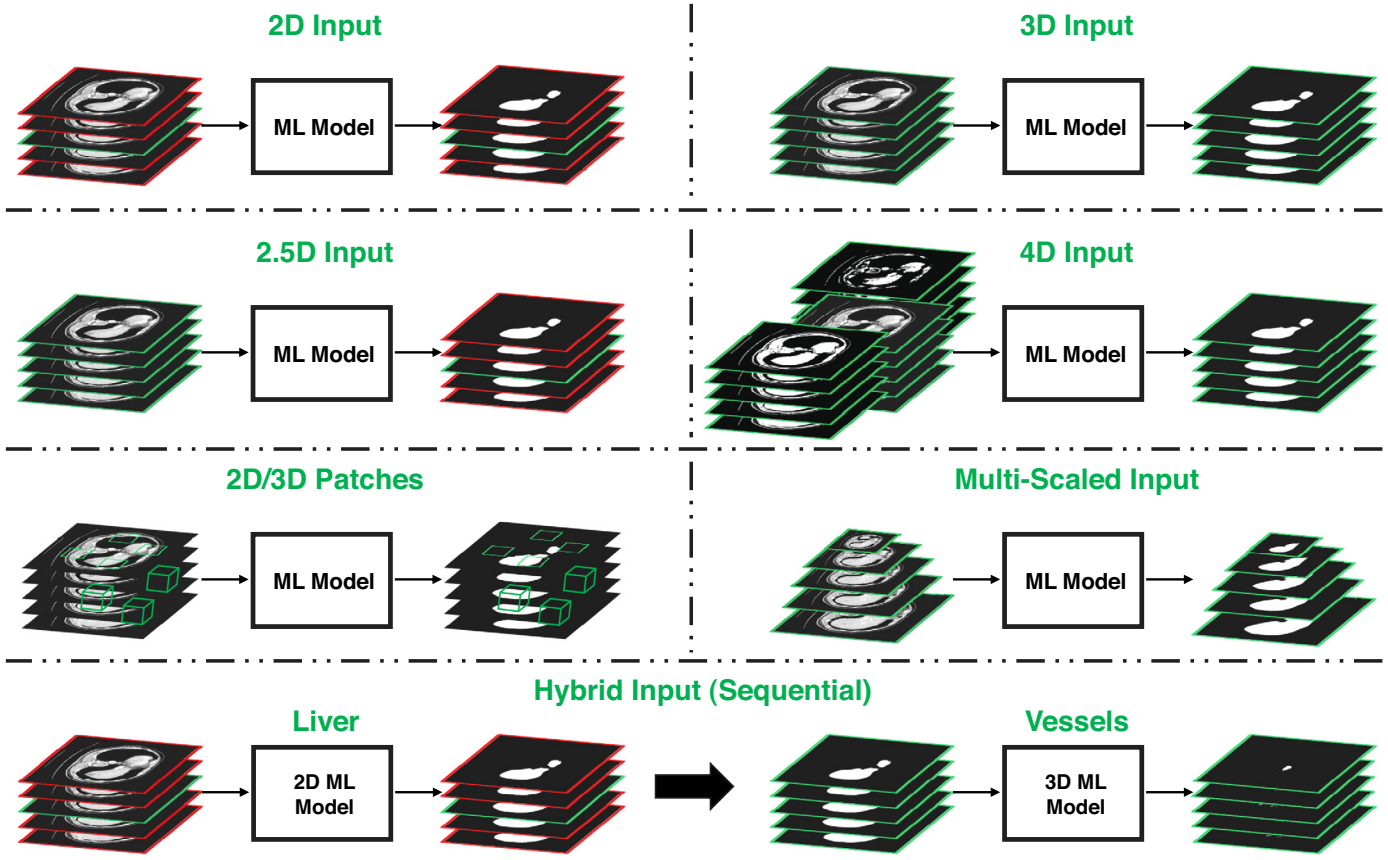

Fig. 3. Different input shapes inserted into an ML model, where green indicates slices being inserted/outputted to/from an ML model, and red means that the slices are not involved in that specific segmentation step for the green slice.
Source: CT images from Cardoso et al. (2018).

inter-slice information is preserved compared to the 2D counterpart. For instance, the famous 2D U-Net (Ronneberger et al., 2015) and its 3D counterpart (Çiçek et al., 2016) demonstrate the changes in the network architecture that follow the transition from receiving a 3D input instead. However, complications are imposed when using the 3D volumes because of the limitations in the graphics processing unit (GPU) memory and the accompanying heavy calculations required by the implementation of 3D CNNs. Thus, researchers would then have to deal with patches of the original volume or a coarsely down-scaled version of it.

To reflect the differences between outside-liver, tumor, and inside-liver tissues, liver and tumor segmentation from 3D abdominal CT volumes are performed in Chi et al. (2021) using a multi-branch U-Net-like model, namely X-Net. Typically, to better extract intra-slice features of liver and tumors, a pyramid-like convolution structure for inner-liver feature extraction and an up-sampling branch for liver region recognition are embedded in the back-bone Dense-UNet. Moreover, conventional 3D U-Net is simplified by adopting fixed-size convolutional kernels (3×3 in the x-y plane) and applying it as a 3D counterpart to aggregate contextual information along the z-axis from the stacked, filtered CT slices. This helps inhibit the influence of neighboring pixels and greatly alleviates the computational burden. In Di et al. (2022), the authors accurately segment liver tumors from CT images by using 3D U-Net to detect liver regions and alleviate the computational cost of the segmentation. Typically, liver regions are first extracted using a 3D U-Net before dividing them into homogeneous superpixels by applying a hierarchical iterative segmentation strategy, which relies on local-information-based simple linear iterative clustering (SLIC). Consequently, this enables classifying every pixel in the liver regions into non-tumor or tumor using the support vector machine (SVM) with its texture features and local intensity. To segment the liver and the tumors, the authors in Alalwan et al. (2021) develop a 3D semantic segmentation deep learning (DL) model, namely 3D DenseU-Net-569. The latter is a fully 3D semantic segmentation model, which encompasses lower training parameters and a considerably deeper network. It also relies on depthwise separable convolution instead of conventional convolution. Fig. 4 presents the flowchart of the 3D U-Net-based liver segmentation scheme proposed in Di et al. (2022).

4.1.3. 2.5D input

2.5D is the middle ground between the 2D and 3D inputs, where it utilizes the 3D context and information while restraining the segmentation to a single slice in a single forward pass. The input is a slice in the middle of its neighboring slices, creating an odd number of slices $2(k-1)$ inserted into the CNN model. In essence, the CNN is built to receive inputs of 2D nature with multiple channels; however, the key difference lies in its output, where the segmentation mask is generated for the center slice only, and the neighboring slices serve only as context and 3D spatial information providers for the model. The idea in itself is not new, it is clearly stated in Roth et al. (2014), but many works opt for this method as it harnesses the benefits of both inputs' dimensions and disposes of their disadvantages (Han, 2017; Li et al., 2018; Chlebus et al., 2018; Vorontsov et al., 2018; Wang et al., 2019a; Zheng et al., 2019; He et al., 2020), and others.

Because 2D DL-based segmentation models are less accurate while 3D ones are accurate but memory and computationally expensive, Tian et al. (2021) automatically annotate functional regions of the liver using a 2.5D class-aware deep neural network (DNN) with spatial adaptation. This framework is based on analyzing abdominal images using a ResU-Net model, which (i) adequately selects a pile of adjacent

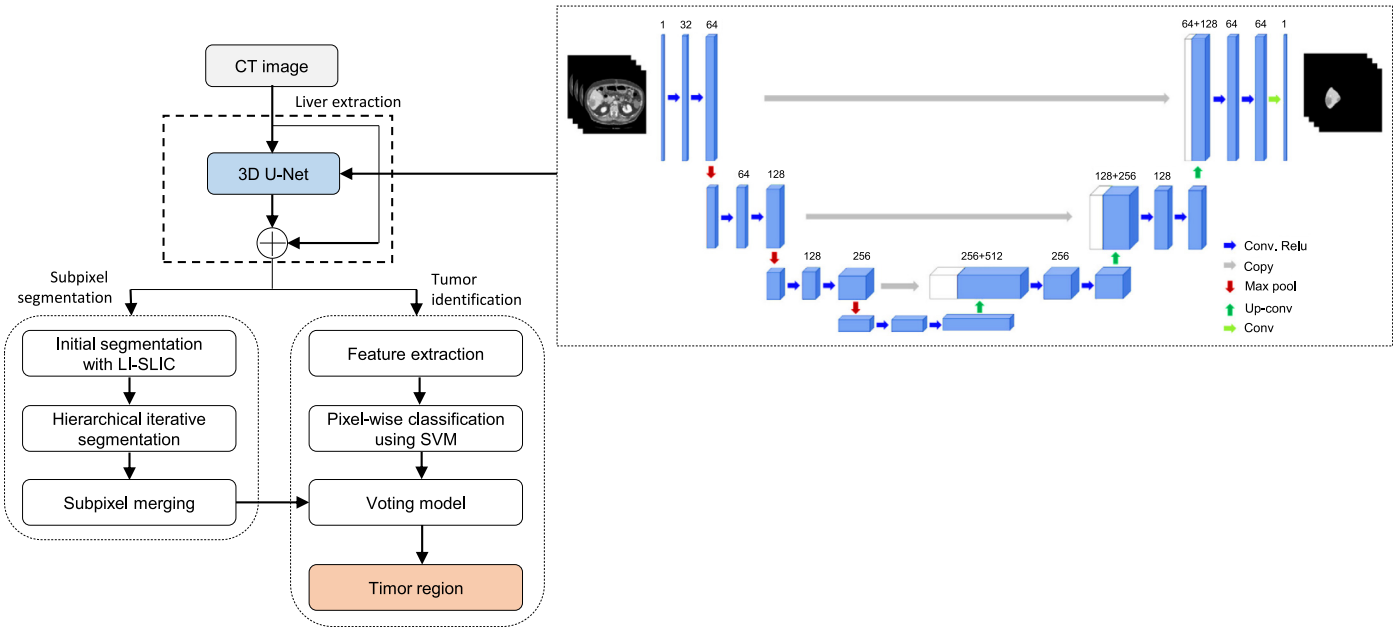

Fig. 4. Flowchart of the 3D U-Net based liver segmentation scheme proposed in Di et al. (2022).

CT slices as input; (ii) generates the center slice; and (iii) automatically annotates the liver functional regions. Besides, in Zhang et al. (2021a), 2.5D UV-Net with multi-scale convolution is utilized to segment the liver tumors. This enables the mining of structured data, reducing data redundancy, strengthening independent characteristics, making features sparse, and enhancing network efficiency and capacity. In Lv et al. (2022), automatic liver and tumor segmentation are conducted using a lightweight "Inception" convolution architecture with residual connections, which significantly reduces the model's parameters. Accordingly, a 2.5D lightweight U-Net equipped with residual and InceptionV3 modules (RIU-Net) model is adopted, which deploys DSC and binary cross-entropy (BCE) loss to reach fast convergence and low fluctuations in training. Similarly, in Han et al. (2021a), a cascaded 2.5D fully convolutional network (FCN) model is considered for liver and tumor segmentation from 3D medical images. Additionally, the FCN model is augmented with a boundary loss incorporating boundary information, area, and distance to learn more contour features and boundaries from the 3D images. In Wardhana et al. (2021), a modified 2.5D SegNet model is used for liver and tumor segmentation by: (i) utilizing the long-range connection from U-Net; and (ii) implementing the short/skip connection that is generally found in ResNet.

4.1.4. 4D input

As controversial as it sounds, the 4D concept comes from the MRI modality since it generates multi-phase 3D volumes of the same shape with a difference in temporal acquisition. They can be grouped when used for segmentation. In Ivashchenko et al. (2020), the multi-phase volumes are used in 4D K-means clustering aided by active contour refinement. On the other hand, in Takenaga et al. (2019), the 3D volumes are inserted into a 3D ResNet-based CNN, where the input is multi-channel (effectively making it 4D). However, this does not reflect architecture change as it can be resolved by channel depth design at the first layer.

In Zheng et al. (2022), a 4D DL network built upon 3D convolution and convolutional long short-term memory (LSTM), namely Conv-LSTM, for HCC lesion segmentation. This DL module uses 4D data corresponding to dynamic CE-MRI images to assist liver tumor segmentation. Accordingly, 3D spatial domain features from every dynamic phase are extracted using a shallow 3D U-Net model before applying a 4-layer Conv-LSTM for time domain information exploitation.

Fig. 5 presents the overall architecture of the 4D framework for HCC segmentation. This includes a 3D CNN module (in pink), and a Conv-LSTM network module (in green). Additionally, a shallow 3D U-Net is utilized to extract spatial domain information in the pre-contrast, arterial, portal venous, and delayed phases, separately. Moreover, a 4-layer Conv-LSTM network has been developed to exploit time domain information via the multiple dynamic phases (m refers to the number of layers of the Conv-LSTM network, and in this case, $m = 4$).

4.1.5. 2D & 3D patches

Taking patches means that the programmer extracts small portions of the slice/volume and then inputs them to the FCN to perform the segmentation. Theoretical background for why it works is provided in Chen et al. (2015), and some of the reasons are mentioned here. Especially for the 3D case, GPU and extensive computations are the barriers to evaluating volumes in one shot. Thus, researchers opt to take 3D chunks from the volumetric scan to process, which can have homogeneous dimensions as in Wang et al. (2019b), Zhang et al. (2018a), Cheema et al. (2019), or can have heterogeneous dimensions (Roth et al., 2018a). It is worth noting that in Roth et al. (2018a), the effect of overlapping patches is studied against non-overlapping ones. In general, for both 2D and 3D, it helps the model generalize better to unseen real-life scenarios when the segmentation is done over patches instead of the whole slice/volume. Moreover, as in Li et al. (2015), 2D patches are very convenient when the TOI is small, e.g., tumors and vessels within the liver, as processing the whole liver would be redundant when segmenting such tissues.

4.1.6. Multi-scaled input

In more recent works, researchers opt to fuse segmentations on different scales. Such algorithms take multi-scaled inputs, concatenate, and fuse them on many levels of the network to generate the segmentation mask either in a sequential manner as in Christ et al. (2016) or in one shot as in Fang et al. (2020).

4.1.7. Hybrid input (sequential)

Hybrid input emphasizes the employment of sequential models with different inputs' dimensions, whereas the model can utilize an input with distinct dimensions compared to the previous/following one. To increase segmentation accuracy, Jin et al. (2020) utilized a 2D network

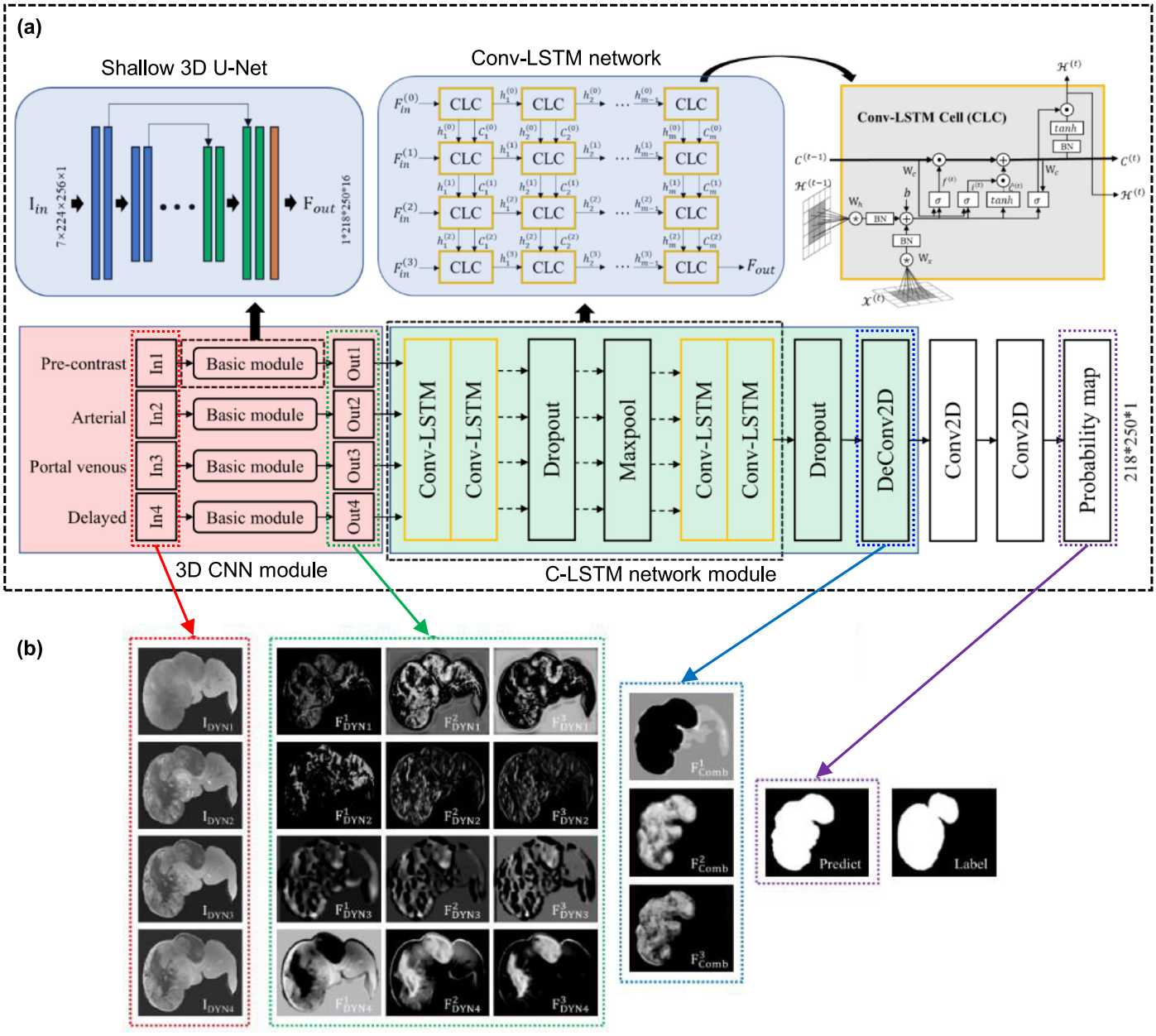

Fig. 5. Overall 4D DL framework for HCC segmentation proposed in Zheng et al. (2022): (a) the architecture of the 4D model, and (b) the feature map analysis for the case of large tumors with internal inhomogeneity.

to acquire a coarse liver segmentation, which is sequentially inserted into a 3D network for segmentation refinement. Another approach is jointly using 2D and 3D networks for liver and tumor segmentation and fusing both networks' outputs (Li et al., 2018). Other methodology uses the first 2D CNN to segment the liver and large tumors and the sequential 3D CNN to focus on segmenting small ones (Dey and Hong, 2020). It is worth noting that the training methodology followed in Liu et al. (2018) initially relied on developing the weights in a 2D network, which is then extrapolated into their 3D counterpart.

4.2. Based on classified tissues

Since it is desired to obtain accurate, automatic, and real-time results for the liver delineation problem, it is intuitive that ML algorithms are utilized. However, providing a measure for selecting a particular ML algorithm for a specific segmentation scenario would certainly help, especially with the technological advancements currently witnessed. Thus, in this subsection, the determination of the ML algorithms, unsupervised and/or supervised, is shown based on the application area, i.e., liver parenchyma, tumors, and/or vessels within the liver.

4.2.1. Liver

The main tissue/organ that is considered in this survey is the liver. Naturally, it is the first tissue we need to survey since it encapsulates all the tissues residing within. Fig. 6 describes the basis of different algorithms used for the liver segmentation challenge.

Miscellaneous Unsupervised

Unsupervised ML algorithms have a fair share in the liver segmentation task. The reason for their efficacy is that the liver is a single large continuous organ with relatively similar pixels' intensities in the same CT/MRI volume. The most prominent unsupervised algorithms are the K-means clustering and fuzzy c-means (FCM) clustering, where

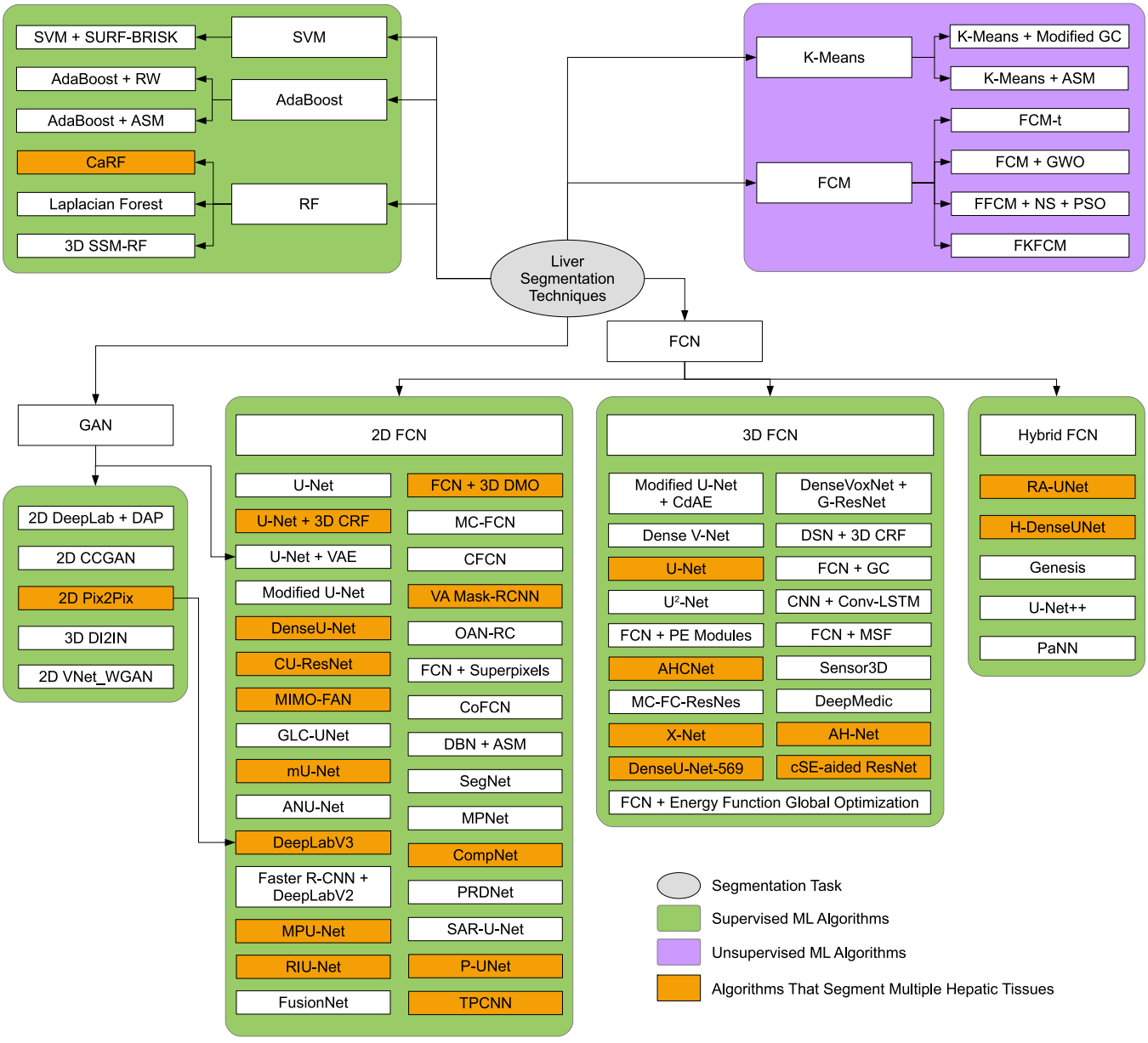

Fig. 6. Liver segmentation techniques from the reviewed literature.

the former only allows the belonging of a certain pixel to a specific centroid (hard), while the latter allows for the pixel to belong to multiple centroids, with a certain value (soft). In Huang et al. (2018a), K-means clustering is used for liver localization in CT slices as a basis for thresholding, followed by modified GC segmentation. However, in Ivashchenko et al. (2020), a 4D K-means is utilized on multi-phase MRI volumes for liver segmentation aided by an ASM technique. It is worth noting that vessel extraction is implemented through multi-scale vesselness filters.

On the other hand, FCM clustering in Alahmer and Ahmed (2016) calculates the degree of belonging for each pixel to three cluster classes, where one of these centroids represents liver pixels. In Ali et al. (2014) the study focuses on choosing an optimum threshold, FCM-t, which best determines the degree of belonging a pixel should convey to be considered a liver pixel. Other researchers use FCM, or an enhanced version of it, for the liver delineation task. For instance, FCM is used with the grey wolf optimization (GWO) algorithm in Sayed et al. (2016), while a fast FCM (FFCM) is utilized with neutrosophic sets (NS) and particle swarm optimization (PSO) in Anter and Hassenian (2018). Lastly, in Cai (2019), a fast kernelized FCM (FKFCM) is used to segment the liver.

Miscellaneous Supervised

Laplacian forest (LF), an improved version of random forest (RF), is used in Lombaert et al. (2014) for the liver segmentation task among other organs. Other works use RF as a landmark detection tool for 3D SSM (Norajitra and Maier-hein, 2017), while cascaded random forest (CaRF) classifiers are used for liver parenchyma segmentation in Treilhard et al. (2017).

In an ensemble of weak classifiers fashion, adaptive boosting (AdaBoost) is used to segment the liver with the aid of the random walks (RW) algorithm in Zhang et al. (2015). A similar work uses the same combination with extra improvements on the RW algorithm in Zheng et al. (2017b), and finally, a three-level ASM is guided by the AdaBoost algorithm in He et al. (2016).

In Liang et al. (2018), speeded up, robust features (SURF) (blob-type), and binary, robust, invariant, scalable key points (BRISK) (corner-type) features are used in a top–bottom flow, aided by the SVM in the bottom-up counterpart pathway to segment the liver.

GAN

A generative adversarial network (GAN) is also employed for this important task, where in Yang et al. (2017), a 3D deep image-to-image network (DI2IN) is used to segment the liver. On the other hand, in Chen et al. (2019a), cascaded conditional GANs (CCGAN) are used for the same task but in 2D form. In Zheng et al. (2019), a GAN network incorporating a deep atlas prior (DAP), where the generator, based on DeepLab (ResNet101), is used for the liver segmentation, and the discriminator is a simple 2D FCN used to challenge the generator segmentation.

2D FCN

FCNs have become the natural choice from various ML and AI algorithms when the data come in more complex forms than the 1-dimensional (1D) form. FCNs are a sector of CNN algorithms, where fully connected layers at the end of the network are replaced by convolutional ones, reducing the number of parameters. Goodfellow et al. mention in Goodfellow et al. (2016): "The hierarchy of concepts allows the computer to learn complicated concepts by building them out of simpler ones. If we draw a graph showing how these concepts are built on top of each other, the graph is deep, with many layers. For this reason, we call this approach AI deep learning." This statement means that a CNN is considered deep if layers build complex structures over simpler structures outputted from the previous ones. Moreover, it is more appropriate for the segmentation task as the output's form of such networks is similar to the input. Nonetheless, FCNs are used for various problems and purposes. For instance, in Tian et al. (2018), a 2D FCN is utilized for liver segmentation, which is then used for diagnosis report generation. In Wang et al. (2018), a 2D FCN-8s training is done via a newly-devised sample selection idea named relaxed upper confident bound (RUCB). In Yuan (2017), cascaded 2D FCN (CFCN) is used for liver segmentation, where the first FCN coarsely segments the liver and the second one refines it. In Zheng et al. (2017a), another 2D FCN is used for the liver segmentation, followed by a 3D deformable model optimization (DMO) based on local cumulative spectral histograms and non-negative matrix factorization (NMF). In Jansen et al. (2019), a 2D multi-channel FCN (MC-FCN) takes six slices as input from multi-phase MRI imagery, where the used structure outperforms the U-Net on the utilized dataset. In Qin et al. (2018), superpixels are computed, forming a map using SLIC algorithm, and then the map is introduced into a 2D FCN to segment the liver. In Aghamohammadi et al. (2021), a two-path CNN (TPCNN) is used to segment the liver using patches of varying sizes, with a novel encoding approach to extract features from CT images. The input is the image itself, the Z-score normalized one, and the encoded image using the local direction of gradient (LDOG) algorithm.

An important FCN architecture that revolutionized the biomedical segmentation field is the U-Net (Ronneberger et al., 2015), playing a similar role to the AlexNet, but for the biomedical field. Thus, it was natural for some researchers to use it. In Christ et al. (2016, 2017), a 2D FCN following the U-Net architecture is utilized along with a 3D CRF for liver segmentation. In Ouhmich et al. (2019), a 2D U-Net is used as the main model, while SegNet is utilized in Nanda et al. (2019). In Zhang et al. (2020a), the U-Net acts as a coarse liver segmenter; however, in Mendizabal et al. (2020), U-Net is used as a replacement for the finite element method to approximate the elastic deformation caused in hyperelastic objects, such as the liver. Interestingly in Wang et al. (2020), the 2D U-Net is used to segment the liver, but the work does not focus on the model's accuracy because the target is to examine whether a slice can be used to make a diagnostic decision or not. In Li et al. (2021a), U-Net is used as the main model, but components such as a Bi-ConvLSTM are integrated to enhance the liver's edge capturing.

Other researchers are inspired by the U-Net structure. A 2D FCN (modified U-Net version) is employed for segmenting the liver parenchyma, excluding vessel ducts, from T1-MRI scans (Irving et al., 2017). In Liu et al. (2020), 16 phases (echoes) of the same slice are generated by employing the multi-echo gradient from the MRI imaging modality, and the kernels at the first layer of the 2D U-Net are modified to accept 16 slices as an input. In a similar approach, unenhanced multi-echo spoiled gradient-echo slices from MRI scans are initially used to train a 2D U-Net, followed by a transfer learning (TL) training step on CE-CT and CE-MRI to segment liver from both modalities (Wang et al., 2019c). Additionally, in Vorontsov et al. (2018), an ensemble of three U-Net-like 2D FCN models is used for the liver segmentation task, and the final mask is the average of those three. Maaref et al. (2020) utilized the same segmentation network as in Vorontsov et al. (2018), but with more interest in tumor classification. In Seo et al. (2020), the skip connections between the encoder and decoder are modified to eliminate the redundant inclusion of low-resolution information, and the network is named modified U-Net (mU-Net). In Guo and Yang (2020), the semantic segmentation of multiple organs is carried via a 2D ResNet equipped with partially dilated convolutions and multiple concatenations and fusion stages.

On the one hand, a multi-planar network (MPNet) is employed to segment the liver in any view (transversal, sagittal, or coronal) (Wang et al., 2019d; Chen et al., 2019b). In their work, MPNet, which is an ensemble of three networks, is trained to segment the liver from each view, and in the end, the segmentation masks from the three networks are fused to generate the final output. A similar approach has been utilized in the organ-attention networks with reverse connections (OAN-RCs) developed by Wang et al. (2019b), where reverse connections are constructed to pass semantic information to the lower layers for coarse organ segmentation, followed by a fine-tuning stage. Finally, the output of the 3 OAN-RCs is combined through statistical similarity fusion. On the other hand, in Perslev et al. (2019), a multi-planar U-Net (MPU-Net) is utilized to capture the organ of interest from different viewing angles (generalizing to more views than the three conventional ones) and, similarly, fusing the output of all planar segmentation to generate the final output. In Yang et al. (2019), a domain adaptation (DA) pipeline is created because the authors aim to create an algorithm that achieves great results on both CT and MRI scans. The first module is concerned with finding a common space between CT and MRI via variational autoencoder (VAE) and GAN. The second module takes the common space output from the first module and inserts it into a 2D U-Net to segment the liver, outperforming a CycleGAN-based solution. In Cheema et al. (2019), a 2D liver extraction residual convolutional network (LER-CN), similar to U-Net architecture, is utilized to segment the liver from low-dose CT scans using two main components: noise removal component (NRC) and structural preservation component (SPC). More modifications have been applied to the U-Net structure. For instance, in Zhang et al. (2018b), a 2D FCN based on U-Net is equipped with ResNet dense forward connections (U-ResNet) for liver segmentation in digitally reconstructed radiographs (DRR) from X-rays via a task-driven generative adversarial network (TD-GAN). In Xi et al. (2020), cascaded U-ResNet (CU-ResNet) is used for liver segmentation, concatenating the middle outputs from the liver U-ResNet with the corresponding output layers in the lesions' network. The work also aims to compare different loss functions, creating an ensemble of models incorporating the different loss functions (Xi et al., 2020). In Han (2017), densely-connected U-Net (DenseU-Net) is used for the liver segmentation task, and in Ahn et al. (2019), a comparison between FusionNet and atlas-based segmentation models is conducted, proving the efficacy of the former to be used in a future clinical environment. A similar architecture is utilized in He et al. (2020), where the 2D FCN is based on DenseU-Net, but interestingly, utilized a shallower decoder scheme and did not witness any reduction in the segmentation performance for the liver and other organs. In Tian et al. (2019), both global and local context U-Net (GLC-UNet) are used to incorporate the global and local context, which also attempts to create Couinaud segmentation of the liver. In another study, a multiple-input and multiple-output feature abstraction network (MIMO-FAN) model adapted the U-Net architecture to generate multi-scale outputs for multi-scale inputs and fusing them to achieve the final output for

liver in Fang et al. (2020), and on partially labeled datasets for multiple organs in Fang and Yan (2020).

Sometimes a different backbone architecture is preferred by some of the researchers. For instance, a 2D FCN based on volume attention (VA) Mask-RCNN (VA Mask-RCNN) to incorporate volume information is employed for liver segmentation (Wang et al., 2019e). In Xia et al. (2019), a 2D FCN based on DeepLabV3 is used for liver segmentation, followed by Pix2Pix GAN in a two-player game competition to enhance the segmentation mask. In Tang et al. (2020a), Faster R-CNN is used for liver localization, while a DeepLabV2 network is used for the segmentation. In Dey and Hong (2020), a complementary network (CompNet) is employed for the segmentation task by attempting to incorporate non-TOI pixels into the learning of TOI ones (Dey and Hong, 2018). A pairwise segmentation technique for sharing supervised segmentation between two paths is investigated by the conjugate FCN (CoFCN) (Wang et al., 2019a), where it takes 2.5D input and learns from adjacent slices explicitly what the segmentation mask should be. In Ahmad et al. (2019), 2D deep belief network (DBN) is deployed to segment the liver, aided by ASM for post-processing refinement.

To overcome the lack of interlayer information in 2D CNN models that can cause profound loss of segmentation performance, the authors in Ma et al. (2021) develop a 2.5-D VNet_WGAN. Moving on, to avoid the sensitivity of liver segmentation models to heterogeneous pathologies and fuzzy boundaries, mainly when the data is scarce, a 3D CNN and a hybrid loss function are deployed in Tan et al. (2021). Typically, compressed codes of liver shapes are obtained using an autoencoder before training a liver segmentation network with a hybrid loss function. In Meng et al. (2021), liver and tumor segmentation is performed using a DenseU-Net. It is applied in two stages by considering both 2D and 3D features as input for DenseU-Net, and then adding an attention mechanism to DenseU-Net for better learning small tumor multi-scale features in the liver.

In Wang et al. (2021), automatic liver segmentation from CT images is performed using a squeeze-and-excitation block and atrous spatial pyramid pooling (ASPP)-based residual U-Net (SAR-U-Net). The attention strategy has been introduced to derive image features adaptively. Moreover, to extract richer multi-scale characteristics, the transition layer and the final output layer of the U-Net decoder are replaced with ASPP. Lastly, a residual block is used instead of the standard convolutional layer of U-Net before attaching a batch normalization layer to speed up the convergence. Aiming at reducing model sizes and increasing segmentation performance, Han et al. (2021b) fuse the output of three 2.5D Res-UNet models to develop perpendicular U-Net (P-UNet) for liver and hepatic tumor segmentation. Post-processing, loss functions, and data augmentation are considered to enhance the overall performance. This results in an accuracy of 96.2% along with a DSC of 73.5%. The flowchart of the developed P-UNet model is portrayed in Fig. 7, where the size has been reduced and augmented with larger receptive fields.

In Araújo et al. (2022), the authors proposed a liver segmentation scheme using CT images and a U-Net, which is employed in a cascaded manner. It adopts a powerful segmentation approach to segment the liver even in the presence of lesions. Typically, this framework has the advantages of (i) reducing CT examination to a region that contains the liver and initial liver segmentation; (ii) using a U-Net-based reconstruction stage for recovering liver regions affected by lesions not included in the initial segmentation; and (iii) reducing the FPR and filling holes to enhance segmentation based on post-processing. In Ahmad et al. (2022), a lightweight CNN model that reduces the computation cost of extracting the liver regions from CT scan images is proposed. The CNN model includes three convolutional and two fully connected layers. To discriminate the liver from the background, softmax has been utilized. Moreover, weight initialization has been made using random Gaussian distribution to achieve distance-preserving-embedding of the information.

3D FCN

To further involve the volumetric information, some researchers opt for the 3D FCN, bearing in mind that the use of 3D FCN is faced with expensive memory and computational necessities.

One of the early works of using 3D FCNs is Lu et al. (2016), whereas a 3D FCN is utilized to segment the liver and is aided by a GC algorithm. In Hu et al. (2016, 2017), the authors base their implementation on the 3D FCN employed in Lu et al. (2016), increasing the kernels' size and modifying some of the activation functions. Then, the 3D FCN output is incorporated in an energy function optimized globally. In Dou et al. (2016, 2017), a 3D FCN is equipped with a deep supervision mechanism creating a 3D deeply supervised network (DSN) aided by 3D CRF to refine the segmentation output. In Tang et al. (2020b), the DeepMedic network, which relies on 3D CNN and 3D CRF (Kamnitsas et al., 2017), is used to segment the liver for selective internal radiation therapy (SIRT). In Gibson et al. (2017), a 3D FCN with dilated convolutional layers is developed for multi-organ segmentation including the liver. Following their work in Gibson et al. (2017), another 3D FCN based on Dense V-Net is subsequently developed for multi-organs segmentation including the liver (Gibson et al., 2018a). The work is extended to create a framework called NiftyNet on Python (Gibson et al., 2018b), which is intended to make it easier to deploy biomedical segmentation algorithms. Another work utilizing Dense V-Net is Chung et al. (2020), where a deeply self-supervised scheme based on adaptive contour features is utilized for the liver segmentation task alone. In Liu et al. (2018), a 3D anisotropic hybrid network (AH-Net) transforms 2D weights trained on a 2D encoder into their 3D counterpart, which is then used for the liver segmentation task. In a model called Sensor3D, a 3D bi-directional cascaded Conv-LSTM in a U-Net architecture theme is used for the segmentation task in Novikov et al. (2019).

To further incorporate the global context information, Rickmann et al. (2019) developed project and excite (PE) modules and employed them within a 3D FCN. A similar approach is utilized in Qayyum et al. (2020), where spatial squeeze and channel excitation (cSE) 3D modules are aiding a 3D FCN, based on ResNet architecture, in the liver segmentation task. Moreover, in Jiang et al. (2019), a 3D FCN composed of multiple attention hybrid connection blocks, hence the name AHCNet, has densely-connected long and short skip connections and soft self-attention modules where two cascaded AHCNets are used for liver localization and segmentation, respectively. In Takenaga et al. (2019), to take advantage of the multi-phase volumes obtained by MRI, a multi-channel 3D FCN based on ResNet (MC-FC-ResNet), or 4D FC-ResNet, is used to segment the liver, utilizing the information each phase provides.

Needless to say, the U-Net architecture also befits in the 3D context (Çiçek et al., 2016). In Bai et al. (2019), a 3D U-Net segments the liver organ, while in Kakeya et al. (2018), a 3D U-JAPA-Net model has a generalized 3D U-Net and a specialized one for each organ. To segment organs from different modalities, a 3D universal U-Net (U^2-Net) is built where domain-specific convolution layers are used for each modality, and a single pipeline of convolutional layers is shared across different ones (Huang et al., 2019). In Zhang et al. (2018a), 3D patches are inserted into a 3D U-Net-like network with context-aware units for multi-phase MRI volumes in a multi-scale fashion. In Mohagheghi and Foruzan (2020), 3D patches were also used; however, some modifications were applied to the 3D U-Net architecture on the pooling layers, activation functions, and channels' depth. Moreover, the work takes advantage of convolutional denoising autoencoders (CdAE) to create shape-prior knowledge and embeds it into a deep data-driven loss (DDL) to enhance the segmentation result. Finally, a 3D U-Net with a multi-scale pyramid-like liver segmentation scheme is employed in Roth et al. (2018b), where it is extended in Roth et al. (2018a) to segment 20 organs in total via TL from the 8 originally segmented abdomenal organs.

It is worth mentioning that some studies use FCNs as a complementary part to the core algorithm. In the case of Zeng et al. (2019), a mean

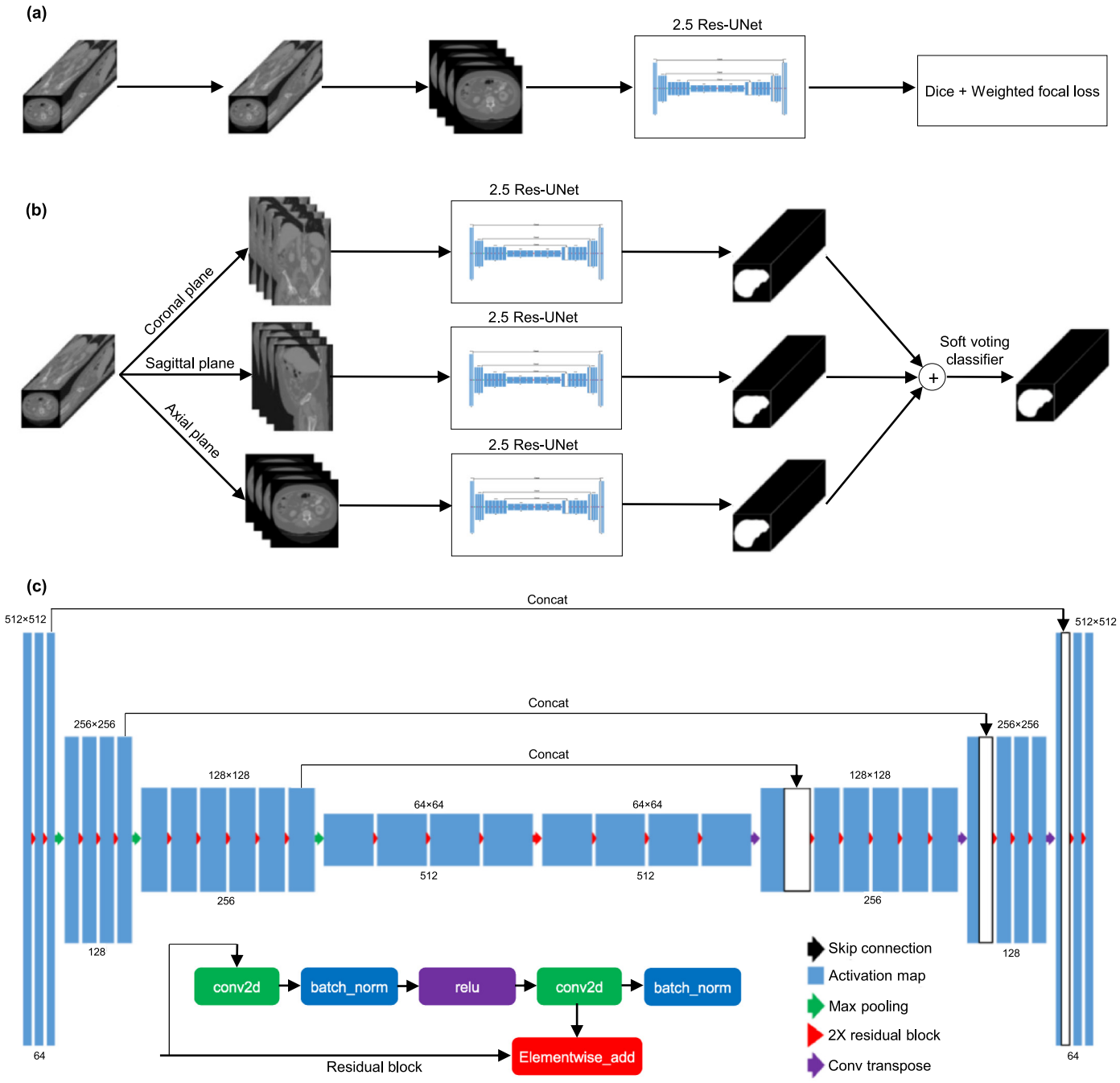

Fig. 7. Flowchart of the P-UNet module proposed in Han et al. (2021b) for liver segmentation: (a) training pipeline, (b) inference pipeline, and (c) network architecture for the Res-UNet model.

shape fitting (MSF) algorithm, which creates an average shape of the liver, is complemented by a 3D FCN that generates a dense deformation field via the calculation of a 3D vector of displacements for each voxel to deform the created prior as necessary. Another work analyzes the inserted CT scans via 3D FCN based on DenseVoxNet, and deforms an initial sphere mesh through the use of 3D graph convolutions-based ResNet (G-ResNet), creating an elegant and smooth 3D mesh representation of the liver (Yao et al., 2019).

Hybrid

In Jin et al. (2020), a 2D residual attention-aware U-Net (RA-UNet) coarsely segments the liver, which is then fed to a 3D RA-UNet counterpart to finely segment it. In Li et al. (2018), both 2D and 3D DenseU-Net models, constituting a hybrid DenseU-Net (H-DenseUNet), are used for liver segmentation. In Zhou et al. (2020), a redesigned U-Net model, called U-Net++, creates an ensemble mechanism from within the architecture itself, allowing the customizability of having DenseU-Nets at various levels. It is also supported by the deep supervision technique, thus, generating outputs at all levels, which then serve as ensemble models. Quickly after that, in Xu et al. (2020), the U-Net++ model is slightly modified and used for both liver segmentation and registration between pre-operative MRI and intra-operative CT. In Li et al. (2020), the attention mechanism and nested U-Net (ANU-Net) builds over the 2D version of the U-Net++, where modifications are applied to the loss function and the dense connections between the nested convolutional blocks.

In Zhou et al. (2019a), a prior-aware neural network (PaNN) single-handedly segments the liver, among other organs, trained over partially labeled datasets, similar to the training scheme deployed in Fang and Yan (2020). The network's 2D and 3D versions are tested and compared with other available networks.

In Zhou et al. (2019b), Models Genesis is a framework that can create a basis for TL to any other organ segmentation via self-supervised training on unlabeled data instead of relying on ImageNet trained weights. The motivation is that the ImageNet dataset is different than the biomedical ones, creating an inappropriate TL process. In their work, both the 2D and 3D models are initially trained on unlabeled data and then transferred for application-specific biomedical segmentation tasks.

From Fig. 6, it is obvious that the ML supervised algorithms of favor are the ones utilizing FCN as the main model, where they have become robust to tackle many problems (localization, registration, classification, or segmentation) in many fields. Moreover, within the FCN models, the majority of works have utilized 2D network models with inclusion techniques for volume information such as 2.5D inputs. The 2D models are usually preferred over 3D ones due to the aforementioned issues of expensive computations and memory shortage. Table 2 historically highlights the most prominent studies that have tackled open-access datasets for the liver segmentation issue, highlighting the DSC score that each study achieved, and if not available, then VOE is reported. The comparison has been conducted in terms of the deployed ML model, method description, dataset, best performance, and advantage/limitation.

4.2.2. Tumors/lesions

The second tissue of importance within the liver is the tumors, where many datasets have focused on the idea of detecting and segmenting the existing tumors within the liver. Fig. 8 have been created, detailing different ML algorithms, supervised and unsupervised, tackling the issue of tumors tissue segmentation. it is worth noting that there are notable intersections that are highlighted (using a light brown color) among the three classified tissues within the liver between Figs. 6 and 8.

To segment tumors, Das and Sabut (2016) initially uses a Kernelized FCM (KFCM), then utilizes spatial-FCM in Das et al. (2019) for the tumor segmentation task, followed by a 4.5C decision tree (DT) algorithm to classify segmented tumors. In Anter and Hassenian (2018), the combination of PSO and FFCM is used for tumor segmentation, while FFCM is utilized for the tumor segmentation task in Sayed et al. (2016) and Anter and Hassenian (2019) along with NS and adaptive watershed algorithm.

2D CNN with fully connected layers is used in Li et al. (2015) to segment tumors on patches, testing different patch sizes for optimal performance. By patching the slices, it allows the model to focus on the tumor itself instead of processing many unrelated pixels simultaneously as they are normally sparse. Also, a comparison is drawn against other ML algorithms such as AdaBoost, RF, and SVM, proving the superiority of CNN-based techniques. In Sun et al. (2017), a single 2D FCN on single-phase CT and 2D MC-FCN utilizing three phases of CE-CT scans are utilized for segmenting tumors within the liver, where the networks are initially trained on the liver segmentation task to allow for faster convergence when trained for tumor segmentation. In Chlebus et al. (2018), a DenseU-Net is utilized for the tumor segmentation task, where post-processing for object identification is based on RF to reduce FPs. In Vivanti et al. (2017), a Markov random field (MRF) registration technique is used to delineate the tumors in a follow-up CT scan from a baseline one. Then, a 2D CNN is used to segment new tumors, an RF is also used for tumor classification. Following their work, in Vivanti et al. (2018), a global 2D CNN and patient-specific 3D CNN are used to segment the tumors on the follow-up CT scans, where if the global CNN achieved low results, the patient-specific CNN is opted for.

An interesting approach is investigated on imprecise labeling of tumors, named "response evaluation criteria in solid tumors (RECIST)". Due to the abundance nature of this kind of data, Cai et al. (2018) use such CT slices for the tumor segmentation via a holistic nested network (HNN), which is originally built for edge detection throughout multiple levels within the network (Xie and Tu, 2015). Thus, utilizing weakly-labeled data instead of relying on pixel-wise labeling. In a similar approach in Cano-Espinosa et al. (2020), a 2D FCN is used to regress biomarker information (area or volume) on CT slices to regress and localize tumors instead of using manually labeled-pixels datasets, which are harder to obtain.

Some of the aforementioned liver segmentation work also use the same model for tumor segmentation. For example, the 2D FCN aided by the 3D DMO and NMF in Zheng et al. (2017a), the 2D FCN in Tian et al. (2018), the 2D FCN based on VA Mask-RCNN in Wang et al. (2019e), the TPCNN in Aghamohammadi et al. (2021), the DeepLabV3 followed by Pix2Pix GAN in Xia et al. (2019), the ensemble of the three U-Net-like 2D FCN in Vorontsov et al. (2018), Maaref et al. (2020), the mU-Net in Seo et al. (2020), the CU-ResNet (Xi et al., 2020), the 3D AH-Net in Liu et al. (2018), the 3D U-Net with context-aware modules in Zhang et al. (2018a), and the H-DenseUNet in Li et al. (2018), all segment the tumors along with the liver simultaneously. In Dey and Hong (2020), the first 2D CompNet, aforementioned in the liver segmentation techniques, helps in segmenting large tumors, followed by a 3D CompNet to segment the smaller ones. In Treilhard et al. (2017), the same CaRF used for liver parenchyma segmentation is also used for viable tumor tissue and necrosis tissues segmentation. In Li et al. (2021a), the same U-Net along with the Bi-ConvLSTM are used to finely capture the tumors borders.

In contrast, some of the works opt to use an extra network for the tumor segmentation task in a cascaded sequence. In Christ et al. (2016, 2017), another 2D FCN is used to segment the tumors, within the segmented liver from the first 2D FCN, in a CFCN fashion, where the 3D CRF refines the output of the CFCN models. Similarly, in Han (2017), another DenseU-Net is used to segment tumors from the segmented liver outputted from the first DenseU-Net. In Yuan (2017), a third 2D FCN, following the first two that segmented the liver, is used for the tumor segmentation task. Moreover, in Jin et al. (2020), a third 3D RA-UNet segments tumors from the liver mask outputted from the first two (2D and 3D) RA-UNet networks. Similarly, a third AHCNet is used for tumor segmentation on the segmented liver from the first two AHC-Nets (Jiang et al., 2019). On the other hand, in Ouhmich et al. (2019), after segmenting the liver with a single U-Net, two other cascaded U-Nets are used for tumor, and its viability segmentation, respectively. In Nanda et al. (2019), the authors opt for a different network than the SegNet employed for segmenting the liver. Laws texture energy measure (LTEM) features are extracted for tumor detection using a normal ANN optimized by a genetic optimizer (GO) algorithm (LTEM-GO-ANN), followed by a 2D U-Net performing the tumors segmentation on detected tumor regions. Similarly, in Chen et al. (2019b), after segmenting the liver using the MPNet, a 3D densely-connected GAN (DC-GAN) is used for the tumor segmentation within the segmented liver. In Bai et al. (2019), after segmenting the liver using 3D U-Net, a multi-scale candidate generation (MCG) algorithm generates candidate tumor areas based on superpixels, which are inserted into a 3D fractal residual network (FRN), and the output is refined by an ASM algorithm. In Jansen et al. (2019), after segmenting the liver using a 2D MC-FCN, another network with dual-pathways is used to segment the tumors using nine phase slices. In Zhang et al. (2020a), after coarsely segmenting the liver using a 2D U-Net, a 3D FCN is used to segment the tumors within, followed by an LSM algorithm to refine the tumor segmentation. In Araújo et al. (2021), a RetinaNet comes before the U-Net to create an initial segmentation for the tumor that is then utilized by the U-Net to complete the task of tumors segmentation, followed

Table 2
Summary of the Liver segmentation techniques based on DL models.

Work	ML model	Method description	Dataset	Best performance[a]	Advantage/limitation
(Dou et al., 2016, 2017)	3D DSN + 3D CRF	3D CNN deeply supervised by auxiliary outputs + 3D CRF for contour refinement for liver and great vessels segmentation	SLIVER07 & HVSMR	VOE=5.42±0.72% (SLIVER07)	Performing well on both heart and liver segmentation, but not reporting DSC
(He et al., 2016)	AdaBoost + ASM	Three-level AdaBoost-guided ASM for liver segmentation in transversal, sagittal & coronal views	3D-IRCADb01, SLIVER07 & VISCERAL Anatomy3	DSC=96.4% (SLIVER07), DSC=93.3% (VISCERAL Anatomy3)	Manual feature engineering highly dependent on the CT modality
(Hu et al., 2016, 2017)	3D FCN based on (Lu et al., 2016)	3D organ delineation using 3D FCN with 10 layers, augmenting training data, and modern convex optimization techniques	SLIVER07 & Private	DSC=96.0±1.5% (on both in (Hu et al., 2017))	Absence of multi-organ datasets at the time of conducting the study
(Gibson et al., 2017)	3D FCN	3D FCN DL algorithm for liver, pancreas, stomach, and esophagus segmentation using dilated convolution units	BtCV & Pancreas-CT	DSC=93% (median, liver)	One of the early attempts to employ dilated convolutional layers for liver segmentation, but has post-processing
(Norajitra and Maier-hein, 2017)	3D SSM + RF	Liver segmentation using 3D SSM where RF utilization appears in omni-directional landmark search	SLIVER07 & BtCV	VOE=5.90% (SLIVER07), DSC=94.7% (BtCV)	Needs flexible shape prior modeling where a case-by-case model is a must; consequently, increasing complexity
(Huang et al., 2018a)	K-means + modified GC	Liver segmentation based on modified GC and feature detection, which relies initially on k-mean clustering	SLIVER07 & 3D-IRCADb	VOE=5.3% (SLIVER07), VOE=8.6% (3D-IRCADb)	Small tumors are under-segmented, GC-based algorithms are not suitable for elongated structures
(Gibson et al., 2018a)	3D Dense-V-Net-based FCN	3D DenseVNet to segment multi-organs from abdominal CT using 3D patches	BtCV & Pancreas-CT	DSC=95% (median, liver)	Multi-abdominal-organ segmentation, with slight enhancement on their previous work in Gibson et al. (2017)
(Roth et al., 2018b,a)	3D U-Net	3D patches input into 3D multi-scale pyramid-like 3D U-Net-based model	Pancreas-CT, VISCERAL Anatomy3 & Private	DSC=95.4±2.0% (liver)	Usage of a single model (consisting of multiple networks) to segment multiple organs is a huge advantage
(Qin et al., 2018)	SLIC + 2D FCN	Superpixel-based and boundary-sensitive CNN for liver segmentation	LiTS	DSC=97.31±0.36%	Using superpixels as input to the FCN
(Yang et al., 2019)	VAE + GAN	Usage of VAE and GANs to transfer content information to common subspace between MRI and CT	LiTS & Private MRI	DSC=81±3%	VAE to disentangle information from MRI and CT modalities to find shared content space
(Cai, 2019)	FKFCM	Use of FKFCM for liver and tumor segmentation	SLIVER07 & 3D-IRCADb01	DSC=87.02% (SLIVER07)	High results given that unsupervised learning is used
(Zhou et al., 2019b)	Genesis	Self-supervised model training to be used as basis for TL to a specific biomedical task (ImageNet biomedical counterpart)	LiTS	DSC=91.13±1.51%	Interesting self-supervised training technique to teach the model human anatomy
(Rickmann et al., 2019)	3D FCN + PE module	3D patches inserted into 3D U-Net implementing PE modules which efficiently replaces extra convolutional layers	VISCERAL Anatomy3 & MALC	DSC=93.1% (VISCERAL Anatomy3, liver)	PE blocks can be inserted into 3D FCNs without significant increase in computational complexity
(Huang et al., 2019)	3D U^2-Net	3D patches from different CT and MRI modalities inserted into 3D U^2-Net for intra- and inter-modal organ segmentation	MSDC (heart, liver, hippocampus, prostate, panceras & spleen)	DSC=93.54% (liver)	Tackles both CT and MRI modalities
(Ahmad et al., 2019)	DBN	Training DBN by unsupervised pre-training followed by supervised fine-tuning for the liver segmentation task	SLIVER07 & 3D-IRCADb01	DSC=94.8±0.6% (SLIVER07), DSC=91.83±1.37% (3D-IRCADb)	The DSC dropped under 3D-IRCADb01 dataset, and further investigation on other datasets is needed
(Zheng et al., 2019)	2D DeepLab + DAP	Semi-supervised adversarial learning model with DAP to improve the accuracy of liver segmentation in CT images	LiTS	DSC=95.23%	Semi-supervised model with unannotated data in training dataset to minimize required medical images' annotation
(Novikov et al., 2019)	Sensor3D	Bi-directional Conv-LSTM following a U-Net architecture for liver segmentation	3D-IRCADb	DSC=95.4%	One of few studies to use LSTM for liver segmentation
(Wang et al., 2019a)	CoFCN	Two inputs into CoFCNs in parallel and share features along segmentation	LiTS	DSC=96.43%	Uses a portion of the dataset, not all of it
(Yao et al., 2019)	3D G-ResNet	3D Liver segmentation based on G-ResNet used with a backbone FCN such as U-Net, V-Net, or VoxDenseNet	MSDC-T3	DSC=96.47%	The study also generates 3D measure of the organ that is segmented
(Cheema et al., 2019)	LER-CN	Segmenting liver from low-dose CT scan by convoluted NRC for coarse extraction and de-convoluted SPC for fine extraction	SLIVER07 & Private	DSC=96.5±1.8% (SLIVER07)	Focuses on the Low-dose CT scans
(Wang et al., 2019d)	3D MPNet	Each network in MPNet specializes in a view and the output is the weighted-average of the 3 views based on their resolutions	LiTS	DSC=96.7%	Multi-plane segmentation and fusion
(Zhou et al., 2019a)	PaNN	Two versions of PaNN (2D & 3D) for organ segmentation using partially annotated datasets for organs' segmentation	BtCV, MSDC-T3 & Pancreas-CT	DSC=97.4% (BtCV, liver)	Multi-organ segmentation, where the model also performs well for pancreas segmentation

(*continued on next page*)

Table 2 (*continued*).

Work	ML model	Method description	Dataset	Best performance[a]	Advantage/limitation
(Tian et al., 2019)	GLC-UNet	2xGLC-UNets to segment liver firstly and then the famous Couinaud segmentation	MSDC-T8	DSC=98.18±0.85% (liver), DSC=92.8±3.08% (Couinaud liver)	Published liver masks (443 records) and Couinaud masks (193 records) for MSDC-T8 dataset, and first work to tackle Couinaud segmentation
(Tang et al., 2020a)	Faster R-CNN	Sequential segmentation of liver over two stages using Faster R-CNN (localize) and DeepLab (segment)	SLIVER07 & 3D-IRCADb	VOE=5.06% (SLIVER07), VOE=8.67% (3D-IRCADb)	Liver detection and then segmentation is interesting to reduce the work needed for the 2nd model
(Zhou et al., 2020)	U-Net++	New U-Net architecture with deep supervision for organs' segmentation where the encoder is redesigned to support inter-level concatenations	LiTS & Others	DSC=82.6±1.11%	A part of the model can be considered a standalone U-Net, and the output of the U-Net++ is the ensemble of all those existing U-Nets within
(Tang et al., 2020b)	DeepMedic (3D CNN + 3D CRF)	Multi-scale segmentation of the liver, with fusion of fully connected layers using DeepMedic CNN	SLIVER07, LiTS & Private	DSC=94% (median, Private)	Inter-observer variability was reduced when the CNN segmentation was used as a baseline
(Fang et al., 2020; Fang and Yan, 2020)	MIMO-FAN	A novel pyramid-like architecture for multi-organ segmentation using multi-scale fusion layers	BtCV, LiTS, KiTS & Spleen	DSC=95.9% (on all datasets)	The input is inserted in different scales
(Chung et al., 2020)	3D Dense V-Net	Deeply self-supervised 3D Dense V-Net to segment liver	SLIVER07, 3D-IRCADb, Gibson et al. (2018c)'s & Private	DSC=96±1% (on all datasets)	Does not investigate tumor segmentation
(Mohagheghi and Foruzan, 2020)	3D U-Net	Usage of 3D U-Net with hybrid loss to encompass 3D liver global knowledge in segmenting the liver	SLIVER07	DSC=97.62%	Model's training initiates as noise removal; but it would be better to test on more recent public datasets
(Li et al., 2020)	2D ANU-Net	Modified U-Net++ architecture and loss function for multi-organ segmentation	LiTS & CHAOS	DSC=98.15% (LiTS), DSC=93.55% (CHAOS)	Work introduces a light ANU-Net version, with a reduction in performance
(Tan et al., 2021)	3D CNN	Automatic liver segmentation using 3D CNN and a hybrid loss function	SLIVER07 & CHAOS	DSC=83.02% (CHAOS)	Can be trained on small datasets; however, moderate performance is reported
(Tian et al., 2021)	2D ResU-Net	Automatic annotation of liver functional regions using a 2.5D class-aware DNN	MSDC-T8	DSC=88.2% (Couinaud liver)	Moderate computational cost with accurate segmentation, and further investigation on other datasets is needed
(Ma et al., 2021)	VNet_WGAN	Fusion of VNet and WGAN for liver Segmentation	LiTS & CHAOS	DSC=92% (LiTS), DSC=90% (CHAOS)	Moderate performance but the loss function part is appropriate for medical image analysis
(Wang et al., 2021)	SAR-U-Net	Liver segmentation using an improved U-Net scheme	LiTS & SLIVER07	DSC=97.3±1.49% (SLIVER07) DSC=95.71±0.55% (LiTS)	High computational cost compared to the state-of-the-art
(Ahmad et al., 2022)	Lightweight CNN	A lightweight CNN architecture to segment liver in CT images	SLIVER07, 3D-IRCADb01 & LiTS	DSC=95% (SLIVER07), DS92.9% (3D-IRCADb01)	The performance dropped on the 3D-IRCADb01 dataset
(Araújo et al., 2022)	U-Net	Liver segmentation from CT images using cascaded DL	LiTS	DSC=95.64%	U-Net parameters defined empirically and liver contours slightly failing
(Al-Kababji et al., 2022)	U-Net	Liver segmentation from CT images with careful image enhancements techniques	MSDC-T8 (liver masks from Tian et al. (2019))	DSC=98.12±0.04%	Compares performance of two learning rate scheduling techniques: ReduceLROnPlateau and OneCycleLR

[a]For the "Best performance" column, we mention DSC and VOE, respectively, if one is unavailable. DSC is Dice per case.

by some post-processing techniques to enhance the final segmentation results.

GANs are also used in the tumor segmentation task. In Xiao et al. (2019), a radiomics-guided GAN utilizes a dilated DenseU-Net as the generator (segmenter), and a VGG network as the discriminator in GAN where the discriminator extracts radiomics features to aid the segmenter in tumor segmentation. However, in Pang et al. (2020), a 2D CTumorGAN is used for the tumor segmentation task in multiple organs, including the liver, and it incorporates a novel generator scheme that integrates a noise vector with the encoder part to generate segmentation masks.

Similar to Table 2, Table 3 historically highlights the studies that focus on the task of tumor segmentation, along with liver segmentation if the same work segments both. They are compared in terms of the deployed ML model, method description, dataset, best performance, advantage/limitation, and segmentation category.

4.2.3. Vessels

Application of unsupervised-based ML algorithms towards segmentation of vessels is rare and only available in Zhang et al. (2018c), where Jerman's vesselness filter based on K-means clustering is followed by an improved fuzzy connectedness (FC) algorithm to segment the vessels. On the other hand, the only supervised-based ML study that segments all the liver's tissues, i.e., liver parenchyma, tumors, and vessels, is in Treilhard et al. (2017), using the same aforementioned CaRF for blood vessels segmentation.

The majority of existing works employ supervised-based ML algorithms for vessels segmentation. In Zeng et al. (2016), an anisotropic filter is used to suppress noise and simultaneously maintain boundary details. Followed by the use of the four filters: (i) Sato; (ii) Frangi (iii) offset medialness; and (iv) strain energy to extract vessel features, which are then normalized. Finally, an extreme learning machine (ELM) is applied to recognize liver vessels from the background.

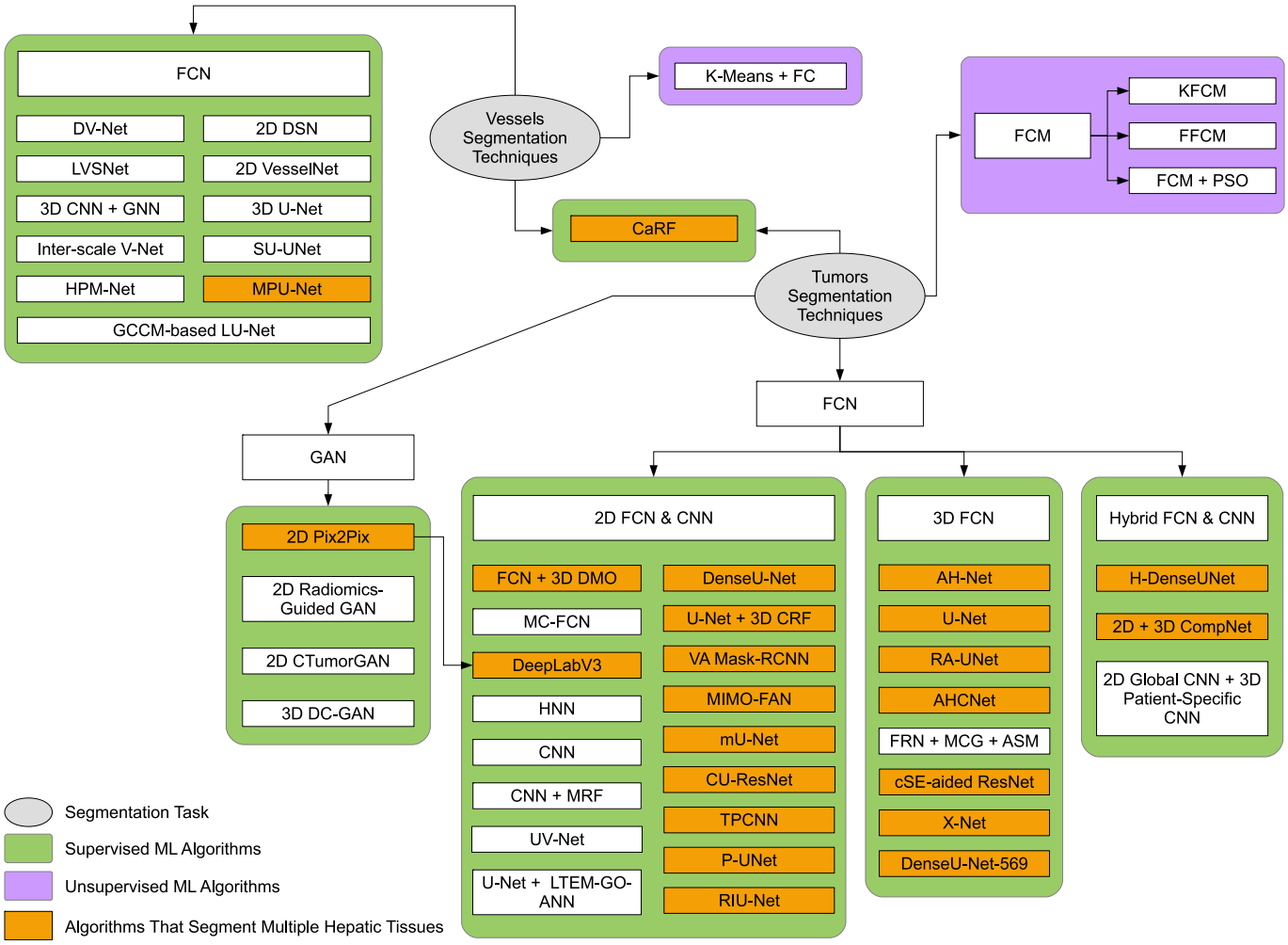

Fig. 8. Tumors and vessels segmentation techniques from the reviewed literature.

In Mishra et al. (2019), a more ML-dependent approach is followed. A 2D DSN based on VGG-16 is used on liver vessels segmentation from US imagery. DSN has three layers: (i) object boundary definition prediction by fine resolution layers aided by auxiliary losses; (ii) coarse resolution layers to discriminate object regions within the boundary; and (iii) a trainable fusion layer. In Kitrungrotsakul et al. (2019), a 2D VesselNet describes an architecture that utilizes three DenseNets aimed at segmenting orthogonal patches, pre-processed by a Frangi filter, from the three planar views (transversal, sagittal, and coronal). Thus, vesselness probability maps are inserted into the orthogonal DenseNets, which are then fused to generate the final segmentation mask. To incorporate the 3D context even further, some researchers developed 3D networks. In Huang et al. (2018b), a 3D U-Net is employed, which is vital in the case of tubular structures traversing narrowly through the slices. The work emphasizes the data imbalance issue and attempts to solve it by carefully designing data augmentation schemes and loss functions. In Zhang et al. (2020b), a 3D CNN for vessel enhancement is used to highlight the vessel centerlines. A 3D tree tracing algorithm initializes the vessel graph tracing with high sensitivity and low specificity. Then, a graph neural network (GNN) equipped with graph attention layers (GAT) is utilized to prune the false-positive branches.

In Zeng et al. (2018), two strategies, namely the 3D region growing and the hybrid active contour model, are combined to segment liver vessels by utilizing the shape and intensity constraints of 3D vessels. The former has been facilitated by a bi-Gaussian filter for thin vessel segmentation, while the latter has been combined with K-means clustering for thick vessel segmentation. Besides, in Su et al. (2021), a dense V-Net (DV-Net) model is proposed to segment liver vessels, which relies on (i) integrating a dense block structure into V-net; and (ii) using data augmentation from abdominal CT volumes with scarce training data. Additionally, a dual-branch dense connection down-sampling strategy and a combined Dice and BCE (D-BCE) loss function have been introduced for capturing vascular features and maximizing image resources' use, respectively. Moving forward, in Hao et al. (2022), a hierarchical progressive multi-scale network (HPM-Net), is proposed to segment liver vessels in CT images. Accordingly, the multiple-scale semantic features of liver vessels are learned using a hierarchical progressive multi-scale learning model, aggregating internal and external progressive learning methods. Moreover, a dual-branch progressive 3D U-Net using a dual-branch progressive down-sampling approach is introduced to capture vessel features better.

Many liver vessel segmentation methods have relied on using U-Net architecture; however, interference can be caused as not all features of the encoder are useful. To avoid this issue, Yan et al. (2020) propose a liver vessel segmentation network (LVSNet) that deploys particular designs to derive the accurate structure of the liver vessels. Typically, an attention-guided concatenation component is designed for adaptively selecting relevant context characteristics from low-level characteristics guided by high-level characteristics. To put it simply, it concentrates on deriving rich complemented data to get more details. In Yang et al. (2021), an inter-scale V-Net model is developed to

Table 3
Summary of the tumors (and liver) segmentation frameworks based on ML and DL models.

Work	ML model	Method description	Dataset	Best performance[a]	Advantage/limitation	Segmentation category
(Christ et al., 2016, 2017)	U-Net-like 2D FCN + 3D CRF	Cascaded U-Nets for liver and lesion segmentation aided by 3D CRF on CT and MRI	3D-IRCADb & 2 Private Datasets	3D-IRCADb: DSC=94% (liver), DSC=56% (tumors)	Created the LiTS dataset, the studies that revolutionized liver/tumors segmentation challenge	Liver & Tumors
(Sun et al., 2017)	2D FCN & 2D MC-FCN	FCNs on 3D-IRCADb and MC-FCNs on JDRD for tumors segmentation	3D-IRCADb & JDRD	3D-IRCADb: VOE=15.6±4.3%, JDRD: VOE=8.1±4.5%	Segments liver from multi-phased CT images, but no mention of MRI	Tumors
(Yuan, 2017)	2D FCN	3 × 2D FCN cascaded for liver and tumor segmentation on LiTS dataset	LiTS	DSC=96.3% (liver), DSC=65.7% (tumors)	A participant of the original LiTS competition, hardware limitations prevented higher performance	Liver & Tumors
(Han, 2017)	DenseU-Net	Use of 32-layered DNN with short (ResNet Connections) and long connections (U-Net connections)	LiTS	DSC=67%	Using better post-processing techniques or ensemble of FCNs	Tumors
(Tian et al., 2018)	2D FCN	FCN to segment CT slices, and an LSTM captions generator to create diagnostic reports	LiTS	DSC=94.2% (liver), DSC=54.9% (tumors)	Opens aspects of report generation and image captions for medical reasons	Liver & Tumors
(Liu et al., 2018)	3D AH-Net	3D AH-Net utilizing inter-slice information to gain intra-slice features (2D to 3D)	Breast tumors Private & LiTS	DSC=96.3% (liver), DSC=63.4% (tumors)	Exceeds state-of-the-art at the time, also the DPC is the one to be compared with the other DSC	Liver & Tumors
(Chlebus et al., 2018)	DenseU-Net + RF	Multiple 2D U-Net for liver and tumor segmentation + RF for FP filtering for tumor segmentation	LiTS	DSC=96% (liver), DSC=68% (tumors)	Smaller tumors pose an issue for the FCN	Liver & Tumors
(Li et al., 2018)	2D & 3D DenseU-Net	2D DenseU-Net to extract intra-slice features and 3D one for aggregating volumetric context for segmentation	LiTS & 3D-IRCADb	LiTS: DSC=96.1% (liver), DSC=72.2% (tumors)	Small tumors are under-segmented	Liver & Tumors
(Cai et al., 2018)	HNN	Weakly supervised approach converts RECIST-based lesion diameter measurements into full 3D lesion volume segmentation	Lymph node & DeepLesion	DSC=92% (RECIST tumors), DSC=76% (tumors volumes)	Utilizes RECIST data to segment different tumors around the body including the liver	Tumors
(Vorontsov et al., 2018)	U-Net-like 2D FCN	Sequential U-Net-like models for liver and tumor segmentation with models ensemble for the liver segmentation	LiTS	DSC=95.1% (liver), DSC=77.3% (tumors)	Tumor segmentation is high, liver not the best, maybe increase 2.5D input size could help	Liver & Tumors
(Jiang et al., 2019)	3D AHCNet	3D AHCNet combines soft and hard attention mechanisms with long and short skip connections	LiTS & 3D-IRCADb & Private	3D-IRCADb: DSC=95.3% (liver), DSC=66.8% (tumors), LiTS: DSC=59.1% (tumors)	Tumor segmentation can be enhanced by post-processing techniques	Liver & Tumors
(Bai et al., 2019)	3D U-Net + MCG + 3D FRN + ASM	3D U-Net for liver segmentation + 3D FRN for tumors and ASM for refining tumors segmentation	LiTS	DSC=67.4% (3D-IRCADb)	Study notes that 3D-IRCADb is part of LiTS; thus, should not be used for training	Tumors
(Chen et al., 2019b)	MPNet + 3D DC-GAN	MPNet to segment the liver + 3D DC-GAN to segment the tumor	LiTS	DSC=96.7% (liver), DSC=68.4% (tumors)	Multi-plane segmentation and fusion	Liver & Tumors
(Nanda et al., 2019)	LTEM-GO-ANN & 2D U-Net	Cascaded SegNet, ANN and U-Net, where former segments liver, middle detects tumors, and latter segments tumors	LiTS	DSC=95.57% (liver), DSC=69.76% (tumors)	Localizes tumors before segmenting it	Liver & Tumors
(Wang et al., 2019e)	VA Mask-RCNN	Using VA modules with CNN to enhance extracted inter-slice information in 2.5D inputs	LiTS & DeepLesion	LiTS: DSC=74.1%	VA modules can be integrated with any type of CNN	Tumors
(Xia et al., 2019)	DeepLabV3 + Pix2Pix GAN	Usage of Pix2Pix GAN after DeepLabV3 network to improve liver and tumor segmentation & detection	LiTS & DeepLesion	LiTS: LiTS: DSC=97.0% (liver), DeepLesion: DSC=87.24% (tumors)	Creating a weighted complex loss function consisting of multi-class cross-entropy, generator, and discriminator loss functions	Liver & Tumors
(Dey and Hong, 2020)	2D & 3D CompNet	Hybrid cascaded 2D CompNet to segment liver & 3D CompNet to segment tumors	LiTS	DSC=68.1% (tumors)	Segments small and large tumors, but affected by LiTS imperfect segmentation of tumors	Liver & Tumors
(Zhang et al., 2020a)	2D U-Net & 3D FCN + LSM & FCM	DL methods for liver and tumor segmentation aided by LSM	LiTS & Private	LiTS: DSC=96.3% (liver), DSC=71.8% (tumors)	Utilizing FCM to help FCN for tumor localization is interesting	Liver & Tumors
(Xi et al., 2020)	CU-ResNet	Comparison between loss functions on CU-ResNet for both liver and tumors segmentation challenges	LiTS	DSC=94.9% (liver), DSC=75.2% (tumors)	Fine-tuning the weight parameters in loss function could enhance the performance	Liver & Tumors
(Pang et al., 2020)	2D CTumorGAN	Universal tumor segmentation using GAN network on CT scans for the whole body	LiTS & Others	LiTS: DSC=80.19%	Work concludes that mean-squared error is the best loss function for tumor segmentation	Tumors
(Qayyum et al., 2020)	3D ResNet-based FCN + cSE	Segmentation of liver and kidneys and their associated tumors via 3D ResNet and cSE blocks	LiTS & KiTS	LiTS: DSC=97.1% (liver), DSC=82.5% (tumors)	Tumor segmentation results are superb	Liver & Tumors

(*continued on next page*)

Table 3 (*continued*).

Work	ML model	Method description	Dataset	Best performance[a]	Advantage/limitation	Segmentation category
(Jin et al., 2020)	2D RA-UNet	3D patches liver and tumors segmentation using cascaded RA-UNet coupled with attention-aware module	LiTS & 3D-IRCADb	LiTS: DSC=96.1% (liver), DSC=59.5% (tumors), 3D-IRCADb: DSC=97.7% (liver), DSC=83% (tumors)	Heavyweight 3D FCN model is used, which is more expensive to train	Liver & Tumors
(Seo et al., 2020)	mU-Net	Modifications to the U-Net skip connection architecture	LiTS & 3D-IRCADb	LiTS: DSC=98.51±1.02% (liver), DSC=89.72±5.07% (tumors)	No preprocessing is required and excellent performance on both segmentation tasks	Liver & Tumors
(Aghamohammadi et al., 2021)	TPCNN	Tumor and liver segmentation using LDOG encoding technique on CT images	Dataset in Ranjbarzadeh and Saadi (2020)	VOE=2.2±0.1% (liver), VOE=9.5±0.9% (tumors)	Validation on real-world scenarios is missing; and DSC in the paper on tumors is higher than liver, which is interesting	Liver & Tumors
(Meng et al., 2021)	DenseU-Net	Two-stage liver and tumor segmentation using 2D and 3D features and attention mechanism	LiTS	DSC=96.7% (liver), DSC=72.5% (tumors)	The performance of tumor segmentation needs further improvement	Liver & Tumors
(Han et al., 2021b)	P-UNet	Liver and tumor segmentation by fusing three perpendicular 2D Res-UNets' outputs (2.5D inputs)	LiTS	DSC=96.2% (liver), DSC=73.5% (tumors)	Trained with less data and GPU memory; however, it is only trained on one dataset	Liver & Tumors
(Han et al., 2021a)	Cascaded 2D FCN	Segmentation of liver and tumor by exploring spatial information in 3D images inputted as 2.5D	LiTS & 3D-IRCADb	LiTS: DSC=94.3% (liver), DSC=74.5% (tumors), 3D-IRCADb: DSC=96.1% (liver), DSC=68% (tumors)	The performance needs further improvement especially for tumors segmentation	Liver & Tumors
(Chi et al., 2021)	X-Net	Segmentation of liver and tumor using using a multi-branch U-Net-like model	LiTS & 3D-IRCADb	LiTS: DSC=96.8% (liver), DSC=76.4% (tumors), 3D-IRCADb: DSC=96.68% (liver), DSC=69.11% (tumors)	The performance slighlty outperforms the one by Han et al. (2021a)	Liver & Tumors
(Alalwan et al., 2021)	3D DenseU-Net-569	A fully 3D semantic segmentation network with lower training parameters and deeper architecture	LiTS	DSC=96.7% (liver), DSC=80.7% (tumors)	Validated only on one dataset and the tumors segmentation needs further improvement	Liver & Tumors
(Zhang et al., 2021a)	Multi-scale UV-Net	Liver tumor segmentation using 2.5D UV-Net with multi-scale convolution	LiTS	DSC=88.92%	Moderate training time but excellent tumor segmentation performance	Tumors
(Di et al., 2022)	3D U-Net	Using hierarchical iterative superpixels and local statistical features for tumor segmentation	LiTS & 3D-IRCADb	DSC=71±7% (3D-IRCADb)	Less computational cost compared to existing methods	Tumors
(Lv et al., 2022)	RIU-Net	Automatic liver and tumor segmentation from CT images by extracting inter-slice spatial information in the form of 2.5D	LiTS & 3D-IRCADb	LiTS: DSC=97.72% (liver), DSC=73.79% (tumors), 3D-IRCADb: DSC=96.71% (liver), DSC=76.55% (tumors)	Improves performance in presence of small tumors or tumors near liver boundary; however, insufficient feature integration still exists	Liver & Tumors
(Zheng et al., 2022)	3D CNN + Conv-LSTM	Automatic tumors segmentation using 4D information	Private	DSC=82.5±7.7%	Small tumors could be missed and motion artifacts generate registration errors in dynamic CE-MRI	Tumors

[a]For the "Best performance" column, we mention DSC, JI, and VOE, respectively, if one is unavailable. DSC is Dice per case.

segment liver vessels by (i) introducing a dilated convolution into the traditional V-Net model to save detailed spatial information and enlarge the receptive field without reducing down-sampling; and (ii) using a 3D deep supervision mechanism into the V-Net to speed up its convergence and to better learn semantic features. Additionally, to efficiently integrate multi-scale features and avoid the loss of high-level semantic information in the decoder, inter-scale dense connections are integrated into the decoder of V-Net. Montaña-Brown et al. (2021) utilize 2D U-Net with batch normalization blocks at each layer for liver vessel segmentation in 2D registration of laparoscopic US images.

In Li et al. (2021b), liver vessel segmentation is performed by introducing a new strategy, namely plug-in mode, which helps in integrating a graphical connectivity constraint module (GCCM) into a 3D lightweight U-Net (LU-Net). In this regard, the 3D LU-Net has been used for segmentation. In contrast, the GCCM, which is based on GAT, has been utilized for supervising the training process of LU-Net with connectivity prior. Because of low contrasts in the CT images and complex structures of hepatic vessels, it is challenging, even for experts, to perform accurate manual annotation. Consequently, most of the labels of existing publicly available datasets are noisy. Fig. 9 portrays the flowchart of the liver vessel segmentation method proposed in Li et al. (2021b). To overcome this issue, Liu et al. (2022a) introduce a self-updating U-Net (SU-UNet), based on soft-constraint, for an accurate vessel segmentation from noisy annotations. Two U-Nets are first used to output different segmentation predictions before designing a self-updating module to optimize noisy vessel labels based on segmentation predictions. This helps better guide the model training using optimized labels. Finally, Table 4 historically summarizes some existing liver vessel segmentation frameworks discussed in the paper. A comparison has been conducted in terms of the deployed ML model, method description, dataset, best performance, and advantage/limitation.

4.2.4. Outlook

Many insights can be drawn from the above survey: (1) The majority of studies in the liver delineation task utilize supervised ML algorithms, especially the 2D and 3D FCN-based models as depicted in Fig. 6 and compared in Table 2; (2) The huge advancements in the ML field to tackle the biomedical problems, such as using 3D or 2.5D instead of 2D, or innovating new interconnected architectures that enables better understanding of the liver's complex structure; (3) The interconnectivity of different algorithms aiming to segment multiple tissues, showing an initiative towards creating a complete algorithm for full liver delineation; (4) The number of studies investigating tumors and vessels delineation, shown in Fig. 8 and summarized in Tables 3 and 4, are low when compared with the ones investigating the liver's delineation,

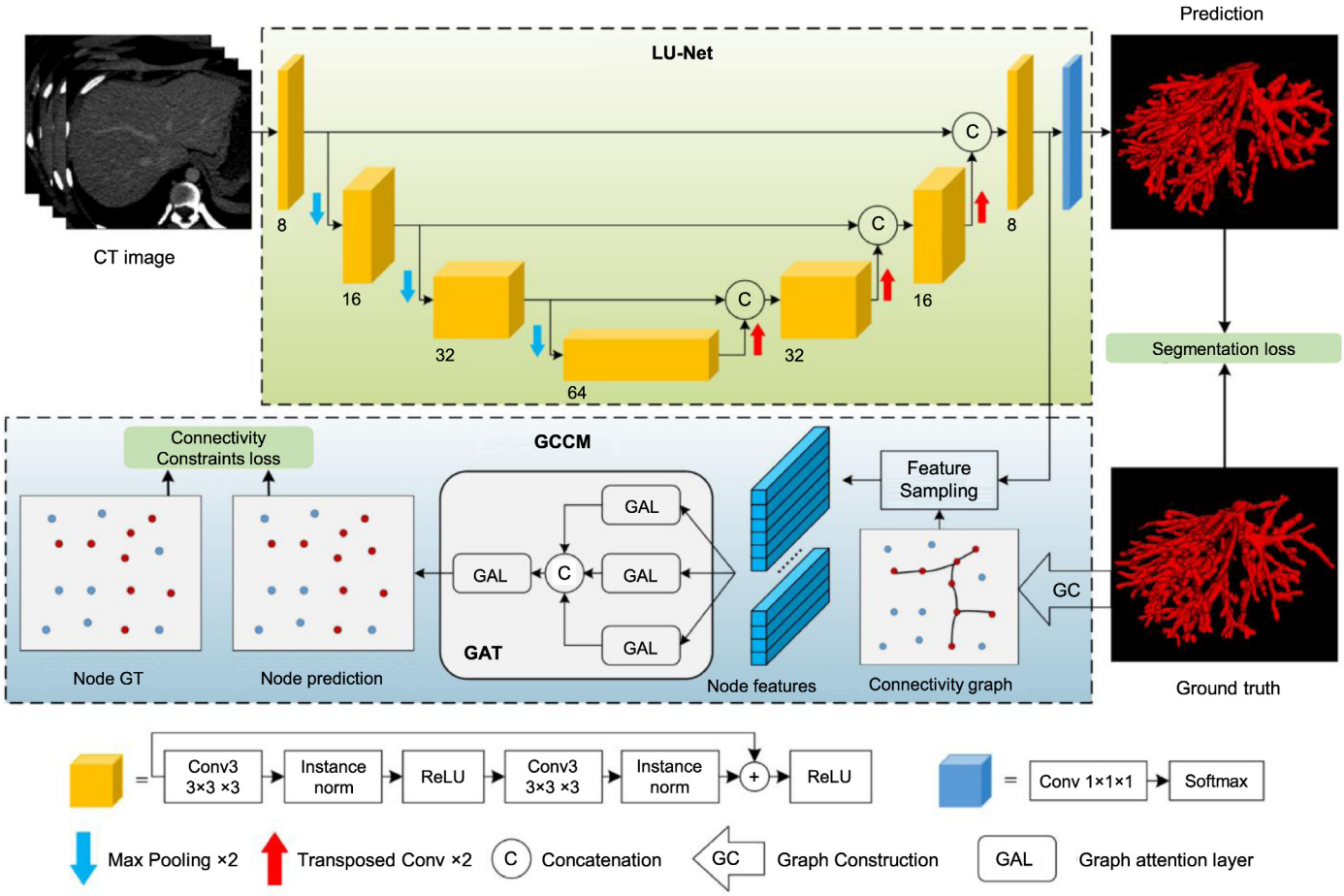

Fig. 9. Flowchart of the liver vessel segmentation method proposed in Li et al. (2021b), which is conducted in two stages by (i) using a 3D LU-Net for segmentation; and (ii) applying a GAT-based GCCM to supervise LU-Net training process with "connectivity prior" information of the hepatic-vessels.

especially the vessels segmentation studies that are rare, pointing at a research area worth further investigation; (5) The severe absence of studies that tackle all liver's different tissues delineation problem. It is worth noting that the studies that worked solely on Private datasets have been removed from the liver segmentation comparison in Table 2 and the tumors segmentation in Table 3. Contrastingly, they were kept for the vessel segmentation comparison in Table 4 due to the scarce number of studies.

5. Critical discussion and open challenges

A wide range of DL-based algorithms have been proposed and have shown state-of-the-art performance for different tasks, including automatic liver segmentation, liver tumors segmentation, and liver vessels segmentation. The performance of DL techniques has been enhanced over time in terms of segmentation accuracy, complexity, and overall "smartness". Moreover, CNN models have been the most utilized architectures for the aforementioned segmentation tasks with 2.5D, 3D, and 4D images. Additionally, some studies have used TL, particularly fine-tuning, in which a pre-trained network (all the layers or part of them) is employed to initialize the weights. However, most DL algorithms have adopted end-to-end training without using any pre-trained models.

On the other hand, it was obvious that most of the studies still have difficulties in simultaneously discriminating between tumors, inside-liver tissues, and outside-liver organs. This is in addition to the fact that extracting features that reflect the axial changes of the liver and the tumor is still challenging because of the high computational cost. This results in limited learning effects and efficiencies.

In this context, although significant progress has been made for semi-automatic or fully automatic liver, liver tumor, and liver vessel CT image segmentation, precise and accurate segmentation is still challenging in many scenarios. For example, in the case of liver segmentation, this is due to various reasons, as visually shown in Fig. 10. Typically, this can be attributed to: (i) the intensity similarity between the liver and its neighboring organs such as the stomach and heart; (ii) the blurring of the liver contour due to the partial volume effects; (iii) the severe pathological changes, e.g., large tumors and cirrhosis, often occur in clinical images, although its intensity is evidently not similar to that of the normal liver; and (iv) the liver shape can vary from one person to another, especially if a hepatectomy has been performed on said person. These issues impede the segmentation of livers with complex contours and small sizes, complicating the automation of liver segmentation when diagnosing and treating CT images (Tang et al., 2020c).

After surveying the literature and understanding the novelty of each work, we believe that the available techniques in literature, especially in the last 3 years, have advanced rapidly so that they can be soon implemented in clinical environments, if that is not the case already. To the best of our knowledge, we have included the key studies that are concerned with the automatic segmentation of liver, tumors, and vessels using ML algorithms. Thus, from that perspective, we see some patterns/gaps in both Figs. 6 and 8 that are worth highlighting. Along

Table 4
Summary of the liver vessel segmentation frameworks based on ML and DL models.

Work	ML model	Method description	Dataset	Best performance	Advantage/limitation
(Zeng et al., 2016)	ELM	Using ELM for segmentation on pre-processed data (anisotropic filter for suppressing noise + Sato, Frangi, offset medialness, and strain energy filters)	Private	Acc=98.1%, Recall=74.2%	One of the earliest work to tackle liver vessels segmentation
(Treilhard et al., 2017)	CaRF	Multi-class tissue segmentation (Parenchyma, viable tumors, necrosis, and vasculature) from MRI	Private (MRI)	DSC=67.8% (viable tumors), DSC=54.4% (necrosis), DSC=55.7% (vessels)	Private dataset, but one of the only studies to tackle all TOIs segmentation
(Zhang et al., 2018c)	K-means + FC	Improved FC method for automatic 3D segmentation in CT images	3D-IRCADb & SLIVER07	DSC=67.3±5.7% (3D-IRCADb), DSC=71.4±7.6% (SLIVER07)	Small dataset size, and the isotropical and anisotropical resampling are time-consuming
(Zeng et al., 2018)	K-means	Automatic segmentation using 3D region growing and hybrid active contour model	Private	DSC=73%	Thick vessels with lower intensities fail to be segmented, and the surface of vessels is not convincingly smooth
(Huang et al., 2018b)	3D U-Net	3D vessels segmentation using 3D U-Net with an adjusted loss function	3D-IRCADb & SLIVER07 & Private	DSC=75.3% (3D-IRCADb)	High vessels segmentation Dice score compared to peers
(Perslev et al., 2019)	MPU-Net	MPU-Net to segment multiple organs from different views with the same simple architecture	MSDC	DSC=76±18% (liver & tumor MSDC-T3), DSC=49% (tumor & vessels, MSDC-T8)	Tackles all challenges in MSDC
(Mishra et al., 2019)	2D VGG-16-based DSN	2D DSN to segment vessels in the liver within US images	Private (US)	DSC=73%	Focuses on the US images, which is rare in literature
(Kitrungrotsakul et al., 2019)	VesselNet	VesselNet segments vessels from Fringi filtered vessels images using orthogonal 2D patches from the 3 different views	3D-IRCADb & ViscuSynth	DSC=90.3% (3D-IRCARDb)	Excellent results, but 2-4 mins for computations (with GPU)
(Ivashchenko et al., 2020)	4D K-means	An automatic algorithm for segmentation of liver (based on 4D K-means) and of vessels (based on Otsu and Frangi filters)	Private (MRI)	N/A	Segmentation of the hepatic veins could be improved, and more common metrics could have been used
(Zhang et al., 2020b)	3D CNN + GNN	3D CNN highlighting vessels on 64 × 64 × 64 patches followed by GNN to properly segment hepatic vessels	Private	F1 Score=87.62±5.49%	Uses GNN as a post-processing scheme to enhance F1 Score
(Yan et al., 2020)	LVSNet	Attention-guided DL with multi-scale feature fusion for vessels segmentation	3D-IRCADb & Private	DSC=90.4% (3D-IRCADb)	Performance drops on the proposed dataset
(Li et al., 2021b)	GCCM-based LU-Net	Liver vessel segmentation using 3D graph-connectivity constrained network	3D-IRCADb & MSDC	DSC=65.41% (3D-IRCADb)	GPU memory consumption increases by decreasing sampling interval; but increasing it leads to poorer performance
(Montaña-Brown et al., 2021)	2D U-Net	Vessel segmentation for automatic registration in 2D untracked laparoscopic US images	Private	DSC=64.81%	Difficulty in segmenting rapidly-varying vessel sections over time, and performance needs to be improved
(Yang et al., 2021)	Inter-scale V-Net	Liver vessel segmentation based on inter-scale V-Net	3D-IRCADb	DSC=71.6%	Performance needs further improvement and investigation on other datasets
(Su et al., 2021)	DV-Net	DV-Net with D-BCE loss function for automatic vessels segmentation	3D-IRCADb & MSDC	DSC=75.46% (3D-IRCADb)	High computational cost and the performance needs further improvement
(Survarachakan et al., 2021)	3D U-Net	Liver vessel segmentation by combining multiple vesselness enhancement filters	OSLO-COMET (Fretland et al., 2015)	DSC=80%	Further investigation on other datasets is required
(Liu et al., 2022a)	SU-UNet	SU-UNet is a novel self-updating network for hepatic vessel segmentation in CT images	MSDC	DSC=62.94%	Further performance improvement and investigation on other datasets are required
(Hao et al., 2022)	HPM-Net	3D CNN for liver vessel segmentation	3D-IRCADb	DSC=75.18%	The network has a complex structure with a huge number of parameters

our survey, we also identified gaps and challenges that need attention to be addressed.

5.1. Tumors and vessels literature availability

The works utilizing ML techniques for tumors and vessel segmentation seem to be a little copious against the ones concerned with the liver as a whole. This is understandable because the advanced ML algorithms have been thoroughly investigated for the liver segmentation task first, which can then be utilized for the tumors and vessels segmentation task in a hierarchical fashion. Nonetheless, they are of scarce nature, especially the vessels segmentation task, due to the fewer available masks for hepatic vasculature needed for ML algorithms. However, with the introduction of the MSDC-T8 dataset, the research fraternity has been boosted up to utilize ML algorithms for tumors and vessel segmentation.

5.2. Classifying all tissues

The most prominent gap that has been identified is the absence of studies that segment all the hepatic tissues within the liver, except for (Treilhard et al., 2017), even though the achieved results are not comparable with the state-of-the-art. One of the possible reasons for this problem might be due to the unavailability of complete masked

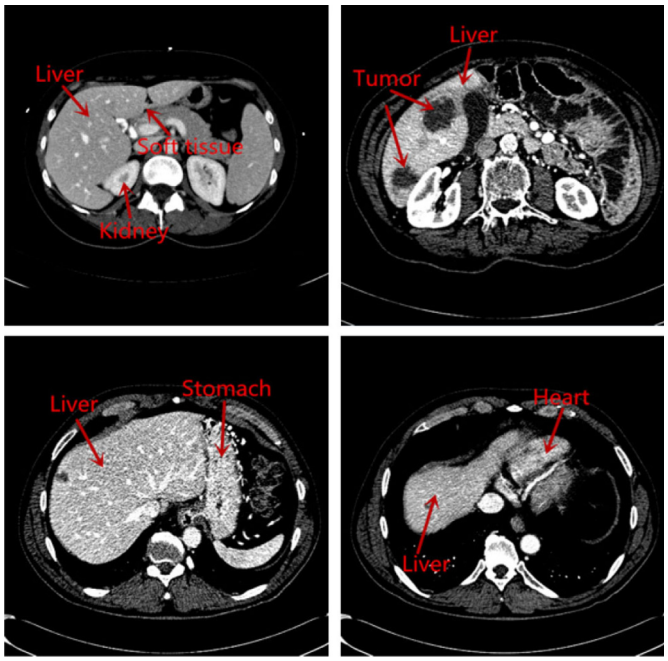

Fig. 10. Some liver segmentation challenges that still impede the development of accurate semi-automatic or automatic segmentation solutions (Tang et al., 2020c).

data, including liver parenchyma, tumors, and vessels. Although the MSDC-T8 dataset provides two of the three elements required, the tumors and vessels masks, there has been another database recently introduced by (Tian et al., 2019) that includes the liver annotations, rendering this dataset a complete one for segmenting all the tissues within the liver.

5.3. Absence of post-operative ground-truth labels and follow-up datasets

After liver resection, the surgeons/interventional radiologists are always concerned about keeping the maximum liver mass, expecting that the lost liver mass would naturally recover (Fausto, 2000). However, the liver's shape is not necessarily maintained in this growth, making it irregular in the "eyes" of ML algorithms. When trained, they are not subjected to these unfamiliar cases, rendering these algorithms helpless in these types of situations. Thus, it is out of necessity to provide a post-operative/follow-up dataset to train the algorithms to ensure that such techniques work in the best way possible, regardless of the liver shape being delineated. Moreover, if both the pre-operative and post-operative volumes of the same patient are available, it is possible to find a mapping transformation that allows the creation of synthetic patient volumes to increase the post-operative dataset size, leading to a more robust methodology for training networks.

6. Future directions

From the surveyed literature, it is evident that a lot of aspects have been tackled; however, we compiled the below aspects that we think require further research, generally related to the imaging modalities, and especially related to the liver. Fig. 11 highlights those aspects.

6.1. Inter- and intra-modality transformation

A transformation neural network should be built to transfer volumes from CT to CE-CT scans from existing datasets or create multi-phase MRI volumes from a single-phase MRI volume to allow the construction of bigger datasets. The motivation for creating a style transfer from normal CT scans to CE-CT is that the administration of contrast agents, such as iodinated contrast medium, can increase the radiation dose that organs absorb (Amato et al., 2013; Sahbaee et al., 2017). Similarly, a transformation from the MRI domain to the CT domain, or vice-versa, can also help in allowing MRI-based images to be fed immediately to a CT-based trained model instead of training the model on volumes from both modalities. Some works tackle the issue at hand, but further investigation can be clearly established to allow better inter- and intra-modality transformations. For instance, Jiang et al. (2018) utilized a GAN model to transfer volumes from CT to MRI, creating synthesized MRI volumes that are combined with a few real ones and training a U-Net for segmenting tumors within the lungs. Another approach that tackles the problem differently is depicted in Yang et al. (2019). An algorithm consists of two modules where the former decomposes volumes from both MRI and CT, using VAEs and GANs, into domain-invariant content space that contains the anatomical information, and domain-specific style space that preserves the modality information. The latter module takes the common space output from the first module and inserts it into a 2D U-Net to segment the liver.

6.2. Data augmentation

Data augmentation is important in the field of DL for increasing the input dataset size, as the input training data is not abundant, and DL models are data hungry. Data augmentation can be implemented via translating the pixels, softly/harshly rotating the slices, and horizontally and/or vertically flipping the images/volumes. All these techniques are employed to increase the dataset size. Utilizing such augmentation schemes on normal images is significant as many of them can be encountered in real-life scenarios. However, in the biomedical field, some of these augmentation techniques can be meaningless in the sense that flipping a slice/volume horizontally or vertically is not something that can be encountered. From that point of view, a better understanding of the data augmentation techniques in the biomedical field should be attained such that data augmentation do not become counter-productive.

6.3. Diagnostic report generation

As ML algorithms are increasingly getting "smarter", it is possible to devise models that can be used in the context of diagnosis. One such piece of work (Wang et al., 2020) classifies if a certain slice can be used to make a diagnostic decision. In another work, an LSTM-based language model inserts diagnostic captions with segmented tumors, which helps radiologists and surgeons in having a machine-perspective opinion of the issue at hand (Tian et al., 2018). This is important, especially in countries with enormous populations. Combining the two aforementioned works could further the technological advancements toward healthcare automation. In this way, it could be planned to automate the healthcare report generation and improve the healthcare system quality overall.

6.4. Explainable and interpretable liver tumor delineation

Explainability and interpretation are among the essential aspects when it comes to using ML and DL models in healthcare. Although ML/DL techniques have demonstrated better performance than humans in many analytical tasks, the absence of interpretations and explanations still impedes the broad utilization of these tools. Additionally, it continues to provoke critics as most ML/DL models are considered as "black-box" methods that lack interpretation (Amann et al., 2020). Thus, this can doubt the credibility of reached decisions and lack compelling evidence for convincing experts. Yet, adding interpretations and explanations is not an entirely technological problem but evokes a multitude of ethical, legal, medical, and societal queries that need to be solved and explored. To that end, an increasing interest has been shown recently in developing explainable and interpretable liver tumor delineation frameworks (Singh et al., 2020).

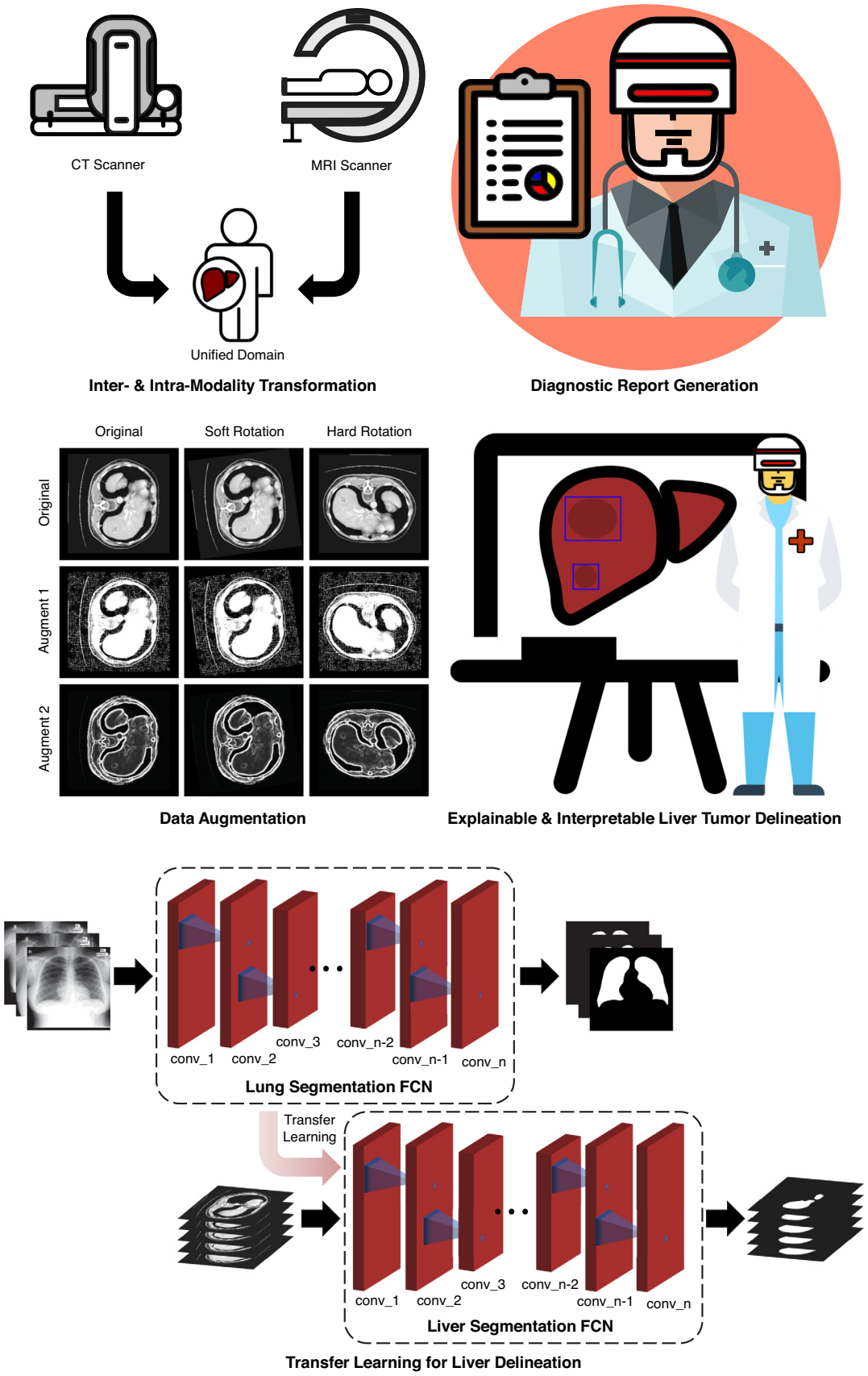

Fig. 11. Reported future directions.
Source: CT scans and liver masks are taken from Cardoso et al. (2018), while chest X-rays and lung masks are taken from Jaeger et al. (2014).

For instance, to improve segmentation defects in liver CT images, Mohagheghi and Foruzan (2022) develop an explainable DL boundary correction model. It incorporates cascaded x-Dim models (1D and 2D), which helps in refining other models' outputs and providing robust and accurate results. Typically, to refine incorrect segmented regions (slice-by-slice), a 2-step loop with a 1D local boundary validation scheme is firstly implemented before applying a 2D image patch segmentation approach. Turco et al. (2022) proposes an interpretable ML approach that characterizes benign/malignant focal liver lesions in contrast-enhanced ultrasound (CE-US) modality. Typically, it relies on defining the regions of interest, extracting spatiotemporal features, filtering for dimensionality reduction using principal component analysis (PCA), and applying different classifiers including, K-nearest neighbor (KNN), RF, SVM, logistic regression (LR), and soft voting classifier (SVC). Lastly, an explainable liver tumor delineation in surgical specimens is proposed by Zhang et al. (2021b), achieving an overall sensitivity of 94.48%, outperforming SVM by a large margin.

6.5. TL for liver delineation

It has been demonstrated in many studies, such as Prasad et al. (2021), Conze et al. (2021) and Liu et al. (2022b), that most DL models cannot accurately segment liver tissues if (i) small training datasets are considered; and/or (ii) there is a discrepancy/data distribution inconsistency between training and testing datasets, where both datasets are not withdrawn from the same distribution (Zoetmulder et al., 2022). To that end, TL has recently received increasing attention due to its ability to (i) provide high-quality decision support; (ii) require less training data compared to conventional DL algorithms; and (iii) reduce the domain shift between source domain data and target domain data. Typically, these properties came from the fact that TL models are already trained on large generic datasets. Thus, only a task-specific dataset is required to customize these models, consequently, the need to train models from scratch is eliminated. TL is based either on fine-tuning pre-trained models or DA. The former is performed by reusing previously fully trained networks with a specific dataset for a particular purpose (Karimi et al., 2021; Nowak et al., 2021). By contrast, DA is accomplished to tackle domain shifts often occuring when the medical images are recorded by different equipment or in different environments (Hong et al., 2022a). DA is mainly based on different approaches: (i) divergence-based DA; (ii) adversarial-based DA using GANs (Hong et al., 2022b); and (iii) reconstruction-based DA using stacked autoencoders (SAEs) or GANs (Yao et al., 2022).

On the other hand, labeling liver/tumor segmentation images in the target domain is a crucial challenge, which necessitates the intervention of experienced radiologists (Yao et al., 2022). Fortunately, unsupervised DA techniques help transfer knowledge across domains without the need for annotated data in the target domain. Hence, they can be beneficial in alleviating the data labeling process, which is costly and time-consuming. For instance, an unsupervised DA scheme is cross-modality liver segmentation using self-learning and joint adversarial learning that is proposed by (Yao et al., 2022). Typically, a post-situ identification strategy along with a shape-entropy-aware and joint semantic-aware adversarial learning are introduced to implicitly align the distributions of task-related characteristics derived from the target and source domains. Moving on, Hong et al. (2022a) introduce cross-modality abdominal multi-organ segmentation using source-free unsupervised DA. Similarly, a DA-based liver tumor segmentation scheme using adversarial learning in multi-phase CT images is presented in Jain et al. (2022).

7. Conclusions

We have created a survey covering the major studies available between 2014 and 2022 employing automatic ML algorithms on the liver, tumors, and/or vessel segmentation. Three tables are created to summarize and compare the different studies that delved into the challenges of the liver, tumors, and vessel segmentations. The following conclusions are drawn: (1) We summarize the existence of full liver, tumor, and vessels manual labeled datasets, highlighting that the MSDC-T8 is the most complete one; (2) For the liver segmentation task, the biggest cluster of ML algorithms fall under the 2D FCN umbrella; (3) Similarly, for the tumors segmentation task, 2D FCNs constituted the majority of ML algorithms used; (4) The common algorithms shared between the liver and tumors segmentation tasks were also highlighted; (5) Even though it is of high importance, few works have addressed the vessels segmentation task using ML techniques; (6) We identified numerous challenges and future directions for the researchers to address and improve, where the most prominent one is the absence of studies that classify all the associated tissues within the liver.

In the end, we believe that this survey is a concise and comprehensive reference that could assist the research fraternity in the field of automatic ML-based liver tissues segmentation techniques. Moreover, even though we specifically targetted the liver organ in our survey, the conclusions we came up with could be generalized to other organs as well, since many also suffer from similar issues.

CRediT authorship contribution statement

Ayman Al-Kababji: Conceptualization, Investigation, Data curation, Writing – original draft, Writing – review & editing, Project administration, Funding acquisition, Visualization. **Faycal Bensaali:** Conceptualization, Validation, Writing – review & editing, Supervision. **Sarada Prasad Dakua:** Conceptualization, Validation, Writing – review & editing, Supervision. **Yassine Himeur:** Methodology, Investigation, Data curation, Writing – review & editing, Visualization.

Declaration of competing interest

The authors declare that they have no known competing financial interests or personal relationships that could have appeared to influence the work reported in this paper.

Acknowledgments

This publication was made possible by an Award [GSRA6-2-0521-19034] from Qatar National Research Fund (a member of Qatar Foundation). The contents herein are solely the responsibility of the authors. Open Access funding provided by the Qatar National Library

References

Aghamohammadi, A., Ranjbarzadeh, R., Naiemi, F., Mogharrebi, M., Dorosti, S., Bendechache, M., 2021. TPCNN: two-path convolutional neural network for tumor and liver segmentation in CT images using a novel encoding approach. Expert Syst. Appl. 183, 115406.

Ahmad, M., Ai, D., Xie, G., Qadri, S.F., Song, H., Huang, Y., Wang, Y., Yang, J., 2019. Deep Belief Network Modeling for Automatic Liver Segmentation. IEEE Access 7, 20585–20595. http://dx.doi.org/10.1109/ACCESS.2019.2896961.

Ahmad, M., Qadri, S.F., Qadri, S., Saeed, I.A., Zareen, S.S., Iqbal, Z., Alabrah, A., Alaghbari, H.M., Rahman, M., Md, S., 2022. A lightweight convolutional neural network model for liver segmentation in medical diagnosis. Comput. Intell. Neurosci. 2022.

Ahn, S.H., Yeo, A.U., Kim, K.H., Kim, C., Goh, Y., Cho, S., Lee, S.B., Lim, Y.K., Kim, H., Shin, D., Kim, T., Kim, T.H., Youn, S.H., Oh, E.S., Jeong, J.H., 2019. Comparative clinical evaluation of atlas and deep-learning-based auto-segmentation of organ structures in liver cancer. Radiat. Oncol. 14 (1), 1–13. http://dx.doi.org/10.1186/s13014-019-1392-z.

Al-Kababji, Ayman, Bensaali, Faycal, Dakua, Sarada Prasad, 2022. Scheduling Techniques for Liver Segmentation: ReduceLRonPlateau vs OneCycleLR. In: Bennour, Akram, Ensari, Tolga, Kessentini, Yousri, Eom, Sean (Eds.), Intelligent Systems and Pattern Recognition. Springer International Publishing, Cham, ISBN: 978-3-031-08277-1, pp. 204–212.

Alahmer, H., Ahmed, A., 2016. Computer-aided Classification of Liver Lesions from CT Images Based on Multiple ROI. Procedia Comput. Sci. 90, 80–86. http://dx.doi.org/10.1016/j.procs.2016.07.027.

Alalwan, N., Abozeid, A., ElHabshy, A.A., Alzahrani, A., 2021. Efficient 3d deep learning model for medical image semantic segmentation. Alexandria Eng. J. 60 (1), 1231–1239.

Ali, A.-R., Couceiro, M., Anter, A.M., Hassanien, A.E., Tolba, M.F., Snášel, V., 2014. Liver CT image segmentation with an optimum threshold using measure of fuzziness. In: Proc. Fifth Int. Conf. Innov. Bio-Inspired Comput. Appl. IBICA 2014, Springer International Publishing, pp. 83–92.

Amann, J., Blasimme, A., Vayena, E., Frey, D., Madai, V.I., 2020. Explainability for artificial intelligence in healthcare: a multidisciplinary perspective. BMC Med. Inf. Decis. Mak. 20 (1), 1–9.

Amato, E., Salamone, I., Naso, S., Bottari, A., Gaeta, M., Blandino, A., 2013. Can Contrast Media Increase Organ Doses in CT Examinations? A Clinical Study. Amer. J. Roentgenol. 200 (6), 1288–1293.

Anter, A.M., Hassenian, A.E., 2018. Computational intelligence optimization approach based on particle swarm optimizer and neutrosophic set for abdominal CT liver tumor segmentation. J. Comput. Sci. 25, 376–387. http://dx.doi.org/10.1016/j.jocs.2018.01.003.

Anter, A.M., Hassenian, A.E., 2019. CT liver tumor segmentation hybrid approach using neutrosophic sets, fast fuzzy c-means and adaptive watershed algorithm. Artif. Intell. Med. 97, 105–117. http://dx.doi.org/10.1016/j.artmed.2018.11.007.

Araújo, J.D.L., da Cruz, L.B., Ferreira, J.L., da Silva Neto, O.P., Silva, A.C., de Paiva, A.C., Gattass, M., 2021. An automatic method for segmentation of liver lesions in computed tomography images using deep neural networks. Expert Syst. Appl. 180 (April), 0–2. http://dx.doi.org/10.1016/j.eswa.2021.115064.

Araújo, J.D.L., da Cruz, L.B., Diniz, J.O.B., Ferreira, J.L., Silva, A.C., de Paiva, A.C., Gattass, M., 2022. Liver segmentation from computed tomography images using cascade deep learning. Comput. Biol. Med. 140, 105095.

Asrani, S.K., Devarbhavi, H., Eaton, J., Kamath, P.S., 2019. Burden of liver diseases in the world. J. Hepatol. 70 (1), 151–171. http://dx.doi.org/10.1016/j.jhep.2018.09.014.

Bai, Z., Jiang, H., Li, S., Yao, Y.D., 2019. Liver Tumor Segmentation Based on Multi-Scale Candidate Generation and Fractal Residual Network. IEEE Access 7, 82122–82133. http://dx.doi.org/10.1109/ACCESS.2019.2923218.

Bilic, P., Christ, P.F., Vorontsov, E., Chlebus, G., Chen, H., Dou, Q., Fu, C., Han, X., Heng, P., Hesser, J., Kadoury, S., Konopczynski, T.K., Le, M., Li, C., Li, X., Lipková, J., Lowengrub, J.S., Meine, H., Moltz, J.H., Pal, C., Piraud, M., Qi, X., Qi, J., Rempfler, M., Roth, K., Schenk, A., Sekuboyina, A., Zhou, P., Hülsemeyer, C., Beetz, M., Ettlinger, F., Grün, F., Kaissis, G., Lohöfer, F., Braren, R., Holch, J., Hofmann, F., Sommer, W.H., Heinemann, V., Jacobs, C., Mamani, G.E.H., van Ginneken, B., Chartrand, G., Tang, A., Drozdzal, M., Ben-Cohen, A., Klang, E., Amitai, M.M., Konen, E., Greenspan, H., Moreau, J., Hostettler, A., Soler, L., Vivanti, R., Szeskin, A., Lev-Cohain, N., Sosna, J., Joskowicz, L., Menze, B.H., 2019. The liver tumor segmentation benchmark (LiTS). arXiv:1901.04056.

Cai, J., 2019. Segmentation and Diagnosis of Liver Carcinoma Based on Adaptive Scale-Kernel Fuzzy Clustering Model for CT Images. J. Med. Syst. 43 (11), http://dx.doi.org/10.1007/s10916-019-1459-2.

Cai, J., Tang, Y., Lu, L., Harrison, A.P., Yan, K., Xiao, J., Yang, L., Summers, R.M., 2018. Accurate weakly-supervised deep lesion segmentation using large-scale clinical annotations: slice-propagated 3D mask generation from 2D RECIST. In: Med. Image Comput. Comput. Interv. MICCAI 2018, Springer International Publishing, pp. 396–404. http://dx.doi.org/10.1007/978-3-030-00937-3.

Campadelli, P., Casiraghi, E., Esposito, A., 2009. Liver segmentation from computed tomography scans: A survey and a new algorithm. Artif. Intell. Med. 45 (2–3), 185–196. http://dx.doi.org/10.1016/j.artmed.2008.07.020.

Cano-Espinosa, C., Gonzalez, G., Washko, G.R., Cazorla, M., Estepar, R.S.J., 2020. Biomarker Localization from Deep Learning Regression Networks. IEEE Trans. Med. Imaging 39 (6), 2121–2132. http://dx.doi.org/10.1109/TMI.2020.2965486.

Cardoso, M.J., Simpson, A., Ronneberger, O., Menze, B., van Ginneken, B., Landman, B., Litjens, G., Farahani, K., Summers, R., Maier-Hein, L., Kopp-Schneider, A., Bakas, S., Antonelli, M., 2018. Medical segmentation decathlon challenge. URL http://medicaldecathlon.com/index.html.

Çiçek, Ö., Abdulkadir, A., Lienkamp, S.S., Brox, T., Ronneberger, O., 2016. 3D U-net: learning dense volumetric segmentation from sparse annotation. In: Med. Image Comput. Comput. Assist. Interv. MICCAI 2016, Springer International Publishing, pp. 424–432. http://dx.doi.org/10.1007/978-3-319-46723-8_49.

Chang, L., 2018. CT scan (CAT scan): purpose, procedure, risks, side-effects, results. URL https://www.webmd.com/cancer/what-is-a-ct-scan#2.

Cheema, M.N., Nazir, A., Sheng, B., Li, P., Qin, J., Feng, D.D., 2019. Liver Extraction Using Residual Convolution Neural Networks From Low-Dose CT Images. IEEE Trans. Biomed. Eng. 66 (9), 2641–2650.

Chen, Y., Li, S., Yang, S., Luo, W., 2019a. Liver segmentation in CT images with adversarial learning. In: Int. Conf. Intell. Comput. Springer International Publishing, pp. 470–480. http://dx.doi.org/10.1007/978-3-030-26763-6_45.

Chen, G.H., Shah, D., Golland, P., 2015. A latent source model for patch-based image segmentation. In: Med. Image Comput. Comput. Interv. MICCAI 2015, Springer International Publishing, pp. 140–148. http://dx.doi.org/10.1007/978-3-319-24574-4_17.

Chen, L., Song, H., Wang, C., Cui, Y., Yang, J., Hu, X., Zhang, L., 2019b. Liver tumor segmentation in CT volumes using an adversarial densely connected network. BMC Bioinformatics 20 (Suppl. 16), 1–13. http://dx.doi.org/10.1186/s12859-019-3069-x.

Chi, J., Han, X., Wu, C., Wang, H., Ji, P., 2021. X-net: Multi-branch unet-like network for liver and tumor segmentation from 3d abdominal ct scans. Neurocomputing 459, 81–96.

Chlebus, G., Schenk, A., Moltz, J.H., van Ginneken, B., Hahn, H.K., Meine, H., 2018. Automatic liver tumor segmentation in CT with fully convolutional neural networks and object-based postprocessing. Sci. Rep. 8 (1), 1–7. http://dx.doi.org/10.1038/s41598-018-33860-7.

Christ, P., 2017. CodaLab - LiTS - liver tumor segmentation challenge. URL https://competitions.codalab.org/competitions/17094#learn_the_details-overview.

Christ, P.F., Elshaer, M.E.A., Ettlinger, F., Tatavarty, S., Bickel, M., Bilic, P., Rempfler, M., Armbruster, M., Hofmann, F., D'Anastasi, M., Sommer, W.H., Ahmadi, S.A., Menze, B.H., 2016. Automatic liver and lesion segmentation in CT using cascaded fully convolutional neural networks and 3D conditional random fields. In: Med. Image Comput. Comput. Interv. MICCAI 2016, Springer International Publishing, pp. 415–423. http://dx.doi.org/10.1007/978-3-319-46723-8_48.

Christ, P.F., Ettlinger, F., Grün, F., Elshaera, M.E.A., Lipkova, J., Schlecht, S., Ahmaddy, F., Tatavarty, S., Bickel, M., Bilic, P., Rempfler, M., Hofmann, F., Anastasi, M.D., Ahmadi, S.-A., Kaissis, G., Holch, J., Sommer, W., Braren, R., Heinemann, V., Menze, B., 2017. Automatic liver and tumor segmentation of CT and MRI volumes using cascaded fully convolutional neural networks. arXiv:1702.05970.

Chung, M., Lee, J., Lee, M., Lee, J., Shin, Y.G., 2020. Deeply self-supervised contour embedded neural network applied to liver segmentation. Comput. Methods Programs Biomed. 192, 105447. http://dx.doi.org/10.1016/j.cmpb.2020.105447.

Clark, Kenneth, Vendt, Bruce, Smith, Kirk, Freymann, John, Kirby, Justin, Koppel, Paul, Moore, Stephen, Phillips, Stanley, Maffitt, David, Pringle, Michael, et al., 2013. The Cancer Imaging Archive (TCIA): maintaining and operating a public information repository. Journal of Digital Imaging 26 (6), 1045–1057. http://dx.doi.org/10.1007/s10278-013-9622-7, https://www.cancerimagingarchive.net/.

Conze, P.-H., Kavur, A.E., Cornec-Le Gall, E., Gezer, N.S., Le Meur, Y., Selver, M.A., Rousseau, F., 2021. Abdominal multi-organ segmentation with cascaded convolutional and adversarial deep networks. Artif. Intell. Med. 117, 102109.

Das, A., Das, P., Panda, S.S., Sabut, S., 2019. Detection of Liver Cancer Using Modified Fuzzy Clustering and Decision Tree Classifier in CT Images. Pattern Recognit. Image Anal. 29 (2), 201–211. http://dx.doi.org/10.1134/S1054661819020056.

Das, A., Sabut, S.K., 2016. Kernelized Fuzzy C-means Clustering with Adaptive Thresholding for Segmenting Liver Tumors. Procedia Comput. Sci. 92, 389–395. http://dx.doi.org/10.1016/j.procs.2016.07.395.

Dey, R., Hong, Y., 2018. CompNet: complementary segmentation network for brain MRI extraction. In: Med. Image Comput. Comput. Assist. Interv. MICCAI 2018, Springer International Publishing, pp. 628–636. http://dx.doi.org/10.1007/978-3-030-00931-1_72.

Dey, R., Hong, Y., 2020. Hybrid cascaded neural network for liver lesion segmentation. In: 2020 IEEE 17th Int. Symp. Biomed. Imaging. pp. 1173–1177. http://dx.doi.org/10.1109/ISBI45749.2020.9098656, arXiv:1909.04797.

Di, S., Zhao, Y., Liao, M., Yang, Z., Zeng, Y., 2022. Automatic liver tumor segmentation from ct images using hierarchical iterative superpixels and local statistical features. Expert Syst. Appl. 203, 117347.

Dou, Q., Chen, H., Jin, Y., Yu, L., Qin, J., Heng, P.-A., 2016. 3D deeply supervised network for automatic liver segmentation from CT volumes. In: Med. Image Comput. Comput. Interv. MICCAI 2016, Springer International Publishing, pp. 149–157. http://dx.doi.org/10.1007/978-3-319-46723-8_18.

Dou, Q., Yu, L., Chen, H., Jin, Y., Yang, X., Qin, J., Heng, P.A., 2017. 3D deeply supervised network for automated segmentation of volumetric medical images. Med. Image Anal. 41, 40–54. http://dx.doi.org/10.1016/j.media.2017.05.001.

Fang, X., Xu, S., Wood, B.J., Yan, P., 2020. Deep learning-based liver segmentation for fusion-guided intervention. Int. J. Comput. Assist. Radiol. Surg. 15 (6), 963–972. http://dx.doi.org/10.1007/s11548-020-02147-6.

Fang, X., Yan, P., 2020. Multi-Organ Segmentation Over Partially Labeled Datasets With Multi-Scale Feature Abstraction. IEEE Trans. Med. Imaging 39 (11), 3619–3629. http://dx.doi.org/10.1109/TMI.2020.3001036.

Fausto, N., 2000. Liver regeneration. J. Hepatol. 32, 19–31.

Fretland, Å.A., Kazaryan, A.M., Bjørnbeth, B.A., Flatmark, K., Andersen, M.H., Tønnessen, T.I., Bjørnelv, G.M.W., Fagerland, M.W., Kristiansen, R., Øyri, K., et al., 2015. Open versus laparoscopic liver resection for colorectal liver metastases (the oslo-comet study): study protocol for a randomized controlled trial. Trials 16 (1), 1–10.

Garg, A., Mago, V., 2021. Role of machine learning in medical research: A survey. Comp. Sci. Rev. 40, 100370.

Gibson, E., Giganti, F., Hu, Y., Bonmati, E., Bandula, S., Gurusamy, K., Davidson, B.R., Pereira, S.P., Clarkson, M.J., Barratt, D.C., 2017. Towards image-guided pancreas and biliary endoscopy: automatic multi-organ segmentation on abdominal CT with dense dilated networks. In: Med. Image Comput. Comput. Interv. MICCAI 2017, Springer International Publishing, pp. 728–736. http://dx.doi.org/10.1007/978-3-319-66182-7_83.

Gibson, E., Giganti, F., Hu, Y., Bonmati, E., Bandula, S., Gurusamy, K., Davidson, B., Pereira, S.P., Clarkson, M.J., Barratt, D.C., 2018a. Automatic Multi-Organ Segmentation on Abdominal CT with Dense V-Networks. IEEE Trans. Med. Imaging 37 (8), 1822–1834. http://dx.doi.org/10.1109/TMI.2018.2806309.

Gibson, E., Giganti, F., Hu, Y., Bonmati, E., Bandula, S., Gurusamy, K., Davidson, B., Pereira, S.P., Clarkson, M.J., Barratt, D.C., 2018c. Multi-organ Abdominal CT Reference Standard Segmentations, This data set was developed as part of independent research supported by Cancer Research UK (Multidisciplinary C28070/A19985) and the National Institute for Health Research UCL/UCL Hospitals Biomedical Research Centre. http://dx.doi.org/10.5281/zenodo.1169361.

Gibson, E., Li, W., Sudre, C., Fidon, L., Shakir, D.I., Wang, G., Eaton-Rosen, Z., Gray, R., Doel, T., Hu, Y., Whyntie, T., Nachev, P., Modat, M., Barratt, D.C., Ourselin, S., Cardoso, M.J., Vercauteren, T., 2018b. NiftyNet: a deep-learning platform for medical imaging. Comput. Methods Programs Biomed. 158, 113–122. http://dx.doi.org/10.1016/j.cmpb.2018.01.025, arXiv:1709.03485.

Goodfellow, I., Bengio, Y., Courville, A., 2016. Deep Learning. MIT Press.

Gotra, A., Sivakumaran, L., Chartrand, G., Vu, K.N., Vandenbroucke-Menu, F., Kauffmann, C., Kadoury, S., Gallix, B., de Guise, J.A., Tang, A., 2017. Liver segmentation: indications, techniques and future directions. Insights Imaging 8 (4), 377–392. http://dx.doi.org/10.1007/s13244-017-0558-1.

Guo, H., Yang, D., 2020. PRDNet: Medical image segmentation based on parallel residual and dilated network. Measurement 173 (October), http://dx.doi.org/10.1016/j.measurement.2020.108661.

Hamarneh, G., Jassi, P., 2010. VascuSynth: Simulating vascular trees for generating volumetric image data with ground-truth segmentation and tree analysis. Comput. Med. Imaging Graph. 34 (8), 605–616.

Han, X., 2017. Automatic liver lesion segmentation using a deep convolutional neural network method. arXiv:arXiv:1704.07239v1.

Han, L., Chen, Y., Li, J., Zhong, B., Lei, Y., Sun, M., 2021b. Liver segmentation with 2.5d perpendicular unets. Comput. Electr. Eng. 91, 107118.

Han, Y., Li, X., Wang, B., Wang, L., 2021a. Boundary loss-based ?2.5 D fully convolutional neural networks approach for segmentation: a case study of the liver and tumor on computed tomography. Algorithms 14 (5), 144.

Hanbury, A., 2016. VISCERAL - Anatomy3 continuous evaluation. URL http://www.visceral.eu/benchmarks/anatomy3-open/.

Hao, W., Zhang, J., Su, J., Song, Y., Liu, Z., 2022. Hpm-net: Hierarchical progressive multiscale network for liver vessel segmentation in ct images. Comput. Methods Programs Biomed. 107003.

He, T., Hu, J., Song, Y., Guo, J., Yi, Z., 2020. Multi-task learning for the segmentation of organs at risk with label dependence. Med. Image Anal. 61, http://dx.doi.org/10.1016/j.media.2020.101666.

He, B., Huang, C., Sharp, G., Zhou, S., Hu, Q., Fang, C., Fan, Y., Jia, F., 2016. Fast automatic 3D liver segmentation based on a three-level AdaBoost-guided active shape model. Med. Phys. 43 (5), 2421–2434. http://dx.doi.org/10.1118/1.4946817.

Heimann, T., van Ginneken, B., Styner, M.A., Humpire, G., 2007. SLIVER07 - grand challenge. URL https://sliver07.grand-challenge.org/Home/.

Heimann, T., Van Ginneken, B., Styner, M.A., Arzhaeva, Y., Aurich, V., Bauer, C., Beck, A., Becker, C., Beichel, R., Bekes, G., Bello, F., Binnig, G., Bischof, H., Bornik, A., Cashman, P.M., Chi, Y., Córdova, A., Dawant, B.M., Fidrich, M., Furst, J.D., Furukawa, D., Grenacher, L., Hornegger, J., Kainmüller, D., Kitney, R.I., Kobatake, H., Lamecker, H., Lange, T., Lee, J., Lennon, B., Li, R., Li, S., Meinzer, H.P., Németh, G., Raicu, D.S., Rau, A.M., Van Rikxoort, E.M., Rousson, M., Ruskó, L., Saddi, K.A., Schmidt, G., Seghers, D., Shimizu, A., Slagmolen, P., Sorantin, E., Soza, G., Susomboon, R., Waite, J.M., Wimmer, A., Wolf, I., 2009. Comparison and Evaluation of Methods for Liver Segmentation from CT Datasets. IEEE Trans. Med. Imaging 28 (8), 1251–1265. http://dx.doi.org/10.1109/TMI.2009.2013851.

Heinrich, M.P., 2019. Closing the gap between deep and conventional image registration using probabilistic dense displacement networks. In: Med. Image Comput. Comput. Assist. Interv. MICCAI 2019, Springer International Publishing, pp. 50–58. http://dx.doi.org/10.1007/978-3-030-32226-7_6.

Hong, J., Yu, S.C.-H., Chen, W., 2022b. Unsupervised domain adaptation for cross-modality liver segmentation via joint adversarial learning and self-learning. Appl. Soft Comput. 121, 108729.

Hong, J., Zhang, Y.-D., Chen, W., 2022a. Source-free unsupervised domain adaptation for cross-modality abdominal multi-organ segmentation. Knowl.-Based Syst. 109155.

Hu, P., Wu, F., Peng, J., Bao, Y., Chen, F., Kong, D., 2017. Automatic abdominal multi-organ segmentation using deep convolutional neural network and time-implicit level sets. Int. J. Comput. Assist. Radiol. Surg. 12 (3), 399–411. http://dx.doi.org/10.1007/s11548-016-1501-5.

Hu, P., Wu, F., Peng, J., Liang, P., Kong, D., 2016. Automatic 3D liver segmentation based on deep learning and globally optimized surface evolution. Phys. Med. Biol. 61 (24), 8676–8698. http://dx.doi.org/10.1088/1361-6560/61/24/8676.

Huang, Q., Ding, H., Wang, X., Wang, G., 2018a. Fully automatic liver segmentation in CT images using modified graph cuts and feature detection. Comput. Biol. Med. 95 (February), 198–208. http://dx.doi.org/10.1016/j.compbiomed.2018.02.012.

Huang, C., Han, H., Yao, Q., Zhu, S., Zhou, K.S., 2019. 3D U^2-net: a 3D universal U-net for multi-domain medical image segmentation. In: Med. Image Comput. Comput. Assist. Interv. MICCAI 2019, Springer International Publishing, pp. 291–299. http://dx.doi.org/10.1007/978-3-030-32245-8_33.

Huang, Q., Sun, J., Ding, H., Wang, X., Wang, G., 2018b. Robust liver vessel extraction using 3D U-Net with variant dice loss function. Comput. Biol. Med. 101 (March), 153–162. http://dx.doi.org/10.1016/j.compbiomed.2018.08.018.

IRCAD, 2010. 3Dircadb | IRCAD France. URL https://www.ircad.fr/research/3dircadb/.

Irving, B., Hutton, C., Dennis, A., Vikal, S., Mavar, M., Kelly, M., Brady, J.M., 2017. Deep quantitative liver segmentation and vessel exclusion to assist in liver assessment. In: Annu. Conf. Med. Image Underst. Anal. Springer International Publishing, pp. 663–673. http://dx.doi.org/10.1007/978-3-319-60964-5_58.

Ivashchenko, O.V., Rijkhorst, E.J., ter Beek, L.C., Hoetjes, N.J., Pouw, B., Nijkamp, J., Kuhlmann, K.F., Ruers, T.J., 2020. A workflow for automated segmentation of the liver surface, hepatic vasculature and biliary tree anatomy from multiphase MR images. Magn. Reson. Imaging 68 (2019), 53–65. http://dx.doi.org/10.1016/j.mri.2019.12.008.

Jaeger, S., Candemir, S., Antani, S., Wáng, Y.-X.J., Lu, P.-X., Thoma, G., 2014. Two public chest X-ray datasets for computer-aided screening of pulmonary diseases. Quant. Imaging Med. Surg. 4 (6), 475.

Jain, R.K., Sato, T., Watasue, T., Nakagawa, T., Iwamoto, Y., Han, X., Lin, L., Hu, H., Ruan, X., Chen, Y.-W., 2022. Unsupervised domain adaptation with adversarial learning for liver tumors detection in multi-phase ct images. In: Innovation in Medicine and Healthcare. Springer, pp. 149–159.

Jansen, M.J.A., Kuijf, H.J., Niekel, M., Veldhuis, W.B., Wessels, F.J., Viergever, M.A., Pluim, J.P.W., 2019. Liver segmentation and metastases detection in MR images using convolutional neural networks. J. Med. Imaging 6 (4), 1. http://dx.doi.org/10.1117/1.jmi.6.4.044003, arXiv:1910.06635.

Jassi, P., Hamarneh, G., 2011. Vascusynth: Vascular tree synthesis software. Insight J. 1–12, URL http://vascusynth.cs.sfu.ca/Welcome.html.

Jiang, J., Hu, Y.-C., Tyagi, N., Zhang, P., Rimner, A., Mageras, G.S., Deasy, J.O., Veeraraghavan, H., 2018. Tumor-aware, adversarial domain adaptation from CT to MRI for lung cancer segmentation. In: Med. Image Comput. Comput. Assist. Interv. MICCAI 2018, Springer International Publishing, pp. 777–785. http://dx.doi.org/10.1007/978-3-030-00934-2_86.

Jiang, H., Shi, T., Bai, Z., Huang, L., 2019. AHCNet: An Application of Attention Mechanism and Hybrid Connection for Liver Tumor Segmentation in CT Volumes. IEEE Access 7, 24898–24909. http://dx.doi.org/10.1109/ACCESS.2019.2899608.

Jimenez-del-Toro, O., Müller, H., Krenn, M., Gruenberg, K., Taha, A.A., Winterstein, M., Eggel, I., Foncubierta-Rodríguez, A., Goksel, O., Jakab, A., Kontokotsios, G., Langs, G., Menze, B.H., Salas Fernandez, T., Schaer, R., Walleyo, A., Weber, M., Dicente Cid, Y., Gass, T., Heinrich, M., Jia, F., Kahl, F., Kechichian, R., Mai, D., Spanier, A.B., Vincent, G., Wang, C., Wyeth, D., Hanbury, A., 2016. Cloud-Based Evaluation of Anatomical Structure Segmentation and Landmark Detection Algorithms: VISCERAL Anatomy Benchmarks. IEEE Trans. Med. Imaging 35 (11), 2459–2475.

Jin, Q., Meng, Z., Sun, C., Cui, H., Su, R., 2020. RA-UNet: A Hybrid Deep Attention-Aware Network to Extract Liver and Tumor in CT Scans. Front. Bioeng. Biotechnol. 8, 1471. http://dx.doi.org/10.3389/fbioe.2020.605132.

Kakeya, H., Okada, T., Oshiro, Y., 2018. 3D U-JAPA-net: mixture of convolutional networks for abdominal multi-organ CT segmentation. In: Med. Image Comput. Comput. Assist. Interv. MICCAI 2018, Springer International Publishing, pp. 426–433. http://dx.doi.org/10.1007/978-3-030-00937-3_49.

Kamnitsas, K., Ledig, C., Newcombe, V.F., Simpson, J.P., Kane, A.D., Menon, D.K., Rueckert, D., Glocker, B., 2017. Efficient multi-scale 3D CNN with fully connected CRF for accurate brain lesion segmentation. Med. Image Anal. 36, 61–78.

Karimi, D., Warfield, S.K., Gholipour, A., 2021. Transfer learning in medical image segmentation: New insights from analysis of the dynamics of model parameters and learned representations. Artif. Intell. Med. 116, 102078.

Kavur, A. Emre, Gezer, N. Sinem, Barış, Mustafa, Aslan, Sinem, Conze, Pierre-Henri, Groza, Vladimir, Pham, Duc Duy, Chatterjee, Soumick, Ernst, Philipp, Özkan, Savaş, Baydar, Bora, Lachinov, Dmitry, Han, Shuo, Pauli, Josef, Isensee, Fabian, Perkonigg, Matthias, Sathish, Rachana, Rajan, Ronnie, Sheet, Debdoot, Dovletov, Gurbandurdy, Speck, Oliver, Nürnberger, Andreas, Maier-Hein, Klaus H., Bozdağı Akar, Gözde, Ünal, Gözde, Dicle, Oğuz, Selver, M. Alper, 2021. CHAOS Challenge - combined (CT-MR) healthy abdominal organ segmentation. Med. Image Anal. (ISSN: 1361-8415) 69, 101950. http://dx.doi.org/10.1016/j.media.2020.101950, https://www.sciencedirect.com/science/article/pii/S1361841520303145.

Kitrungrotsakul, T., Han, X.H., Iwamoto, Y., Lin, L., Foruzan, A.H., Xiong, W., Chen, Y.W., 2019. VesselNet: A deep convolutional neural network with multi pathways for robust hepatic vessel segmentation. Comput. Med. Imaging Graph. 75, 74–83. http://dx.doi.org/10.1016/j.compmedimag.2019.05.002.

Kitware Inc., 2010a. MIDAS - the digital archiving system. URL https://www.insight-journal.org/midas/.

Kitware Inc., 2010b. MIDAS - Collection livers and liver tumors with expert hand segmentations. URL https://www.insight-journal.org/midas/collection/view/38.

Landman, B., Xu, Z., Igelsias, J.E., Styner, M., Langerak, T.R., Klein, A., 2015. 2015 MICCAI multi-atlas labeling beyond the cranial vault - workshop and challenge. http://dx.doi.org/10.7303/syn3193805.

Li, X., Chen, H., Qi, X., Dou, Q., Fu, C.W., Heng, P.A., 2018. H-DenseUNet: Hybrid Densely Connected UNet for Liver and Tumor Segmentation from CT Volumes. IEEE Trans. Med. Imaging 37 (12), 2663–2674. http://dx.doi.org/10.1109/TMI.2018.2845918, arXiv:1709.07330.

Li, R., Huang, Y.-J., Chen, H., Liu, X., Yu, Y., Qian, D., Wang, L., 2021b. 3d graph-connectivity constrained network for hepatic vessel segmentation. IEEE J. Biomed. Health Inf. 26 (3), 1251–1262.

Li, W., Jia, F., Hu, Q., 2015. Automatic Segmentation of Liver Tumor in CT Images with Deep Convolutional Neural Networks. J. Comput. Commun. 03 (11), 146–151. http://dx.doi.org/10.4236/jcc.2015.311023.

Li, J., Ou, X., Shen, N., Sun, J., Ding, J., Zhang, J., Yao, J., Wang, Z., 2021a. Study on strategy of CT image sequence segmentation for liver and tumor based on U-Net and Bi-ConvLSTM. Expert Syst. Appl. 180 (333), 115008. http://dx.doi.org/10.1016/j.eswa.2021.115008.

Li, C., Tan, Y., Chen, W., Luo, X., He, Y., Gao, Y., Li, F., 2020. ANU-Net: Attention-based nested U-Net to exploit full resolution features for medical image segmentation. Comput. Graph. 90, 11–20. http://dx.doi.org/10.1016/j.cag.2020.05.003.

Liang, F., Qian, P., Su, K.H., Baydoun, A., Leisser, A., Van Hedent, S., Kuo, J.W., Zhao, K., Parikh, P., Lu, Y., Traughber, B.J., Muzic, R.F., 2018. Abdominal, multi-organ, auto-contouring method for online adaptive magnetic resonance guided radiotherapy: An intelligent, multi-level fusion approach. Artif. Intell. Med. 90 (2017), 34–41. http://dx.doi.org/10.1016/j.artmed.2018.07.001.

Liu, M., Vanguri, R., Mutasa, S., Ha, R., Liu, Y.C., Button, T., Jambawalikar, S., 2020. Channel width optimized neural networks for liver and vessel segmentation in liver iron quantification. Comput. Biol. Med. 122 (May), 103798. http://dx.doi.org/10.1016/j.compbiomed.2020.103798.

Liu, S., Xu, D., Zhou, S.K., Pauly, O., Grbic, S., Mertelmeier, T., Wicklein, J., Jerebko, A., Cai, W., Comaniciu, D., 2018. 3D anisotropic hybrid network: transferring convolutional features from 2D images to 3D anisotropic volumes. In: Med. Image Comput. Comput. Interv. MICCAI 2018, Springer International Publishing, pp. 851–858. http://dx.doi.org/10.1007/978-3-030-00934-2_94.

Liu, Y., Yang, F., Yang, Y., 2022b. Free-form lesion synthesis using a partial convolution generative adversarial network for enhanced deep learning liver tumor segmentation. arXiv preprint arXiv:2206.09065.

Liu, Y., Zhang, X., Kuang, H., Yang, Z., Yan, S., Zhai, P., Zhang, L., 2022a. Su-unet: A novel self-updating network for hepatic vessel segmentation in ct images. In: 2022 the 5th International Conference on Image and Graphics Processing. ICIGP, pp. 214–219.

Lombaert, H., Zikic, D., Criminisi, A., Ayache, N., 2014. Laplacian forests: semantic image segmentation by guided bagging. In: Med. Image Comput. Comput. Interv. MICCAI 2014, Springer International Publishing, pp. 496–504. http://dx.doi.org/10.1007/978-3-319-10470-6_62.

Lu, F., Wu, F., Hu, P., Peng, Z., Kong, D., 2016. Automatic 3D liver location and segmentation via convolutional neural network and graph cut. Int. J. Comput. Assist. Radiol. Surg. 12 (2), 171–182. http://dx.doi.org/10.1007/s11548-016-1467-3, arXiv:1605.03012.

Lv, P., Wang, J., Wang, H., 2022. ?2.5D lightweight ?RIU-Net for automatic liver and tumor segmentation from ?CT. Biomed. Signal Process. Control 75, 103567.

Ma, J., Deng, Y., Ma, Z., Mao, K., Chen, Y., 2021. A liver segmentation method based on the fusion of vnet and wgan. Comput. Math. Methods Med. 2021.

Maaref, A., Romero, F.P., Montagnon, E., Cerny, M., Nguyen, B., Vandenbroucke, F., Soucy, G., Turcotte, S., Tang, A., Kadoury, S., 2020. Predicting the Response to FOLFOX-Based Chemotherapy Regimen from Untreated Liver Metastases on Baseline CT: a Deep Neural Network Approach. J. Digit. Imaging http://dx.doi.org/10.1007/s10278-020-00332-2.

Mendizabal, A., Márquez-Neila, P., Cotin, S., 2020. Simulation of hyperelastic materials in real-time using deep learning. Med. Image Anal. 59, 101569. http://dx.doi.org/10.1016/j.media.2019.101569, arXiv:1904.06197.

Meng, L., Zhang, Q., Bu, S., 2021. Two-stage liver and tumor segmentation algorithm based on convolutional neural network. Diagnostics 11 (10), 1806.

Mishra, D., Chaudhury, S., Sarkar, M., Soin, A.S., 2019. Ultrasound Image Segmentation: A Deeply Supervised Network With Attention to Boundaries. IEEE Trans. Biomed. Eng. 66 (6), 1637–1648. http://dx.doi.org/10.1109/TBME.2018.2877577.

Mohagheghi, S., Foruzan, A.H., 2020. Incorporating prior shape knowledge via data-driven loss model to improve 3D liver segmentation in deep CNNs. Int. J. Comput. Assist. Radiol. Surg. 15 (2), 249–257. http://dx.doi.org/10.1007/s11548-019-02085-y.

Mohagheghi, S., Foruzan, A.H., 2022. Developing an explainable deep learning boundary correction method by incorporating cascaded x-dim models to improve segmentation defects in liver ct images. Comput. Biol. Med. 140, 105106.

Montaña-Brown, N., Ramalhinho, J., Allam, M., Davidson, B., Hu, Y., Clarkson, M.J., 2021. Vessel segmentation for automatic registration of untracked laparoscopic ultrasound to ct of the liver. Int. J. Comput. Assist. Radiol. Surg. 16 (7), 1151–1160.

Nanda, N., Kakkar, P., Nagpal, S., 2019. Computer-Aided Segmentation of Liver Lesions in CT Scans Using Cascaded Convolutional Neural Networks and Genetically Optimised Classifier. Arab. J. Sci. Eng. 44 (4), 4049–4062. http://dx.doi.org/10.1007/s13369-019-03735-8.

Nasiri, N., Foruzan, A.H., Chen, Y.-W., 2020. Integration of a knowledge-based constraint into generative models with applications in semi-automatic segmentation of liver tumors. Biomed. Signal Process. Control 57, 101725. http://dx.doi.org/10.1016/j.bspc.2019.101725, URL https://www.sciencedirect.com/science/article/pii/S1746809419303064.

Norajitra, T., Maier-hein, K.H., 2017. 3D Statistical Shape Models Incorporating Landmark-Wise Random Regression Forests for Omni-Directional Landmark Detection. IEEE Trans. Med. Imaging 36 (1), 155–168.

Novikov, A.A., Major, D., Wimmer, M., Lenis, D., Buhler, K., 2019. Deep sequential segmentation of organs in volumetric medical scans. IEEE Trans. Med. Imaging 38 (5), 1207–1215. http://dx.doi.org/10.1109/TMI.2018.2881678, arXiv:1807.02437.

Nowak, S., Mesropyan, N., Faron, A., Block, W., Reuter, M., Attenberger, U.I., Luetkens, J.A., Sprinkart, A.M., 2021. Detection of liver cirrhosis in standard t2-weighted mri using deep transfer learning. Eur. Radiol. 31 (11), 8807–8815.

Ouhmich, F., Agnus, V., Noblet, V., Heitz, F., Pessaux, P., 2019. Liver tissue segmentation in multiphase CT scans using cascaded convolutional neural networks. Int. J. Comput. Assist. Radiol. Surg. 14 (8), 1275–1284. http://dx.doi.org/10.1007/s11548-019-01989-z.

Pang, S., Du, A., Orgun, M.A., Yu, Z., Wang, Y., Wang, Y., Liu, G., 2020. CTumorGAN: a unified framework for automatic computed tomography tumor segmentation. Eur. J. Nucl. Med. Mol. Imaging 47 (10), 2248–2268. http://dx.doi.org/10.1007/s00259-020-04781-3.

Perslev, M., Dam, E.B., Pai, A., Igel, C., 2019. One network to segment them all: a general, lightweight system for accurate 3D medical image segmentation. In: Med. Image Comput. Comput. Assist. Interv. MICCAI 2019, pp. 30–38. http://dx.doi.org/10.1007/978-3-030-32245-8_4.

Prasad, P.J.R., Elle, O.J., Lindseth, F., Albregtsen, F., Kumar, R.P., 2021. Modifying u-net for small dataset: a simplified u-net version for liver parenchyma segmentation. In: Medical Imaging 2021: Computer-Aided Diagnosis, Vol. 11597. SPIE, pp. 396–405.

Qayyum, A., Lalande, A., Meriaudeau, F., 2020. Automatic segmentation of tumors and affected organs in the abdomen using a 3D hybrid model for computed tomography imaging. Comput. Biol. Med. 127 (October), 104097. http://dx.doi.org/10.1016/j.compbiomed.2020.104097.

Qin, W., Wu, J., Han, F., Yuan, Y., Zhao, W., Ibragimov, B., Gu, J., Xing, L., 2018. Superpixel-based and boundary sensitive convolutional neural network for automated liver segmentation. Phys. Med. Biol. 63 (9), http://dx.doi.org/10.1088/1361-6560/aabd19.

Ranjbarzadeh, R., Saadi, S.B., 2020. Automated liver and tumor segmentation based on concave and convex points using fuzzy c-means and mean shift clustering. Measurement 150, 107086.

Rickmann, A.-M., Roy, A.G., Sarasua, I., Navab, N., Wachinger, C., 2019. 'Project & excite' modules for segmentation of volumetric medical scans. In: Med. Image Comput. Comput. Assist. Interv. MICCAI 2019, pp. 39–47. http://dx.doi.org/10.1007/978-3-030-32245-8_5.

Rister, B., Shivakumar, K., Nobashi, T., Rubin, D.L., 2019. CT-ORG: CT volumes with multiple organ segmentations [Dataset]. http://dx.doi.org/10.7937/TCIA.2019.TT7F4V7O, URL https://wiki.cancerimagingarchive.net/x/OgWkAw.

Ronneberger, O., Fischer, P., Brox, T., 2015. U-net: Convolutional networks for biomedical image segmentation. In: Med. Image Comput. Comput. Assist. Interv.. MICCAI 2015, Springer International Publishing, pp. 234–241. http://dx.doi.org/10.1007/978-3-319-24574-4_28.

Roth, H.R., Farag, A., Turkbey, E.B., Lu, L., Liu, J., Summers, R.M., 2016. Data from pancreas-CT. http://dx.doi.org/10.7937/K9/TCIA.2016.tNB1kqBU.

Roth, H.R., Lu, L., Seff, A., Cherry, K.M., Hoffman, J., Wang, S., Liu, J., Turkbey, E., Summers, R.M., 2014. A new 2.5 D representation for lymph node detection using random sets of deep convolutional neural network observations. In: Med. Image Comput. Comput. Assist. Interv. MICCAI 2014, Springer International Publishing, pp. 520–527. http://dx.doi.org/10.1007/978-3-319-10404-1_65.

Roth, H.R., Oda, H., Zhou, X., Shimizu, N., Yang, Y., Hayashi, Y., Oda, M., Fujiwara, M., Misawa, K., Mori, K., 2018a. An application of cascaded 3D fully convolutional networks for medical image segmentation. Comput. Med. Imaging Graph. 66 (2017), 90–99. http://dx.doi.org/10.1016/j.compmedimag.2018.03.001, arXiv:1803.05431.

Roth, H.R., Shen, C., Oda, H., Sugino, T., Oda, M., Hayashi, Y., Misawa, K., Mori, K., 2018b. A multi-scale pyramid of 3D fully convolutional networks for abdominal multi-organ segmentation. In: Med. Image Comput. Comput. Assist. Interv. MICCAI 2018, Springer International Publishing, pp. 417–425. http://dx.doi.org/10.1007/978-3-030-00937-3_48.

Sahbaee, P., Abadi, E., Segars, W.P., Marin, D., Nelson, R.C., Samei, E., 2017. The effect of contrast material on radiation dose at CT: Part II. A systematic evaluation across 58 patient models. Radiology 283 (3), 749–757.

Sayed, G.I., Hassanien, A.E., Schaefer, G., 2016. An Automated Computer-aided Diagnosis System for Abdominal CT Liver Images. Procedia Comput. Sci. 90, 68–73. http://dx.doi.org/10.1016/j.procs.2016.07.012.

Selver, M.A., Ünal, G., Dicle, O., Gezer, N.S., Barış, M., Aslan, S., Candemir, C., Kavur, A.E., Kazaz, E., 2019. CHAOS - grand challenge. URL https://chaos.grand-challenge.org/Combined_Healthy_Abdominal_Organ_Segmentation.

Seo, H., Huang, C., Bassenne, M., Xiao, R., Xing, L., 2020. Modified U-Net (mU-Net) with Incorporation of Object-Dependent High Level Features for Improved Liver and Liver-Tumor Segmentation in CT Images. IEEE Trans. Med. Imaging 39 (5), 1316–1325. http://dx.doi.org/10.1109/TMI.2019.2948320, arXiv:1911.00140.

Simpson, Amber L, Antonelli, Michela, Bakas, Spyridon, Bilello, Michel, Farahani, Keyvan, Van Ginneken, Bram, Kopp-Schneider, Annette, Landman, Bennett A, Litjens, Geert, Menze, Bjoern, et al., 2019. A large annotated medical image dataset for the development and evaluation of segmentation algorithms. arXiv preprint arXiv:1902.09063.

Singh, A., Sengupta, S., Lakshminarayanan, V., 2020. Explainable deep learning models in medical image analysis. J. Imaging 6 (6), 52.

Su, J., Liu, Z., Zhang, J., Sheng, V.S., Song, Y., Zhu, Y., Liu, Y., 2021. Dv-net: Accurate liver vessel segmentation via dense connection model with d-bce loss function. Knowl.-Based Syst. 232, 107471.

Sun, C., Guo, S., Zhang, H., Li, J., Chen, M., Ma, S., Jin, L., Liu, X., Li, X., Qian, X., 2017. Automatic segmentation of liver tumors from multiphase contrast-enhanced CT images based on FCNs. Artif. Intell. Med. 83, 58–66. http://dx.doi.org/10.1016/j.artmed.2017.03.008.

Survarachakan, S., Pelanis, E., Khan, Z.A., Kumar, R.P., Edwin, B., Lindseth, F., 2021. Effects of enhancement on deep learning based hepatic vessel segmentation. Electronics 10 (10), 1165.

Taha, A.A, Hanbury, A., 2015. Metrics for evaluating 3d medical image segmentation: analysis, selection, and tool. BMC Med. Imaging 15 (1), 1–28.

Takenaga, T., Hanaoka, S., Nomura, Y., Nemoto, M., Murata, M., Nakao, T., Miki, S., Yoshikawa, T., Hayashi, N., Abe, O., 2019. Four-dimensional fully convolutional residual network-based liver segmentation in Gd-EOB-DTPA-enhanced MRI. Int. J. Comput. Assist. Radiol. Surg. 14 (8), 1259–1266. http://dx.doi.org/10.1007/s11548-019-01935-z.

Tan, M., Wu, F., Kong, D., Mao, X., 2021. Automatic liver segmentation using 3d convolutional neural networks with a hybrid loss function. Med. Phys. 48 (4), 1707–1719.

Tang, X., Jafargholi Rangraz, E., Coudyzer, W., Bertels, J., Robben, D., Schramm, G., Deckers, W., Maleux, G., Baete, K., Verslype, C., Gooding, M.J., Deroose, C.M., Nuyts, J., 2020b. Whole liver segmentation based on deep learning and manual adjustment for clinical use in SIRT. Eur. J. Nucl. Med. Mol. Imaging http://dx.doi.org/10.1007/s00259-020-04800-3.

Tang, W., Zou, D., Yang, S., Shi, J., Dan, J., Song, G., 2020a. A two-stage approach for automatic liver segmentation with Faster R-CNN and DeepLab. Neural Comput. Appl. 32 (11), 6769–6778. http://dx.doi.org/10.1007/s00521-019-04700-0.

Tang, W., Zou, D., Yang, S., Shi, J., Dan, J., Song, G., 2020c. A two-stage approach for automatic liver segmentation with faster r-cnn and deeplab. Neural Comput. Appl. 32 (11), 6769–6778.

Tian, J., Li, C., Shi, Z., Xu, F., 2018. A diagnostic report generator from CT volumes on liver tumor with semi-supervised attention mechanism. In: Med. Image Comput. Comput. Assist. Interv. MICCAI 2018, pp. 702–710. http://dx.doi.org/10.1007/978-3-030-00934-2_78.

Tian, J., Liu, L., Shi, Z., Xu, F., 2019. Automatic couinaud segmentation from CT volumes on liver using GLC-UNet. In: Med. Image Comput. Comput. Assist. Interv. MICCAI 2019, Springer International Publishing, pp. 274–282. http://dx.doi.org/10.1007/978-3-030-32692-0_32.

Tian, Y., Xue, F., Lambo, R., He, J., An, C., Xie, Y., Cao, H., Qin, W., 2021. Fully-automated functional region annotation of liver via a 2.5 d class-aware deep neural network with spatial adaptation. Comput. Methods Programs Biomed. 200, 105818.

Treilhard, J., Smolka, S., Staib, L., Chapiro, J., Lin, M., Shakirin, G., Duncan, J.S., 2017. Liver tissue classification in patients with hepatocellular carcinoma by fusing structured and rotationally invariant context representation. In: Med. Image Comput. Comput. Interv. MICCAI 2017, Springer International Publishing, pp. 81–88. http://dx.doi.org/10.1007/978-3-319-66179-7_10.

Turco, S., Tiyarattanachai, T., Ebrahimkheil, K., Eisenbrey, J., Kamaya, A., Mischi, M., Lyshchik, A., El Kaffas, A., 2022. Interpretable machine learning for characterization of focal liver lesions by contrast-enhanced ultrasound. IEEE Trans. Ultrason. Ferroelectr. Freq. Control 69 (5), 1670–1681.

UCSF Department of Surgery, 2020. Liver metastases. URL https://surgery.ucsf.edu/conditions--procedures/liver-metastases.aspx.

Vivanti, R., Joskowicz, L., Lev-Cohain, N., Ephrat, A., Sosna, J., 2018. Patient-specific and global convolutional neural networks for robust automatic liver tumor delineation in follow-up CT studies. Med. Biol. Eng. Comput. 56 (9), 1699–1713. http://dx.doi.org/10.1007/s11517-018-1803-6.

Vivanti, R., Szeskin, A., Lev-Cohain, N., Sosna, J., Joskowicz, L., 2017. Automatic detection of new tumors and tumor burden evaluation in longitudinal liver CT scan studies. Int. J. Comput. Assist. Radiol. Surg. 12 (11), 1945–1957. http://dx.doi.org/10.1007/s11548-017-1660-z.

Vorontsov, E., Tang, A., Pal, C., Kadoury, S., 2018. Liver lesion segmentation informed by joint liver segmentation. In: 2018 IEEE 15th Int. Symp. Biomed. Imaging. ISBI 2018, IEEE, pp. 1332–1335. http://dx.doi.org/10.1109/ISBI.2018.8363817.

Wang, R., Cao, S., Ma, K., Meng, D., Zheng, Y., 2019a. Pairwise semantic segmentation via conjugate fully convolutional network. In: Med. Image Comput. Comput. Assist. Interv. MICCAI 2019, Springer International Publishing, pp. 157–165. http://dx.doi.org/10.1007/978-3-030-32226-7_18.

Wang, X., Han, S., Chen, Y., Gao, D., Vasconcelos, N., 2019e. Volumetric attention for 3D medical image segmentation and detection. In: Med. Image Comput. Comput. Assist. Interv. MICCAI 2019, Springer International Publishing, pp. 175–184. http://dx.doi.org/10.1007/978-3-030-32226-7_20.

Wang, J., Lv, P., Wang, H., Shi, C., 2021. Sar-u-net: squeeze-and-excitation block and atrous spatial pyramid pooling based residual u-net for automatic liver segmentation in computed tomography. Comput. Methods Programs Biomed. 208, 106268.

Wang, K., Mamidipalli, A., Retson, T., Bahrami, N., Hasenstab, K., Blansit, K., Bass, E., Delgado, T., Cunha, G., Middleton, M.S., Loomba, R., Neuschwander-Tetri, B.A., Sirlin, C.B., Hsiao, A., 2019c. Automated CT and MRI Liver Segmentation and Biometry Using a Generalized Convolutional Neural Network. Radiol. Artif. Intell. 1 (2), 180022. http://dx.doi.org/10.1148/ryai.2019180022.

Wang, C., Song, H., Chen, L., Li, Q., Yang, J., Hu, X.T., Zhang, L., 2019d. Automatic liver segmentation using multi-plane integrated fully convolutional neural networks. In: Proc. - 2018 IEEE Int. Conf. Bioinforma. Biomed. BIBM 2018, pp. 518–523. http://dx.doi.org/10.1109/BIBM.2018.8621257.

Wang, Y., Song, Y., Wang, F., Sun, J., Gao, X., Han, Z., Shi, L., Shao, G., Fan, M., Yang, G., 2020. A two-step automated quality assessment for liver MR images based on convolutional neural network. Eur. J. Radiol. 124 (January), 108822. http://dx.doi.org/10.1016/j.ejrad.2020.108822.

Wang, Y., Zhou, Y., Shen, W., Park, S., Fishman, E.K., Yuille, A.L., 2019b. Abdominal multi-organ segmentation with organ-attention networks and statistical fusion. Med. Image Anal. 55, 88–102. http://dx.doi.org/10.1016/j.media.2019.04.005, arXiv:1804.08414.

Wang, Y., Zhou, Y., Tang, P., Shen, W., Fishman, E.K., Yuille, A.L., 2018. Training multi-organ segmentation networks with sample selection by relaxed upper confident bound. In: Med. Image Comput. Comput. Assist. Interv. MICCAI 2018, Springer International Publishing, pp. 434–442. http://dx.doi.org/10.1007/978-3-030-00937-3.

Wardhana, G., Naghibi, H., Sirmacek, B., Abayazid, M., 2021. Toward reliable automatic liver and tumor segmentation using convolutional neural network based on 2.5 d models. Int. J. Comput. Assist. Radiol. Surgery 16 (1), 41–51.

Xi, X.F., Wang, L., Sheng, V.S., Cui, Z., Fu, B., Hu, F., 2020. Cascade U-ResNets for Simultaneous Liver and Lesion Segmentation. IEEE Access 8, 68944–68952. http://dx.doi.org/10.1109/ACCESS.2020.2985671.

Xia, K., Yin, H., Qian, P., Jiang, Y., Wang, S., 2019. Liver semantic segmentation algorithm based on improved deep adversarial networks in combination of weighted loss function on abdominal CT images. IEEE Access 7, 96349–96358. http://dx.doi.org/10.1109/ACCESS.2019.2929270.

Xiao, X., Zhao, J., Qiang, Y., Chong, J., Yang, X.T., Kazihise, N.G.F., Chen, B., Li, S., 2019. Radiomics-guided GAN for segmentation of liver tumor without contrast agents. In: Med. Image Comput. Comput. Assist. Interv. MICCAI 2019, Springer International Publishing, pp. 237–245. http://dx.doi.org/10.1007/978-3-030-32245-8_27.

Xie, S., Tu, Z., 2015. Holistically-nested edge detection. In: IEEE Int. Conf. Comput. Vis. pp. 1395–1403.

Xu, P., Chen, C., Wang, X., Li, W., Sun, J., 2020. ROI-Based Intraoperative MR-CT Registration for Image-Guided Multimode Tumor ablation Therapy in Hepatic Malignant Tumors. IEEE Access 8, 13613–13619. http://dx.doi.org/10.1109/aCCESS.2020.2966518.

Yan, Q., Wang, B., Zhang, W., Luo, C., Xu, W., Xu, Z., Zhang, Y., Shi, Q., Zhang, L., You, Z., 2020. Attention-guided deep neural network with multi-scale feature fusion for liver vessel segmentation. IEEE J. Biomed. Health Inf. 25 (7), 2629–2642.

Yang, J., Dvornek, N.C., Zhang, F., Chapiro, J., Lin, M.D., Duncan, J.S., 2019. Unsupervised domain adaptation via disentangled representations: application to cross-modality liver segmentation. In: Med. Image Comput. Comput. Assist. Interv. MICCAI 2019, Springer International Publishing, pp. 255–263. http://dx.doi.org/10.1007/978-3-030-32245-8_29.

Yang, J., Fu, M., Hu, Y., 2021. Liver vessel segmentation based on inter-scale v-net. Math. Biosci. Eng. 18 (4), 4327–4340.

Yang, D., Xu, D., Zhou, S.K., Georgescu, B., Chen, M., Grbic, S., Metaxas, D., Comaniciu, D., 2017. Automatic liver segmentation using an adversarial image-to-image network. In: Med. Image Comput. Comput. Interv. MICCAI 2017, Springer International Publishing, pp. 507–515. http://dx.doi.org/10.1007/978-3-319-66179-7_58.

Yao, J., Cai, J., Yang, D., Xu, D., Huang, J., 2019. Integrating 3D geometry of organ for improving medical image segmentation. In: Med. Image Comput. Comput. Assist. Interv. MICCAI 2019, Springer International Publishing, pp. 318–326. http://dx.doi.org/10.1007/978-3-030-32254-0_36.

Yao, K., Su, Z., Huang, K., Yang, X., Sun, J., Hussain, A., Coenen, F., 2022. A novel 3d unsupervised domain adaptation framework for cross-modality medical image segmentation. IEEE J. Biomed. Health Inf.

Yeghiazaryan, V., Voiculescu, I., 2015. An Overview of Current Evaluation Methods Used in Medical Image Segmentation. Tech. Rep. RR-15-08, Department of Computer Science, Oxford, UK.

Yuan, Y., 2017. Hierarchical convolutional-deconvolutional neural networks for automatic liver and tumor segmentation. arXiv:1710.04540.

Yushkevich, P.A., Piven, J., Cody Hazlett, H., Gimpel Smith, R., Ho, S., Gee, J.C., Gerig, G., 2006. User-guided 3D active contour segmentation of anatomical structures: significantly improved efficiency and reliability. Neuroimage 31 (3), 1116–1128, URL www.itksnap.org.

Zeng, Q., Karimi, D., Pang, E.H., Mohammed, S., Schneider, C., Honarvar, M., Salcudean, S.E., 2019. Liver segmentation in magnetic resonance imaging via mean shape fitting with fully convolutional neural networks. In: Med. Image Comput. Comput. Assist. Interv. MICCAI 2019, Springer International Publishing, pp. 246–254. http://dx.doi.org/10.1007/978-3-030-32245-8_28.

Zeng, Y.-z., Liao, S.-h., Tang, P., Zhao, Y.-q., Liao, M., Chen, Y., Liang, Y.-x., 2018. Automatic liver vessel segmentation using 3d region growing and hybrid active contour model. Comput. Biol. Med. 97, 63–73.

Zeng, Y.Z., Zhao, Y.Q., Liao, M., Zou, B.J., Wang, X.F., Wang, W., 2016. Liver vessel segmentation based on extreme learning machine. Phys. Med. 32 (5), 709–716. http://dx.doi.org/10.1016/j.ejmp.2016.04.003.

Zhang, C., Hua, Q., Chu, Y., Wang, P., 2021a. Liver tumor segmentation using 2.5d uv-net with multi-scale convolution. Comput. Biol. Med. 133, 104424.

Zhang, Y., Jiang, B., Wu, J., Ji, D., Liu, Y., Chen, Y., Wu, E.X., Tang, X., 2020a. Deep Learning Initialized and Gradient Enhanced Level-Set Based Segmentation for Liver Tumor from CT Images. IEEE Access 8, 76056–76068. http://dx.doi.org/10.1109/ACCESS.2020.2988647.

Zhang, D., Liu, S., Chaganti, S., Gibson, E., Xu, Z., Grbic, S., Cai, W., Comaniciu, D., 2020b. Graph attention network based pruning for reconstructing 3D liver vessel morphology from contrasted CT images. arXiv:2003.07999.

Zhang, Y., Miao, S., Mansi, T., Liao, R., 2018b. Task driven generative modeling for unsupervised domain adaptation: application to X-ray image segmentation. In: Med. Image Comput. Comput. Assist. Interv. MICCAI 2018, Springer International Publishing, pp. 599–607. http://dx.doi.org/10.1007/978-3-030-00934-2_67.

Zhang, P., Yang, J., Ai, D., Xie, Z., Liu, Y., 2015. Learning based random walks for automatic liver segmentation in CT image. In: Chinese Conf. Image Graph. Technol. Springer International Publishing, pp. 251–259. http://dx.doi.org/10.1007/978-3-662-47791-5.

Zhang, F., Yang, J., Nezami, N., Laage-gaupp, F., Chapiro, J., De Lin, M., Duncan, J., 2018a. Liver tissue classification using an auto-context-based deep neural network with a multi-phase training framework. In: Int. Work. Patch-Based Tech. Med. Imaging. Springer International Publishing, pp. 59–66. http://dx.doi.org/10.1007/978-3-030-00500-9_7.

Zhang, Y., Yu, S., Zhu, X., Ning, X., Liu, W., Wang, C., Liu, X., Zhao, D., Zheng, Y., Bao, J., 2021b. Explainable liver tumor delineation in surgical specimens using hyperspectral imaging and deep learning. Biomed. Opt. Express 12 (7), 4510–4529.

Zhang, R., Zhou, Z., Wu, W., Lin, C.C., Tsui, P.H., Wu, S., 2018c. An improved fuzzy connectedness method for automatic three-dimensional liver vessel segmentation in CT images. J. Healthc. Eng. 2018, 1–17. http://dx.doi.org/10.1155/2018/2376317.

Zheng, Y., Ai, D., Mu, J., Cong, W., Wang, X., Zhao, H., Yang, J., 2017b. Automatic liver segmentation based on appearance and context information. Biomed. Eng. Online 16 (1), 1–12. http://dx.doi.org/10.1186/s12938-016-0296-5.

Zheng, S., Fang, B., Li, L., Gao, M., Wang, Y., Peng, K., 2017a. Automatic liver lesion segmentation in CT combining fully convolutional networks and non-negative matrix factorization. In: Imaging Patient-Customized Simulations Syst. Point-of-Care Ultrasound, Int. Work. BIVPCS 2017 POCUS 2017. Springer International Publishing, pp. 44–51. http://dx.doi.org/10.1007/978-3-319-67552-7_6.

Zheng, H., Lin, L., Hu, H., Zhang, Q., Chen, Q., Iwamoto, Y., Han, X., Chen, Y.-W., Tong, R., Wu, J., 2019. Semi-supervised segmentation of liver using adversarial learning with deep atlas prior. In: Med. Image Comput. Comput. Assist. Interv. MICCAI 2019, Springer International Publishing, pp. 148–156. http://dx.doi.org/10.1007/978-3-030-32226-7_17.

Zheng, R., Wang, Q., Lv, S., Li, C., Wang, C., Chen, W., Wang, H., 2022. Automatic liver tumor segmentation on dynamic contrast enhanced mri using 4D information: Deep learning model based on 3D convolution and convolutional LSTM. IEEE Trans. Med. Imaging.

Zhou, Y., Li, Z., Bai, S., Chen, X., Han, M., Wang, C., Fishman, E., Yuille, A., 2019a. Prior-aware neural network for partially-supervised multi-organ segmentation. In: IEEE Int. Conf. Comput. Vis. pp. 10671–10680. http://dx.doi.org/10.1109/ICCV.2019.01077.

Zhou, Z., Siddiquee, M.R., Tajbakhsh, N., Liang, J., 2020. UNet++: Redesigning Skip Connections to Exploit Multiscale Features in Image Segmentation. IEEE Trans. Med. Imaging 39 (6), 1856–1867.

Zhou, Z., Sodha, V., Siddiquee, M.M.R., Feng, R., Tajbakhsh, N., Gotway, M.B., Liang, J., 2019b. Models genesis: generic autodidactic models for 3D medical image analysis. In: Med. Image Comput. Comput. Assist. Interv. MICCAI 2019, Springer International Publishing, pp. 384–393. http://dx.doi.org/10.1007/978-3-030-32251-9_42.

Zoetmulder, R., Gavves, E., Caan, M., Marquering, H., 2022. Domain-and task-specific transfer learning for medical segmentation tasks. Comput. Methods Programs Biomed. 214, 106539.